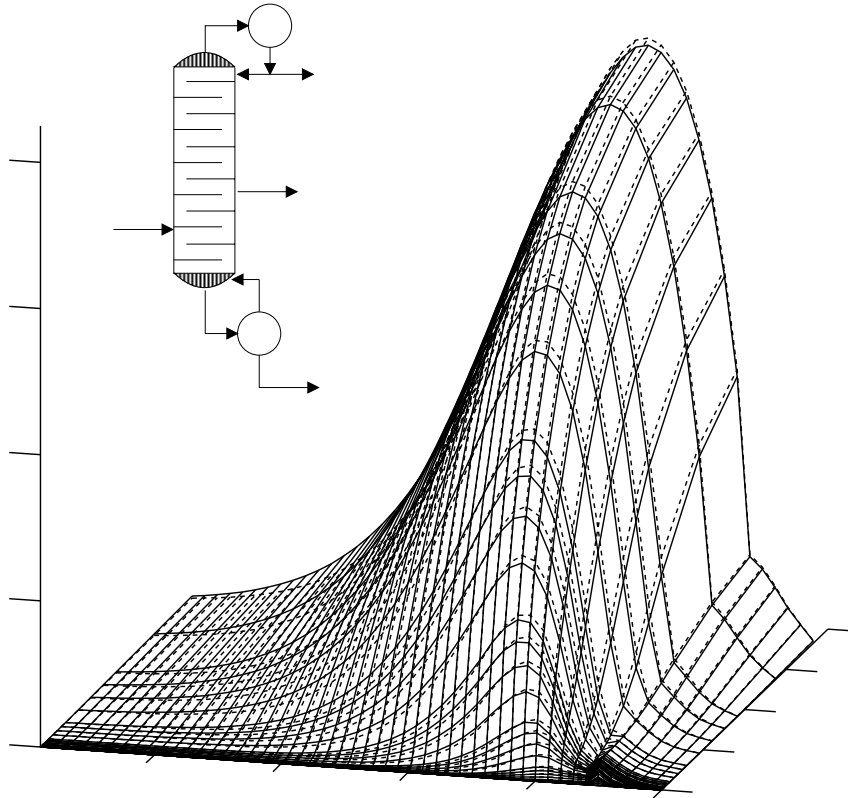


Clarkson University

Dynamic Nonequilibrium Column Simulation



A Dissertation
by
Hendrik Adriaan Kooijman

Clarkson University

Dynamic Nonequilibrium Column Simulation

A Dissertation

by

Hendrik Adriaan Kooijman

Department of Chemical Engineering

Submitted in partial fulfillment of the requirements

for the degree of

Doctor of Philosophy

(Chemical Engineering)

February, 1995

CIP-DATA KONINKLIJKE BIBLIOTHEEK, DEN HAAG

Kooijman, Hendrik Adriaan
Dynamic Nonequilibrium Column Simulation/Dissertation
Thesis Clarkson University, Department of Chemical Engineering

ISBN 90-900-8430-4
NUGI 841

Published and distributed by:
Buro Kooijman, Marco Polorede 10, 2725 KR Zoetermeer, The Netherlands

Copyright © 1995 by H.A. Kooijman. All rights reserved.

No part of the material protected by this copyright notice may be reproduced or utilized in any form or by any means, electronic or mechanical, including photocopying, recording or by any information storage and retrieval system, without permission in writing from the publisher and/or the author.

The undersigned have examined the thesis/dissertation entitled "Dynamic Nonequilibrium Column Simulation" presented by Hendrik A. Kooijman, a candidate for the degree of Doctor of Philosophy in Chemical Engineering, and hereby certify that it is worthy of acceptance.

Date

Prof. Ross Taylor, Advisor

Prof. Angelo Lucia (Committee)

Prof. Don Rasmussen (Committee)

Prof. Babu (Committee)

Prof. Abdul Jerri (Committee)

Abstract

Simulation of distillation columns usually is carried out using an equilibrium model based on the assumption that thermodynamic and thermal equilibrium exists on each tray in the column. To deal with departures from thermodynamic equilibrium it is common practice to specify an efficiency that is the same for all components on all stages. However, component efficiencies are *not* equal in systems with more than two components and cannot be correlated, especially for nonideal systems. This makes the equilibrium model inappropriate for dynamic simulations where these efficiencies are subject to change and cannot be specified beforehand. Using constant efficiencies neglects the influence of the tray hydrodynamics on the mass transfer and the consequences for the column dynamics. Additionally, in certain column operations there is a departure from thermal equilibrium which cannot be modeled with the equilibrium model either.

In this thesis a nonequilibrium model for the dynamic simulation of distillation columns is described. The nonequilibrium model incorporates the rigorous calculation of the mass and energy transfer rates and avoids the use of efficiencies. The influence of mass transfer correlations on column dynamics has been investigated. A new design mode is implemented that eliminates the need for a previously known column layout in order to do a nonequilibrium (dynamic) simulation, which enlarges the range of application of the model. Alternative plug-flow models are proposed to improve the modeling of mass transfer on large trays.

Acknowledgments

I would like to express my appreciation to all the people who helped me during my research period at Clarkson University. Foremost is my advisor Professor Ross Taylor. When he asked me back in 1988 at Delft University to help him develop an educational software program, I never guessed that through this collaboration I would later come to the United States to do my PhD. Ross, it has been a pleasure working with you! I would also like to thank Professor Hans Wesselingh, who, through his use of our programs in his classes and courses, has contributed to their success. Furthermore, I would like to thank Professor Angelo Lucia for many fruitful discussions and comments on numerous topics. I am grateful for the financial support of the National Science Foundation (grant number CBT 88821005) and BP International which enabled me to do my research. Also, I would like to thank all my fellow graduate students for making my stay in Potsdam a joyful one. Finally, I want to thank Sharon Sweeney, who has helped me to get through all the frustrations that go along with pursuing a PhD.

I dedicate this thesis to Jacobus Cornelis Kooijman.

Contents

Abstract	iv
Acknowledgments	v
1 Introduction and Motivation	1
1.1 Need for Dynamic Process Modeling	1
1.2 Dynamic Column Simulation	2
1.3 Nonequilibrium column models	4
1.4 Objectives	6
2 Steady-State Simulation of Nonequilibrium Columns	11
2.1 The Nonequilibrium Model	11
2.2 The Design Mode	18
3 Flow Models	29
3.1 Mass Transfer Modeling Inconsistencies	29
3.2 Flow Models	34
3.3 Evaluation of Flow Models	38
3.4 Evaluation of Mass Transfer Coefficient Correlations	40

3.5	Maxwell-Stefan or Not?	42
4	Dynamic Model Development	47
4.1	Nonequilibrium Model Assumptions	47
4.2	Nonequilibrium Model Equations	48
4.3	Reboiler and Condenser	53
4.4	Equilibrium models	56
4.5	Physical Property Models	58
4.6	Solving the Dynamic Nonequilibrium Model	58
5	Simulation Results	67
5.1	Steady-State Simulations	67
5.2	Design mode	68
5.3	Equilibrium Versus Nonequilibrium	70
5.4	Different Holdup Models	75
5.5	Mass Transfer Coefficients Models	76
5.6	Mass Transfer Sensitivity	77
5.7	Multicomponent and Effective Diffusivity	79
5.8	Tray Layout and Operation	82
5.9	Neglecting Jacobian Terms	84
6	Conclusions	85
	Appendix A. Correlations	89
	Appendix B. Flow model derivation	95
	Appendix C. Flow and Mass Transfer models	97

List of Figures

2.1	Schematic diagram of a nonequilibrium stage (Taylor and Krishna, 1993).	11
3.1	Murphree efficiencies for a depropanizer predicted by a nonequilibrium model assuming both vapor and liquid phases are completely mixed.	30
3.2	Liquid composition profiles for a depropanizer predicted by a nonequilibrium model with the molar fluxes calculated using overall mass transfer coefficients and the energy balance includes the sensible heat transfer terms.	32
3.3	Interphase mass transfer rates for the depropanizer for the same combination of models used in Figure 3.2.	32
3.4	Murphree efficiencies for a depropanizer predicted by a nonequilibrium model assuming the vapor rises in plug flow through a well-mixed liquid phase.	36
3.5	Murphree efficiencies for a depropanizer predicted by a nonequilibrium model assuming both vapor and liquid phases are in plug flow.	37
3.6	Liquid composition profiles for a depropanizer predicted by a nonequilibrium model with the molar fluxes calculated using the plug flow models derived in this paper.	37
3.7	Murphree efficiencies for different flow models for a (8% hole area) sieve tray column with the cyclohexane - <i>n</i> -heptane system operating at 165 <i>kPa</i> . Mixed-Mixed flow (thick dotted line), Plug flow vapor - Mixed flow Liquid (thick dashed line), Plug flow vapor - Dispersion flow liquid (dashed line), and Plug-Plug flow (solid line). Mass transfer coefficients from the Chan and Fair correlation.	40
3.8	Murphree efficiencies for different flow models for a (8% hole area) sieve tray column with the <i>i</i> -butane - <i>n</i> -butane system operating at 2068 <i>kPa</i> . Mixed-Mixed flow (thick dotted line), Plug flow vapor - Mixed flow Liquid (thick dashed line), Plug flow vapor - Dispersion flow liquid (dashed line), and Plug-Plug flow (solid line), Mass transfer coefficients from the Chan and Fair correlation.	40

3.9	Murphree efficiencies for different Mass Transfer Coefficient models for a (14% hole area) sieve tray column with cyclohexane - <i>n</i> -heptane system operating at 34 <i>kPa</i> . Chan and Fair (thick dotted line), AIChE (thick dashed line), Zuiderweg (dashed line), and Chen and Chuang (solid line).	41
3.10	Murphree efficiencies for different Mass Transfer Coefficient models for a (14% hole area) sieve tray column with <i>i</i> -butane - <i>n</i> -butane system operating at 1138 <i>kPa</i> . Chan and Fair (thick dotted line), AIChE (thick dashed line), Zuiderweg (dashed line), and Chen and Chuang (solid line).	41
3.11	Liquid phase composition profiles for acetone - methanol - water extractive distillation column. Solid line - Maxwell-Stefan model, dashed line - equal diffusivity model. . . .	42
3.12	Liquid temperature profiles for acetone - methanol - water extractive distillation column. Solid line - Maxwell-Stefan model, dashed line - equal diffusivity model.	43
3.13	Liquid phase composition profiles for ethanol - <i>t</i> -butanol - water distillation column. Solid line - Maxwell-Stefan model, dashed line - equal diffusivity model.	43
4.1	Schematic diagram of a general tray.	47
4.2	Schematic diagram of the holdups and connecting flows.	48
5.1	BTX distillation column internal liquid flows (<i>kmol/s</i>) as function of time (<i>s</i>) after increasing the boilup ratio. Flows in the rectification section (solid lines) use the left axis and the flows in the stripping section (dashed lines) use the right axis.	69
5.2	BTX distillation column internal liquid flows (<i>kmol/s</i>) after increasing the reflux ratio and decreasing the feed flow simultaneously. Flows in the rectification section (solid lines) use the right axis and the flows in the stripping section (dashed lines) use the left axis.	69
5.3	Extractive Distillation Column Configuration	70
5.4	Murphree efficiencies backcalculated from nonequilibrium simulation for the extractive distillation of <i>n</i> -heptane and toluene with phenol.	70
5.5	Murphree efficiencies backcalculated from nonequilibrium simulation for the extractive distillation after a drop in phenol feed temperature.	72
5.6	Temperatures (K) of trays 10 through 30 and the reboiler for the extractive distillation column as a function of time.	72
5.7	Internal liquid flows for the extractive distillation column.	72

5.8	Internal vapor flows for the extractive distillation column.	73
5.9	Temperature profiles for the acetone absorber simulated with the equilibrium model. . .	73
5.10	Temperature profiles for the acetone absorber simulated with the nonequilibrium model.	73
5.11	Molefraction of acetone of absorber off-gas as a function of time for the equilibrium (dashed line) and nonequilibrium (solid line) model.	75
5.12	Liquid flows in Debutanizer	75
5.13	Temperatures of trays 12, 15, and 18 in a depropanizer modeled by the nonequilibrium model with 2 holdups (dashed lines) and the 4 holdup model (solid lines), after an in- crease in the reflux ratio.	76
5.14	n-Butane composition in the distillate of the depropanizer. The equilibrium model pre- dicts high concentration transients: the EQLV model (solid line), and the EQLV model with lumped downcomer liquid (dashed lines). The nonequilibrium model has low con- centration transients: the NEQ2H model (solid line), the NEQ2H model with the lumped downcomer liquid (dotted line), the NEQ4H model (dashed line), and the NEQ4H model with constant vapor volume above the froth (thick dashed line).	76
5.15	Propane composition in the bottoms of the depropanizer. The equilibrium model pre- dicts high concentration transients (and uses the left axis): the EQLV model (solid line), and the EQLV model with lumped downcomer liquid (dashed lines). The nonequi- librium model has low concentration transients (and uses the right axis): the NEQ2H model (solid line), the NEQ2H model with the lumped downcomer liquid (dotted line), the NEQ4H model (dashed line), and the NEQ4H model with constant vapor volume above the froth (thick dashed line).	77
5.16	Methanol/i-propanol/water column configuration.	77
5.17	Dynamics of various mass transfer model for the methanol/i-propanol/water column. . .	77
5.18	Dynamics of various mass transfer model for the methanol/i-propanol/water column. . .	77
5.19	Propanol mole fraction transient on the 25th tray. The interfacial area is decreased (a, left) or increased (b, right) by 50% (right axis). The normal transient is shown with a dotted line (left axis).	79
5.20	Propanol mole fraction transient on the 25th tray. The vapor and liquid mass transfer coefficients are decreased (a, left) or increased (b, right) by 50% (right axis). The normal transient is shown with a dotted line (left axis).	79

5.21	Propanol mole fraction transient on the 25th tray. The vapor mass transfer coefficients are increased by 100% (a, left) or the liquid mass transfer coefficients are increased by 100% (b, right), using the right axis. The normal transient is shown with a dotted line (left axis).	79
5.22	Ethanol/water column with side-draw for the removal of propanol.	80
5.23	Mole fraction of n-propanol as function of the time using the full Maxwell-Stefan matrix diffusivity approach (solid line, left axis) and the effective diffusivity approach (dotted line, right axis).	80
5.24	Mole fraction of n-propanol as function of time using the full Maxwell-Stefan approach (solid line) and the effective diffusivity approach (dotted line).	80
5.25	Mole fraction of i-propanol as function of time using the full Maxwell-Stefan approach (solid line) and the effective diffusivity approach (dotted line).	82
5.26	Internal liquid flow profiles ($kmol/s$) as function of time for the equilibrium (solid lines) and nonequilibrium (dotted lines) models using a double pass sieve tray.	82
5.27	Mole fraction of i-propanol in the distillate as function of the time for the equilibrium (thin lines) and nonequilibrium (thick lines), using single pass sieve tray (solid lines) and double pass sieve trays (dashed lines). The methanol/i-propanol/water column was simulated with the Chan-Fair model.	83
5.28	i-Propanol mole fractions as function of the time simulated with the nonequilibrium model for single (solid lines) and two pass (dotted lines) sieve trays.	83
5.29	Distillate i-propanol mole fractions as function of the time simulated with the equilibrium (thin lines) and the nonequilibrium model (thick lines) with two different weir heights; one inch (dashed lines) and two inch (solid lines).	83
5.30	Distillate i-propanol mole fractions as function of the time after increasing the reflux ratio simulated with the equilibrium (thin lines, left axis) and the nonequilibrium model (thick lines, right axis).	83
C.1	Experimental FRI data cC6-nC7 at 34 kPa , 14% Sieve plate.	97
C.2	Experimental FRI data cC6-nC7 at 165 kPa , 14% Sieve plate.	97
C.3	Experimental FRI data cC6-nC7 at 165 kPa , 8% Sieve plate.	97
C.4	Experimental FRI data cC6-nC7 at 28 kPa , 8% Sieve plate.	97
C.5	Experimental FRI data iC4-nC4 at 1138 kPa , 14% Sieve plate.	98

C.6	Experimental FRI data iC4-nC4 at 1138 <i>kPa</i> , 8% Sieve plate.	98
C.7	Experimental FRI data iC4-nC4 at 2068 <i>kPa</i> , 8% Sieve plate.	98
C.8	Experimental FRI data iC4-nC4 at 2756 <i>kPa</i> , 8% Sieve plate.	98

List of Tables

2.1	Available mass transfer coefficient correlations per internals type	14
2.2	Pressure drop correlations per internals type	16
2.3	Nonequilibrium model equations type and number	17
2.4	Tray layout data	20
2.5	Tray design checks and adjustments	22
3.1	Column Design Parameters for Depropanizer	31
3.2	Sieve Plate Dimensions of FRI Column	40
4.1	Variables and equations for the full dynamic model	52
4.2	Variables and equations for the reboiler model	54
4.3	Variables and equations for the condenser model	56
4.4	Variables and equations for the EQL model	57
5.1	BTX Distillation Column Specifications	68
5.2	Extractive Distillation Column Specifications	71
5.3	Acetone Absorber Specifications	74
5.4	Methanol/i-propanol/water Column Specifications	78
5.5	Propanol Side-draw Column Specifications	81

D.1	Results for the test problems with and without updating of the Jacobian. Absolute tolerances of 10^{-4} are used and the initial step is 10^{-3}	103
D.2	Results for the test problems using DAES, IMR, and DASSL. Absolute tolerances of 10^{-4} are used and the initial step is 10^{-3}	105

Publications that resulted from this work:

- H.A. Kooijman, R. Taylor, “On the Estimation of Diffusion Coefficients in Multicomponent Liquid Systems”, *Ind. Eng. Chem. Res.*, Vol **30**, No. 6, (1991) pp. 1217-1222.
- R. Taylor, H.A. Kooijman, “Composition Derivatives of Activity Coefficient Models (For the estimation of Thermodynamic Factors in Diffusion)”, *Chem. Eng. Comm.*, Vol. **102**, (1991) pp. 87-106.
- R. Taylor, H.A. Kooijman, M.R. Woodman, “Industrial Applications of a NonEquilibrium Model of Distillation and Absorption Operations”, *I.Chem.E. Symp. Ser.*, No. 128, Birmingham UK (September 1992), pp. A415-427.
- R. Taylor, H.A. Kooijman, J-S. Hung, “A Second Generation Nonequilibrium Model for Computer Simulation of Multicomponent Separation Processes”, *Comp. Chem. Eng.*, Vol **18**, No. 3, (1994) pp. 205-217.
- H.A. Kooijman, R. Taylor, “A Nonequilibrium Model for Dynamic Simulation of Tray Distillation Columns”, accepted for publication in *AIChE J.*
- H.A. Kooijman, R. Taylor, “Modelling Mass Transfer in Multicomponent Distillation”, accepted for publication in *Chem. Eng. J.*

Chapter 1

Introduction and Motivation

To improve the economics, flexibility, operability, and safety of column-based separation processes, design that considers steady-state as well as dynamic behavior is desired. This requires a fundamentally sound model that is capable of accurately describing the separation process. A nonequilibrium model can provide accurate predictions of column performance without the need to fit experimental column data. Our objective is to construct an improved nonequilibrium model which allows both steady-state and dynamic behavior of columns to be studied.

1.1 Need for Dynamic Process Modeling

Current industry design practices feature separate process design and process control groups. Process design remains a largely sequential process with each process unit being sized individually with the emphasis on minimizing capital expenditures instead of an emphasis on overall performance. The resulting dynamic system of the connected equipment can be ill-behaved or difficult to control. Especially designs that minimize holdups may lead to severe control problems. Control engineers often are involved only after the design is already complete. This may lead to redesign of the control system or equipment, unnecessarily complicated control systems, and revenue lost due to delays or not meeting promised product deliveries.

In the process design phase, dynamic simulation is needed to determine dynamic responses to process disturbances such as surge tank levels, column sump levels, product flow rates, or product compositions required for sizing of the relevant equipment as well as for the selection and location of control sensors and actuators. Dynamic modeling can also identify whether the product goals are attainable and detect control schemes which are not adequate or appropriate for meeting given product specification goals. This is specifically of interest with the installation of advanced control algorithms. Initial tuning

and optimization of control parameters can result in faster process start-up and control problems will be detected earlier when the process design can be altered without a considerable increase in costs. Controllability of alternative flowsheets can be investigated and auxiliary equipment for startup or shut-down can be located and designed. A side benefit from dynamic simulation is that process engineers will become familiar with the process dynamics and control issues (and control engineers with process design).

For process safety assessments, dynamic simulation can be used to check whether environmental constraints will be met during transitions or to test various emergency shut down procedures without performing actual experiments. Start-up and shutdown of current processes can be optimized and while interfacing with the control structure dynamic simulation can facilitate online process optimization and operator training. It can also be a tool for testing the controls robustness, e.g., in relation to measurement errors or valve malfunctioning.

Clearly, dynamic simulation provides process *and* control engineers with a powerful tool to improve process design and production in various ways which can lead to improved revenues. However, dynamic process simulation is only yet starting to become of importance due to the fact that dynamic simulation programs and packages have suffered from a number of deficiencies. Most engineers could not use them because they were geared for use by specialists, they were not user-friendly nor interactive. Usually, even the more simple models required large computer resources. Simulators were not portable, fast, flexible, extendable, maintainable, or affordable.

The immense increase in available computer power now allows the engineer to do dynamic simulations on a personal computer or workstation (instead of having to use a mainframe or supercomputer). Maintainability and extendibility is possible by use of equation oriented simulators where models are described in high level declarative languages. Examples are SPEEDUP (Perkins and Sargent, 1982, Pantelides, 1988a), ASCEND (Piela *et al.*, 1991) and gPROMS (Barton and Pantelides, 1991). Pantelides and Barton (1993) and Wozny and Jeromin (1994) discuss the current status and possible future of (equation oriented) dynamic simulation.

1.2 Dynamic Column Simulation

The simulation of separation processes – in particular the simulation of distillation columns – is an essential part of dynamic process simulators. Distillation is a high energy consumer in most chemical processes and the interactions between columns can be significant from the design as well as the operability point of view.

Simulation of separation processes by equilibrium stage calculations dates back to 1893 when Sorel published equations for simple, continuous, steady-state distillation. These equations included total and component material balances and a corresponding energy balance that could account for heat losses. Sorel's equations were not widely applied until 1921 when they were used in a graphical solu-

tion technique for binary systems by Ponchon (1921) and Savarit (1922), who employed an enthalpy-concentration diagram. In 1925 a much simpler, but restricted, graphical technique was developed by McCabe and Thiele. The simplification was achieved by assuming constant molar overflow, eliminating the energy balance equations. Lewis and Matheson (1932) and Thiele and Geddes (1933) were the first to propose methods to solve the systems of equations in a tray by tray manner. Thiele and Geddes (1933) were also the first to solve each type of the MESH equations in turn (MESH is the acronym referring to the different types of equations: M=Material balance, E=Equilibrium, S=Summation, H=Heat balance).

After the introduction of the digital computer in the 1950's, the rate of development of algorithms and simulators has increased dramatically. Equilibrium stage calculations enabled engineers to design a column for the separation of simple mixtures without the need to build a pilot plant again and to scaleup. This had a big impact on the investment costs and design time for a new (part of a) plant. Several textbooks describe the development of the equilibrium stage simulation (see King, 1980; Henley and Seader, 1981; Holland, 1981). Seader (1985) has discussed some recent advances in numerical methods for application to mathematical modeling in process design. By the late 1970's, the steady-state equilibrium stage simulators had made substantial strides, particularly in the area of the physical property prediction. By the end of the 1970's some commercial simulators had gained a wide acceptance by chemical engineers working in process design.

Chemical engineers first used dynamic simulation to evaluate control and safety system designs in the mid 1950's. Only the simplest models could be used, even if just a single unit was to be simulated, since computers were, at that time, far too slow. For the dynamic simulation time derivatives of the holdups on the stages are required making the equations to solve differential ones. A model described by as many as fifty differential equations was then a large model. Early computer models and experiments that appeared in the literature were reported by Mah *et al.* (1962), Huckaba and coworkers (1963, 1965), Luyben *et al.* (1964), Waggoner and Holland (1965), Distefano (1968), and Howard (1970). Howard (1970) discussed a continuous distillation simulator and compared results with experiments. Constant molar holdups were assumed, derivative terms in the energy equation were eliminated and a Runge-Kutta method was used for integration. Boston and Britt (1981) developed a commercial batch distillation simulator, based mainly on the model of Distefano. Gallun and Holland (1982) used Gear's method (1971a,b) to solve the equations involved in dynamic simulation. Holland and Liapis (1983) discuss the use of semi-implicit Runge-Kutta methods as well as the multi-step methods of Gear for the integration. Prokopakis and Seider (1983) simulated azeotropic distillation towers.

Gani *et al.* (1986, 1987a,b, 1989), Cameron (1988), and Ruiz (1988) proposed an extended model for the continuous dynamic simulation of distillation columns. They also discussed the optimization of the dynamic startup/shutdown operations (Gani *et al.*, 1987a,b) and the hydraulics involved. Their model is, perhaps, the most comprehensive dynamic equilibrium stage model described in the literature. They neglected vapor holdup (which is much smaller than the liquid holdup) and assumed the equilibrium model for each stage in the column, using the Murphree plate efficiency. The equations are solved with an ODE solver which solves the algebraic equations through a procedural approach. Gani *et al.* (1987a,b) discuss startup/shutdown operations and the hydraulics involved which they reported to play a major role in these kinds of simulations. Cuille *et al.* (1986) simulated batch distillation with chemical

reactions present. Holl *et al.* (1988) made a dynamic simulator called DIVA and Pantelides (1988) included dynamic simulation in SPEEDUP. Gani and Cameron (1989) proposed a general simulator for steady-state as well as dynamic simulation. The dynamic model could even help with steady-state calculations that are very hard to converge.

Several authors discuss the assumptions used in the dynamic simulation of separation columns that introduce errors. Ranzi *et al.* (1988) discussed the effects of the energy balances and the way they affect the simulation. They found that the energy balances must be evaluated completely in order to predict correct behavior. Choe and Luyben (1987) conclude that vapor holdups cannot be neglected (especially for columns operating at high pressures) and that column pressures should be calculated (especially for low pressure columns, where the tray pressure has a large influence on the tray temperature).

1.3 Nonequilibrium column models

Although the equilibrium model has been the basis of the dynamic simulation of distillation columns, its shortcomings are well known. The model is based on the assumption that both phases leaving a stage are in thermal and thermodynamic equilibrium. In practice equilibrium is rarely attained since mass and heat transfer are actually *rate* processes that are driven by the gradients in chemical potential and temperature.

The traditional method of coping with finite rates of mass transfer in stagewise processes has been through the concept of a stage efficiency. There are various definitions of stage efficiencies, but the most popular is the Murphree (1925) component vapor efficiency:

$$\xi = \frac{y_{ij} - y_{i,j-1}}{y_{ij}^* - y_{i,j-1}} \quad (1.1)$$

where y_{ij} is the actual vapor composition of component i leaving stage j , $y_{i,j-1}$ the vapor composition entering from the previous stage $j-1$, and y_{ij}^* the vapor composition that is in equilibrium with the liquid leaving stage j . This stage efficiency *reflects* the ratio of actual mass transfer over the mass transfer that would be accomplished by an equilibrium stage. For lack of other information, the stage efficiency is taken to be the same for all components, obtained from some empirical correlation depending on the components in the mixture.

For a binary system both component efficiencies are equal, but unfortunately this is not the case in systems with more than two components. Diffusional interaction phenomena (for example *reverse diffusion* or *osmotic diffusion*, have proven that mass transfer can occur against a gradient or in absence of a gradient (Toor, 1964). If a component diffuses against its gradient the component efficiency will be negative (since the direction of mass transfer is the opposite of that what the equilibrium model would predict), and, if it diffuses without a gradient, the components efficiency will be infinite (since the equilibrium model predicts no mass transfer). Because diffusional interactions influence the fluxes differently for each component, component efficiencies in mixtures with three or more components do not have to be

equal. In fact they can vary over a range from $-\infty$ to $+\infty$. This surprising result has been confirmed by experiment (Krishna *et al.*, 1977). For ideal and moderately ideal systems the component efficiencies are only a weak function of the composition, in contrast to nonideal systems where the opposite is true. Consequently, in the distillation of nonideal systems the concentration transients could cause large component efficiency changes that might significantly alter the simulation. Therefore, any good model must be based on diffusion calculations that include diffusional interactions. However, dynamic simulators based on the equilibrium model use Murphree efficiencies which are assumed constant and equal for all components.

Efficiencies also depend on the type of operation, as they differ in distillation and absorption operations for the same mixture at hand. Plate hydraulics (including weeping and entrainment) influence the flows on a tray. Different vapor and liquid flows result into various flow regimes of the two phases on the tray (such as spray, emulsion, or bubble flow) which each have their own transfer properties (and thus, efficiencies). Thus, transients in the tray hydraulics imply possible changes in the component efficiencies but with a constant efficiency model such effects are totally neglected.

Another assumption of the equilibrium model, thermal equilibrium, forces the liquid and vapor leaving a stage to have the same temperature. In reality, heat transfer between the two phases is limited and the separate phases have their own temperatures. The assumption of thermal equilibrium makes it difficult to model the dynamics of sections in a column that are purposely used for heat transfer, or columns where feeds are normally subcooled or superheated (such as extractive distillation or strippers/absorbers).

To eliminate the problems discussed above we need to construct a new dynamic column model which does not employ overall thermodynamic and thermal equilibrium assumptions! A nonequilibrium model was developed by Krishnamurthy and Taylor (1985a-d, 1986) (see, also, Sivasubramanian *et al.*, 1987; Powers *et al.*, 1988; Lao *et al.*, 1989, 1994; Taylor and Krishna, 1993) for steady-state simulation of separation processes. The nonequilibrium model splits the stage material and energy balances into balances for each phase, adding rate equations for the calculation of mass and energy *interphase* transfer rates. The mass transfer rates are computed through matrix routines directly from fundamental diffusion equations and mass transfer correlations. A second generation model was developed by Taylor *et al.* (1994) which incorporated the pressure as a variable. Taylor *et al.* (1992) have demonstrated application of the nonequilibrium model to industrial column operations. Since the nonequilibrium model avoids the use of tray efficiencies and includes the column hydraulics (which are very important in dynamic column simulation) it is suitable as a basis for developing a better dynamic column model.

As very few unsteady-state column data is available, dynamic simulations of columns or linked columns provide an ideal opportunity to study and analyze the dynamic behavior when no other model is available. However, it also makes it difficult to validate the results of a dynamic simulator other than by checking general trends.

1.4 Objectives

The purpose of this work has been to construct and implement dynamic equilibrium and nonequilibrium models into a dynamic column simulator. Requirements of the simulator were

- Portable implementation (Fortran)
- Easily switch between Steady-State (SS) mode and Dynamic State (DS) mode
- Contain an extensive collection of models for handling the dynamics of many different kinds of trays
- Contain a variety of models for multicomponent diffusion coefficients, mass transfer coefficients, thermodynamic properties, and physical properties. Accurate models for these properties are needed in order to use the nonequilibrium model.
- Numerically robust as well as efficient in terms of computer time and storage
- Easy to use (interactive)
- Flexible and extendible
- Graphical output

The simulator was to be used to investigate influences of different holdup models, tray layout parameters, mass transfer coefficient and diffusion models on open loop simulations. Optional were the inclusion of controllers (closed loop simulations) and the operation outside normal operation to study startup and shutdown operations. Since dynamic experimental measurements are virtually absent, no comparison with data is carried out.

Literature

P.I. Barton, C.C. Pantelides, "The Modeling and Simulation of Combined Discrete / Continuous Processes", *Proc. PSE'91 Conf.*, Montebello, Canada (1991).

J.F. Boston, H.B. Britt, "An Advanced System for the Simulation of Batch distillation Operations", *Foundation of computer-aided chemical process design*, Ed. R.S.H. Mah, W.D. Seider, New York (1981).

I.T. Cameron, C.A. Ruiz, R. Gani, "A Generalized Model for Distillation Columns II – Numerical and Computational Aspects", *Comp. Chem. Eng.*, Vol. **12**, No. 5 (1988) pp. 377–382.

J. Choe, W.L. Luyben, "Rigorous dynamic models of distillation columns", *Ind. Eng. Chem. Res.*, Vol. 26, (1987) pp. 2158–2161.

- P.E. Cuille, G.V Reklatis, "Dynamic Simulation of Multicomponent Batch Rectification with Chemical Reactions", *Comp. Chem. Eng.*, Vol. **10**, No. 4 (1986) pp. 389–398.
- G.P. Distefano, "Mathematical Modeling and Numerical Integration of Multicomponent Batch Distillation Equations", *AIChE J.*, Vol. **14** (1968) pp. 190–199.
- S.E. Gallun, C.D. Holland, "Gear's Procedure for the Simultaneous Solution of Differential and Algebraic Equations with Application in Unsteady-State Simulation", *Comp. Chem. Eng.*, Vol. **6** (1982) pp. 231.
- R. Gani, C.A. Ruiz, I.T. Cameron, "A Generalized Model for Distillation Columns I – Model Description and Applications", *Comp. Chem. Eng.*, Vol. **10**, No. 3 (1986) pp. 181–198.
- R. Gani, C.A. Ruiz, I.T. Cameron, "Studies in the Dynamics of Startup and Shutdown operations of Distillation Columns", *Proceedings of XVIII congress: The use of computers in Chemical Engineering*, CEF 87, April 26–30, Giardini Naxos (Sicily,Italy) (1987a).
- R. Gani, C.A. Ruiz, "Simulation of startup and shutdown Behavior of Distillation Operations", *I.Chem.E. Symp. Ser.*, No. 104 (1987b), pp. B39–B50.
- R. Gani, I.T. Cameron, "Extension of Dynamic Model of Distillation Columns to Steady-State Simulation", *Comp. Chem. Eng.*, Vol. **13**, No. 3 (1989) pp. 271–280.
- C.W. Gear, *Numerical Initial Value Problems in Ordinary Differential Equations*, Prentice-Hall, Inc. Englewood Cliffs, New Jersey (1971a).
- C.W. Gear, "Simultaneous Numerical Solution of Differential-Algebraic Equations", *IEEE Trans. Circuit Theory*, CT-18 (1971b) pp. 89–95.
- E.J. Henley. J.D. Seader, *Equilibrium-Stage Separation operations in Chemical Engineering*, Wiley (1981).
- P. Holl, W. Marquardt, E.D. Gilles, "DIVA – A Powerfull Tool for Dynamic Process Simulation", *Comp. Chem. Eng.*, Vol. **12** (1988) pp. 421–426.
- C.D. Holland, *Multicomponent Distillation*, Pentice Hall inc., N.J. (1981).
- C.D. Holland, A.L. Liapis, *Computer Methods for Solving Dynamic Separation Problems*, McGraw-Hill, New York (1983).
- G.M. Howard, "Unsteady-State Behaviour of Multicomponent Distillation Columns", *AIChE. J.*, Vol. **16** (1970) pp. 1023.
- C.E. Huckaba, F.P. May, F.R. Franke, "An Analysis of Transient Conditions in Continuous Distillation Operations", *Chem. Eng. Prog. Symp. Ser.*, No. 46, Vol. **59** (1963) pp. 38.
- C.E. Huckaba, F.R. Franke, F.P. May, B.T. Fairchild, G.P. Distefano, "Experimental Confirmation of a Predictive Model for Dynamic Distillation", *Chem. Eng. Prog. Symp. Ser.*, No. 55, Vol. **61** (1965) pp. 126.
- C.J. King, *Separation Processes*, McGraw-Hill, New York (1980).

- R. Krishna, H.F. Martinez, R. Sreedhar, G.L. Standart, "Murphree Efficiencies in Multicomponent Systems", *Trans. I. Chem. E.*, Vol. **55** (1977) pp. 178.
- R. Krishnamurthy, R. Taylor, "A Nonequilibrium Stage Model of Multicomponent Separation Processes. Part I: Model Description and Method of Solution", *AIChE J.*, Vol. **31**, No. 3 (1985a), pp. 449–455.
- R. Krishnamurthy, R. Taylor, "A Nonequilibrium Stage Model of Multicomponent Separation Processes. Part II: Comparison with Experiment", *AIChE J.*, Vol. **31**, No. 3 (1985b), pp. 456–465.
- R. Krishnamurthy, R. Taylor, "A Nonequilibrium Stage Model of Multicomponent Separation Processes. Part III: The Influence of Unequal Component Efficiencies in Process Design Problems", *AIChE J.*, Vol. **31**, No. 12 (1985c), pp. 1973–1985.
- R. Krishnamurthy, R. Taylor, "Simulation of Packed Distillation and Absorption Columns", *Ind. Eng. Chem. Process Des. Dev.*, Vol. **24** (1985d) pp. 513.
- R. Krishnamurthy, R. Taylor, "Absorber Simulation and Design Using a Nonequilibrium Stage Model", *Can. J. Chem. Eng.*, Vol. **64** (1986) pp. 1976.
- M. Lao, J.P. Kingsley, R. Krishnamurthy, R. Taylor, "A Nonequilibrium Stage Model of Multicomponent Separation Processes. Part VI: Simulation of Liquid-Liquid Extraction", *Chem. Eng. Commun.*, Vol. **86** (1989) pp. 73.
- M. Lao, R. Taylor, "Modeling Mass Transfer in Three Phase Distillation", *Ind. Eng. Chem. Res.*, Vol. **33** (1994) pp. 2637–2650.
- W.K. Lewis, G.L. Matheson, "Studies in Distillation: Design of Rectifying Columns for Natural and Refinery Gasoline", *Ind. Eng. Chem.*, Vol. **24**, No. 5 (1932) pp. 496–498.
- W.L. Luyben, V.S. Verneuil Jr., J.A. Gerster, "Experimental Transient Response of a Pilot-Plant Distillation Column. Part IV: Response of a Ten-Tray Column", *AIChE J.*, Vol. **10** (1964) pp. 357.
- R.S. Mah, S. Michaelson, R.W.H. Sargent, "Dynamic Behaviour of Multicomponent Multistage Systems", *Chem. Eng. Sci.*, Vol. **17** (1962) pp. 619.
- W.L. McCabe, E.W. Thiele, *Ind. Eng. Chem.*, Vol. **17** (1925) pp. 605–611.
- E.V. Murphree, *Ind. Eng. Chem.*, Vol. **17** (1925) 747–750, pp. 960–964.
- C.C. Pantelides, "SPEEDUP – Recent Advances in Process Simulation", *Comp. Chem. Eng.*, Vol. **12** (1988a) pp. 745–755.
- C.C. Pantelides, P.I. Barton, "Equation Oriented Dynamic Simulation, Current Status and Future Perspectives", *ESCAPE 2* (1993).
- J.D. Perkins, R.W.H. Sargent, "SPEEDUP – A Computer Program for Steady-State and Dynamic Simulation and Design of Chemical Processes", *AIChE Symp. Ser.*, No. 214 (1982) pp. 1–11.
- P. Piela, T.G. Epperly, K.M. Westerberg, A.W. Westerberg, "ASCEND: An Object-Oriented Computer Environment for Modeling and Analysis: The Modeling Language", *Comp. Chem. Eng.*, Vol. **15** (1991) pp. 53–72.

M. Ponchon, *Tech. Moderne*, Vol. **13**, No. 20 (1921) pp. 55.

M.F. Powers, D.J. Vickery, A. Arehole, R. Taylor, "A Nonequilibrium Stage Model of Multicomponent Separation Processes. Part V: Computational Methods for Solving the Model Equations", *Comp. Chem. Eng.*, Vol. **12**, No. 12 (1988), pp. 1229–1241.

G.J. Prokopakis, W.D. Seider, "Dynamic Simulation of Azeotropic Distillation Towers", *AIChE J.*, No. 6, Vol. **29** (1983) pp. 1017–1029.

E. Ranzi, M. Rovaglio, T. Faravelli, G. Biardi, "Role of Energy Balances in Dynamic Simulation of Multicomponent Distillation Columns", *Comp. Chem. Eng.*, Vol. **12**, No. 8, (1988) pp. 783–786.

C.A. Ruiz, I.T. Cameron, R. Gani, "A Generalized Model for Distillation Columns III – Study of Startup Operations", *Comp. Chem. Eng.*, Vol. **12**, No. 1 (1988) pp. 1–14.

R. Savarit, *Arts et Metiers*, pp. 65, 142, 178, 241, 266, 307 (1922).

J.D. Seader, "The B.C. (Before Computers) and A.D of Equilibrium Stage Operations", *Chem. Eng. Educ.*, Vol. **19**, No. 2 (1985) pp. 88–103.

M.S. Sivasubramanian, R. Taylor, R. Krishnamurthy, "A Nonequilibrium Stage Model of Multicomponent Separation Processes. Part IV: A Novel Approach to Packed Column Design", *AIChE J.*, Vol. **33**, No. 2 (1987), pp. 325–327.

R. Taylor, H.A. Kooijman, M.R. Woodman, "Industrial Applications of a Nonequilibrium Model of Distillation and Absorption Operations", *I. Chem. E. Symp. Ser.*, No. 128, Birmingham UK (1992) pp. A415–427.

R. Taylor, H.A. Kooijman, J-S. Hung, "A Second Generation Nonequilibrium Model for Computer Simulation of Multicomponent Separation Processes", *Comp. Chem. Eng.*, Vol **18**, No. 3, (1994) pp. 205–217.

R. Taylor, R. Krishna, *Multicomponent Mass Transfer*, Wiley NY (1993).

E.W. Thiele, R.L. Geddes, "Computation of Distillation Apparatus for Hydrocarbon mixtures", *Ind. Eng. Chem.*, Vol. **25** (1933) pp. 289.

H.L. Toor, "Solution of the Linearized Equations of Multicomponent Transfer", *AIChE J.*, Vol. **10** (1964) pp. 448–460.

R.C. Waggoner, C.D. Holland, "Solution of Problems Involving Conventional and Complex Distillation Columns at Unsteady-State Operation", *AIChE J.*, Vol. **11** (1965) pp. 112.

G. Wozny, L. Jeromin, "Dynamic Process Simulation in Industry", *Int. Chem. Eng.*, Vol. 34, No. 2, (1994) pp. 159–177.

Chapter 2

Steady-State Simulation of Nonequilibrium Columns

The steady-state nonequilibrium model and its equations are introduced. Extra specifications required by the nonequilibrium model in comparison with the equilibrium model are identified. A new *design mode* which enables the simultaneous design of the column layout and column simulation is explained. This design mode enables the use of the nonequilibrium model in flowsheet design calculations

2.1 The Nonequilibrium Model

A second generation nonequilibrium model was developed by Taylor and coworkers and is described in detail by Taylor *et al.* (1994). It can be used to simulate trayed columns as well as packed columns. Packed columns are simulated with stages representing a discrete integration over the packed bed. The more stages are used the better the integration, and the more accurate the results will be. A schematic diagram of a nonequilibrium stage is shown in Figure 2.1. This stage may represent one (or more than one) tray in a trayed column or a section of packing in a packed column. The vertical wavy line in the middle of the diagram represents the interface between the two phases which may be vapor and liquid (distillation), gas and liquid (absorption) or two liquids (extraction).

Figure 2.1 also serves to introduce the notation used in writing down the equations that model the behavior of this nonequilibrium stage. The flow rates of vapor and liquid phases leaving the j -th stage are denoted by V_j and L_j respectively. The mole fractions in these streams are y_{ij} and x_{ij} . The N_{ij} are the molar fluxes of species i on stage j . When multiplied by the area available for interphase mass transfer we obtain the rates of interphase mass transfer. The temperatures of the vapor and liquid phases are not assumed to be equal and we must allow for heat transfer as well as mass transfer across the

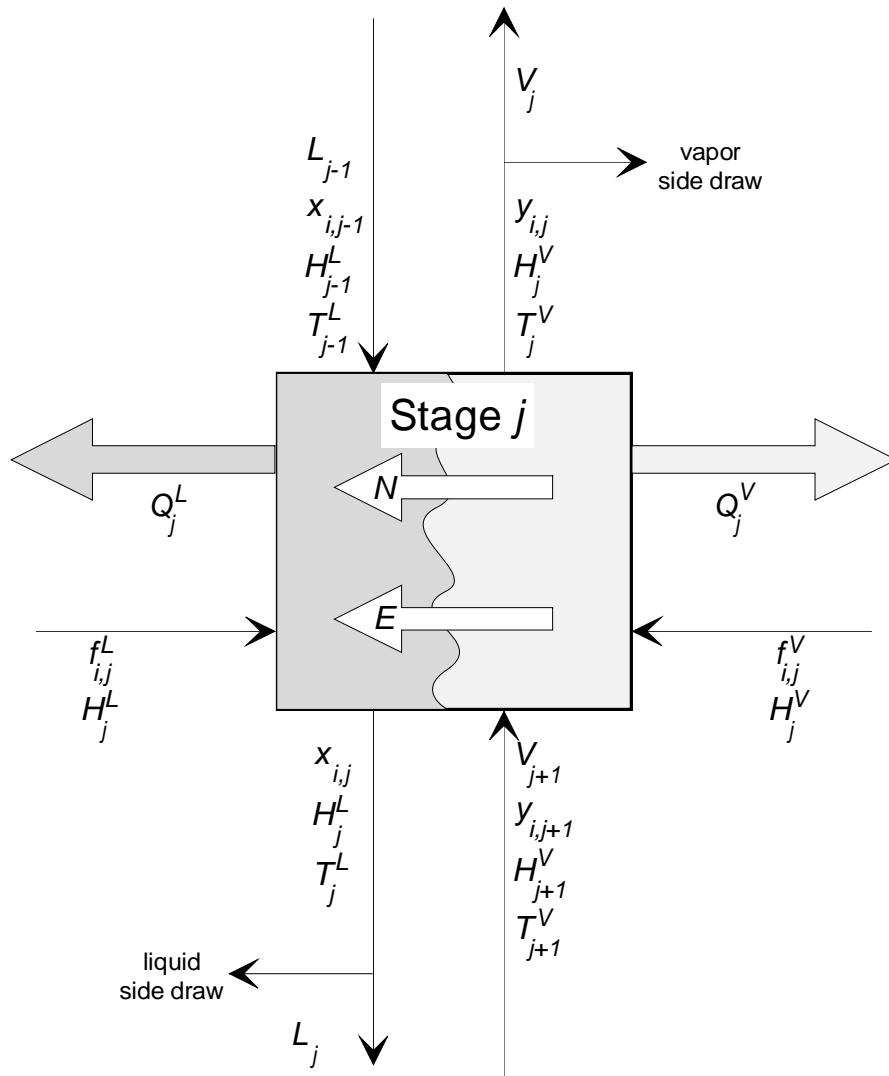


Figure 2.1: Schematic diagram of a nonequilibrium stage (Taylor and Krishna, 1993).

interface.

If Figure 2.1 represents a single tray then the term ϕ_j^L is the fractional liquid entrainment defined as the ratio of the moles of liquid entrained in the vapor phase in stage j to the moles of downflowing liquid

from stage j . Similarly, ϕ_j^V is the ratio of vapor entrained in the liquid leaving stage j (carried down to the tray below under the downcomer) to the interstage vapor flow. For packed columns, this term represents axial dispersion. Weeping in tray columns may be accounted for with a similar term. The component **(M)aterial** balance equations for each phase may be written as follows:

$$\begin{aligned} M_{ij}^V &\equiv (1 + r_j^V + \phi_j^V)V_j y_{ij} - V_{j+1} y_{i,j+1} - \phi_{j-1}^V V_{j-1} y_{i,j-1} - f_{ij}^V - \sum_{\nu=1}^n G_{ij\nu}^V + N_{ij} \\ &= 0 \quad i = 1, 2, \dots, c \end{aligned} \quad (2.1)$$

$$\begin{aligned} M_{ij}^L &\equiv (1 + r_j^L + \phi_j^L)L_j x_{ij} - L_{j-1} x_{i,j-1} - \phi_{j+1}^L L_{j+1} x_{i,j+1} - f_{ij}^L - \sum_{\nu=1}^n G_{ij\nu}^L - N_{ij} \\ &= 0 \quad i = 1, 2, \dots, c \end{aligned} \quad (2.2)$$

where $G_{ij\nu}$ is the interlinked flow rate for component i from stage ν to stage j , n is the number of total stages (trays or sections of packing), r_j is the sidestreams flowratio, and f_{ij} is the component feed rate. The last terms in Equations (2.1) and (2.2) are the mass transfer rates (in $kmol/s$). At the V/L interface we have continuity of mass and, thus, the mass transfer rates in both phases must be equal. Mass transfer from the “V” phase to the “L” phase is defined as positive.

The total material balances for the two phases are obtained by summing Equations (2.1) and (2.2) over the component index i .

$$\begin{aligned} M_{tj}^V &\equiv (1 + r_j^V + \phi_j^V)V_j - V_{j+1} - \phi_{j-1}^V V_{j-1} - F_j^V - \sum_{i=1}^c \sum_{\nu=1}^n G_{ij\nu}^V + N_{tj} \\ &= 0 \end{aligned} \quad (2.3)$$

$$\begin{aligned} M_{tj}^L &\equiv (1 + r_j^L + \phi_j^L)L_j - L_{j-1} - \phi_{j+1}^L L_{j+1} - F_j^L - \sum_{i=1}^c \sum_{\nu=1}^n G_{ij\nu}^L - N_{tj} \\ &= 0 \end{aligned} \quad (2.4)$$

F_j denotes the total feed flow rate for stage j , $F_j = \sum_{i=1}^c f_{ij}$.

Here total flow rates and mole fractions are used as independent variables and total as well as component material balances are included in the set of independent model equations. In the nonequilibrium model of Krishnamurthy and Taylor (1985) component flow rates were treated as variables.

The nonequilibrium model uses two sets of **(R)ate** equations for each stage:

$$R_{ij}^V \equiv N_{ij} - N_{ij}^V = 0 \quad i = 1, 2, \dots, c-1 \quad (2.5)$$

$$R_{ij}^L \equiv N_{ij} - N_{ij}^L = 0 \quad i = 1, 2, \dots, c-1 \quad (2.6)$$

where N_{ij} is the mass transfer rate of component i on stage j . The mass transfer rate in each phase is computed from a diffusive and a convective contribution with

$$N_{ij}^V = J_{ij}^V a_j^I + y_{ij} N_{tj} \quad (2.7)$$

$$N_{ij}^L = J_{ij}^L a_j^I + x_{ij} N_{tj} \quad (2.8)$$

where a_j^I is the total interfacial area for stage j and N_{tj} is the total rate on stage j ($N_{tj} = \sum_{i=1}^c N_{ij}$). The diffusion fluxes J are given by (in matrix form):

$$(J^V) = c_t^V [k^V] (\overline{y^V - y^I}) \quad (2.9)$$

$$(J^L) = c_t^L [k^L] (\overline{x^I - x^L}) \quad (2.10)$$

where $(\overline{y^V - y^I})$ and $(\overline{x^I - x^L})$ are the average mole fraction differences between the bulk and the interface mole fractions (Note that the *fluxes* are multiplied by the interfacial *area* to obtain mass transfer *rates*). How the average mole fraction differences are calculated depends on the selected flow model (see Chapter 3). The matrices of mass transfer coefficients, $[k]$, are calculated from

$$[k^P] = [R^P]^{-1} [\Gamma^P] \quad (2.11)$$

where $[\Gamma^P]$ is a matrix of thermodynamic factors for phase P . For systems where an activity coefficient model is used for the phase equilibrium properties the thermodynamic factor matrix Γ (order $c - 1$) is defined by

$$\Gamma_{ij} = \delta_{ij} + x_i \left(\frac{\partial \ln \gamma_i}{\partial x_j} \right)_{T,P,x_k, k \neq j=1 \dots c-1} \quad (2.12)$$

If an equation of state is used γ_i is replaced by ϕ_i . Expressions for the composition derivatives of $\ln \gamma_i$ are given by Taylor and Kooijman (1991). The rate matrix $[R]$ (order $c - 1$) is a matrix of mass transfer resistances calculated from the following formulae:

$$R_{ii}^P = \frac{z_i}{k_{ic}^P} + \sum_{k=1, k \neq i}^c \frac{z_k}{k_{ik}^P} \quad (2.13)$$

$$R_{ij}^P = -z_i \left(\frac{1}{k_{ij}^P} - \frac{1}{k_{ic}^P} \right) \quad (2.14)$$

where k_{ij}^P are binary pair mass transfer coefficients for phase P . Mass transfer coefficients, k_{ij} , are computed from empirical models (Taylor and Krishna, 1993) and multicomponent diffusion coefficients evaluated from an interpolation formula (Kooijman and Taylor, 1991). Equations (2.13) and (2.14) are suggested by the Maxwell-Stefan equations that describe mass transfer in multicomponent systems (see Taylor and Krishna, 1993). The matrix of thermodynamic factors appears because the fundamental driving force for mass transfer is the chemical potential gradient and not the mole fraction or concentration gradient. This matrix is calculated from an appropriate thermodynamic model.

The binary mass transfer coefficients are estimated from empirical correlations as functions of column internal type as well as design, operational parameters, and physical properties including the binary pair Maxwell-Stefan diffusion coefficients. Thus, the mass transfer coefficient models form the basis of the nonequilibrium model and it is possible to change the behavior of a column by selecting a different mass transfer coefficient correlation. Table 2.1 gives a summary of the correlations per type of column internals which are currently supported by our steady-state nonequilibrium model, they are described in detail by Taylor and Krishna (1993).

Note that there are c times c binary pair Maxwell-Stefan diffusion coefficients, but only $c - 1$ times $c - 1$ elements in the $[R^P]$ and $[k^P]$ matrices and, therefore, only $c - 1$ rate equations per phase. This is

Table 2.1: Available mass transfer coefficient correlations per internals type

Bubble-Cap tray	Sieve tray	Valve tray	Dumped packing	Structured packing
AIChE Hughmark	AIChE Chan-Fair Zuiderweg Harris	AIChE	Onda 68 Bravo 82 Billet 92	Bravo 85 Bravo 92 Billet 92

the result of the fact that diffusion calculations only yield relative transfer rates. We will need an extra equation that will "bootstrap" the mass transfer rates: the energy balance for the interface. Note also that, in this model, the flux correction on the mass transfer coefficients has been neglected.

The **(E)nergy** balance equations on stage j are written for each phase as follows:

$$E_j^V \equiv (1 + r_j^V + \phi_j^V)V_j H_j^V - V_{j+1} H_{j+1}^V - \phi_{j-1}^V V_{j-1} H_{j-1}^V - F_j^V H_j^{VF} - \sum_{\nu=1}^n G_{j\nu}^V H_{j\nu}^V + Q_j^V + e_j^V = 0 \quad (2.15)$$

$$E_j^L \equiv (1 + r_j^L + \phi_j^L)L_j H_j^L - L_{j-1} H_{j-1}^L - \phi_{j+1}^L L_{j+1} H_{j+1}^L - F_j^L H_j^{LF} - \sum_{\nu=1}^n G_{j\nu}^L H_{j\nu}^L + Q_j^L - e_j^L = 0 \quad (2.16)$$

where $G_{j\nu}$ is the interlink flow rate from stage ν to stage j . The last term in the left-hand-side of Equations (2.15) and (2.16), e_j , represents the energy transfer rates for the vapor and liquid phase which are defined by

$$e_j^V = a_j^I h^V (T^V - T^I) + \sum_{i=1}^c N_{ij}^V \bar{H}_{ij}^V \quad (2.17)$$

$$e_j^L = a_j^I h^L (T^I - T^L) + \sum_{i=1}^c N_{ij}^L \bar{H}_{ij}^L \quad (2.18)$$

where \bar{H}_{ij} are the partial molar enthalpies of component i for stage j . We also have continuity of the energy fluxes across the V/L interface which gives the interface energy balance:

$$E_j^I \equiv e_j^V - e_j^L = 0 \quad (2.19)$$

where h^V and h^L are the vapor and liquid heat transfer coefficients respectively, and T^V , T^I , and T^L the vapor, interface, and liquid temperatures. For the calculation of the vapor heat transfer coefficients the Chilton-Colburn analogy between mass and heat transfer is used:

$$\text{Le} = \frac{\lambda}{DC_p \rho} = \frac{\text{Sc}}{\text{Pr}} \quad (2.20)$$

$$h^V = k \rho C_p \text{Le}^{2/3} \quad (2.21)$$

For the calculation of the liquid heat transfer coefficients a penetration model is used:

$$h^L = k\rho C_p \sqrt{Le} \quad (2.22)$$

where k is the average mass transfer coefficient and D the average diffusion coefficient.

In the nonequilibrium model of Krishnamurthy and Taylor (1985) the pressure was taken to be specified on all stages, as is normally done in equilibrium model simulations. However, column pressure drop is a function of tray (or packing) type as well as the column design and column operating conditions, information that is required for or available during the solution of the nonequilibrium model equations. It was, therefore, quite straightforward to add an **hydraulic** equation to the set of independent equations for each stage and to make the pressure of each stage (tray or packed section) an unknown variable. The stage is assumed to be at mechanical equilibrium so $p_j^V = p_j^L = p_j$.

In the second generation model, the pressure of the top tray (or top of the packing) is specified along with the pressure of any condenser. The pressure of trays (or packed sections) below the topmost are calculated from the pressure of the stage above and the pressure drop on that tray (or over that packed section). If the column has a condenser (which is numbered as stage 1 here) the hydraulic equations are expressed as follows:

$$P_1 \equiv p_c - p_1 = 0 \quad (2.23)$$

$$P_2 \equiv p_{spec} - p_2 = 0 \quad (2.24)$$

$$P_j \equiv p_j - p_{j-1} - (\Delta p_{j-1}) = 0 \quad j = 3, 4, \dots, n \quad (2.25)$$

where p_c is the specified condenser pressure, p_{spec} is the specified pressure of the tray or section of packing at the top of the column, and Δp_{j-1} is the pressure drop per tray or section of packing from section/stage $j - 1$ to section/stage j . If the top stage is not a condenser, the **(H)hydraulic** equations are expressed as

$$H_1 \equiv p_{spec} - p_1 = 0 \quad (2.26)$$

$$H_j \equiv p_j - p_{j-1} - (\Delta p_{j-1}) = 0 \quad j = 2, 3, \dots, n \quad (2.27)$$

In general we may consider the pressure drop to be a function of the internal flows, the fluid densities, and equipment layout parameters.

$$\Delta p_{j-1} = f(V_{j-1}, L_{j-1}, \rho_{j-1}^V, \rho_{j-1}^L, Layout) \quad (2.28)$$

Tray pressure drop calculations consist of the addition of various contributions which can be estimated with various correlations. Bubble cap tray pressure drop calculations were given by Bolles(1963), correlations for sieve and valve trays are found in Lockett (1986) and Kister (1992). There are two types of packed column pressure drop correlations; Generalized Pressure Drop Correlations (GPDC) and more theoretically based correlations that compute the liquid holdup which make them superior in predicting the pressure drop above the loading point (> 70 % of flooding). Table 2.2 gives a summary of the correlations for each type of column internal that are implemented in our steady-state nonequilibrium model. Pressure drop can also be *fixed* to impose a known pressure profile.

Table 2.2: Pressure drop correlations per internals type

Bubble-Cap tray	Sieve tray	Valve tray	Dumped packing	Structured packing
Fixed Bolles	Fixed Lockett/ Kister	Fixed Lockett/ Kister	Fixed Ludwig 79 Leva 92 Billet 92 Stichlmair 89	Fixed Billet 92 Bravo 86 Stichlmair 89 Bravo 92

Phase **(E)quilibrium** is assumed to exist only at the interface with the mole fractions in both phases related by:

$$Q_{ij}^I \equiv K_{ij}x_{ij}^I - y_{ij}^I = 0 \quad i = 1, 2, \dots, c \quad (2.29)$$

where K_{ij} is the equilibrium ratio for component i on stage j . The K_{ij} are evaluated at the (calculated) temperature, pressure, and mole fractions at the interface.

The mole fractions must **(S)um** to unity in each phase:

$$S_j^V \equiv \sum_{i=1}^c y_{ij} - 1 = 0 \quad (2.30)$$

$$S_j^L \equiv \sum_{i=1}^c x_{ij} - 1 = 0 \quad (2.31)$$

as well as at the interface:

$$S_j^{VI} \equiv \sum_{i=1}^c y_{ij}^I - 1 = 0 \quad (2.32)$$

$$S_j^{LI} \equiv \sum_{i=1}^c x_{ij}^I - 1 = 0 \quad (2.33)$$

Table 2.3 lists the type and number of equations for the nonequilibrium model. The model consist of $5c + 6$ equations and variables, where c is the number of components. The equations are solved simultaneously using Newton's method.

Nonequilibrium and equilibrium models require many similar specifications. Feed flows and their thermal condition must be specified for both models, as must the column configuration (number of stages, feed and sidestream locations etc.). Additional specifications that are the same for both simulation models include the specification of, for example, reflux ratios or bottom product flow rates if the column is equipped with a condenser and/or a reboiler. The specification of the pressure on each stage is necessary if the pressure drop is not computed; if it is, only the top stage pressure needs be specified (the pressure of all other stages being determined from the pressure drop equations that are part of the model described above).

Table 2.3: Nonequilibrium model equations type and number

Equation	Number
Material balances	$2c + 2$
Energy balances	3
transfer Rate equations	$2c - 2$
Summations equations	2
Hydraulic equation	1
interface eQuilibrium relations	c
Total MERSHQ	$5c + 6$

If we solve the nonequilibrium model with Newton's method, we also require initial guesses for all the variables. This is done with an initial guess routine normally used for equilibrium stage simulation which uses a bottoms flowrate and reflux ratio specification and solves the column using the ideal Wilson K-value model. Temperatures of the vapor, interface, and liquid are then initialized as being equal to the temperature from this guess. Mass and energy transfer rates are initialized as zero and the interface mole fractions are set equal to the bulk mole fractions which are also provided by the initial guess. Pressure drops are initially assumed to be zero.

A nonequilibrium simulation needs the following **extra** specifications (in comparison with an equilibrium model):

- The column internals type and the layout
- Mass transfer coefficient model
- Flow model for both phases
- Entrainment and weeping models
- Pressure drop model
- Physical properties models

For the estimation of transport properties the nonequilibrium model requires the evaluation of many more physical properties (such as densities, viscosities, diffusivities, heat capacities, thermal conductivities, surface tension) which the equilibrium model does not need.

In addition, a nonequilibrium simulation cannot proceed without some knowledge of the column type and the internals layout in order to determine mass transfer coefficients, interfacial area, and pressure drop. Tray type and mechanical layout data, for example, is needed in order to calculate the mass transfer coefficients for each tray. For packed columns the packing type, size and material must be known. Column layout is specified per section of the column, where a section is represented by one or

more trays (or packed bed). Standard tray or packing layout and data can be stored on-line in libraries to be easily accessible.

For designers this restriction resulted in first simulating the column with an equilibrium model, rating the column and only then using a nonequilibrium model. If the flows in the column changed - due to different specifications or a change in the feeds - the column had to be recalculated with the equilibrium model and re-rated. Therefore, the nonequilibrium model could not be used in the design of flowsheets, where changes in the flows required a continuous re-rating of the column.

To alleviate the nonequilibrium model from this "chicken and egg" problem, a **design-mode** was developed where the rating of the column occurs simultaneously with the simulation and the only required specification is the selection of a specific internals type.

2.2 The Design Mode

For each type of internal a specific design mode routine needs to be written that will determine the column layout given a set of flowrates and physical properties on the tray or in the section of packing. However, similarities in tray- and packing-design allow combination for similar types of internals. Liquid-liquid extractors require completely different design methods, even if a similar internals layout is used as in distillation (this is due to the smaller difference in the properties of the contacting phases). Since the layout must be adapted for changes in both flowrates and properties the column layout is input as well (this facilitates the user to make specifications that the design mode will not change as far as possible).

The initial layout is determined after the flows are known from the initial guess. Each stage in the column is designed separately and independently of adjacent stages. Then, after each iteration (that is, an update of the flows) the same design routine is called for re-design. Since the flowrates are also dependent on the layout (to a smaller degree than the layout is dependent on the flowrates) it is important that the design routine is only executed if the flowrates have changed more than by a certain fraction (which can be specified). After convergence has been attained, the internals design is rationalized, making the design for each stage in a column section the same. Then the simulation is restarted with the previously converged answer as starting point. The design method provides a complete design of any trayed or packed section in the column. In this manner trayed and packed sections can be freely mixed in a column simulation/design.

Different design methods can be employed:

- Fraction of flooding; this is the standard design method for trays, we have employed a modified version of the method published by Barnicki and Davis (1989).
- Pressure drop; this is the usual design method for packed columns, but is very useful as well for tray design with pressure drop constraints.

Table 2.4: Tray layout data

General (sieve) tray layout data:	
Column diameter	Active area
Number of flow passes	Total hole area
Tray spacing	Downcomer area
Liquid flow path length	Weir length
Hole diameter	Weir height
Hole pitch	Deck thickness
Downcomer clearance	
Additional data for bubble caps:	
Cap diameter	Slot area
Slot height	Riser area
Skirt clearance	Annual area
Additional data for valves:	
Closed Loss K	Open Loss K
Eddy Loss C	Ratio Valve Legs
Valve Density	Valve Thickness
Fraction Heavy Valves	Heavy Valve Thickness

The methods generate a column-design that might not be optimal from an engineers viewpoint. They must be seen as starting points for the actual design layouts. Also, the design does not include constructional calculations to determine tray support constructions or thicknesses of trays or the column. Design mode is automatically triggered if the column diameter is not specified. Other layout parameters can be specified but they may be changed by the design routine. Each of these methods behaves differently and they are discussed in more detail below. An additional and very important de-rating factor is the system factor (SF). It represents the uncertainty in design correlations with regard to phenomena which are currently still not properly modeled, such as foaming.

Tray layout parameters that specify a complete design (for the calculation of mass transfer coefficients and pressure drops) are shown in Table 2.4. For packings only the column diameter and bed height are design parameters, other parameters are fixed with the selection of the type of packing (such as void fraction, nominal packing diameter, etc.). The packed bed height must be specified since it determines the desired separation and the capacity.

2.2.1 Tray Design: Fraction of flooding

The first task in this approach to tray design is to assign all layout parameters to consistent values corresponding to the required capacity defined by the fraction of flooding and current flowrates. These defaults function as starting points for subsequent designs.

The initial free area ratio is taken to be 15 % of the active area. The active area is determined with capacity factor calculation with internals specific methods (for sieve and bubble-cap trays the default is Fair's correlation by Ogboja and Kuye (19), and the Glitsch method for valve trays). The tray spacing is initially set to the default value (of $0.5m$) and the downcomer area is calculated according the Glitsch manual (limited by a minimum time residence check). From the combined areas the column diameter is computed. The number of liquid passes on a tray is initially set by the column diameter; under $5ft$ one pass, under $8ft$ two, $10ft$ three, under $13ft$ four, else five passes. With the number of passes and the column diameter the total weir length is computed. Once the weir length is determined the liquid weir load is checked, if too high the number of passes is incremented and a new weir length is evaluated until the weir load is below a specified maximum.

Initial weir height is taken as 2", but limited to a maximum of 15 % of the tray spacing. For notched or serrated weirs the notch depth is a third of the weir height. For serrated weirs the angle of serration is 45 degrees. Circular weirs have diameters 0.9 times the weir length. Hole diameter is set to $3/16$ " for sieve trays and tray thickness 0.43 times the hole diameter (or $1/10$ "). The hole pitch is computed from the free area ratio and hole diameter according to a triangular pitch. The default downcomer clearance is 1.5" but is limited by the maximum allowed downcomer velocity according to the Glitch method de-rated with the system factor. The clearance is set to be at least half an inch lower than the weir height to maintain a positive liquid seal but is limited to a minimum of half an inch.

For bubble-cap trays the cap diameter is 3" for column diameters below 4.5 ft and 4" for above. The hole diameter can vary between 60 % to 71 % of the cap diameter, and default taken as 70 %. Default skirt clearance is 1" with minimum of 0.5" and maximum of 1.5". slot height can vary in between 0.5" and 1.5", default 1" for cap diameters below 3.5" and 1.25" for larger cap diameters. The pitch can vary from 1.25" to half the flow path length (minimum number of rows is two), default set to 1.25".

Valve trays are initialized to be Venturi orifice uncaged, carbon steel valves of 3 mm thick with 3 legs (see Kister, 1992, p312). The hole diameter is 1" for column smaller than 4.5 ft, otherwise 2". No double weight valves are present.

The second task in the fraction of flooding method consists of finding the proper free area ratio ($\beta = A_h/A_b = \text{hole area} / \text{active area}$) so that no weeping occurs. This ratio can vary between a minimum of 5% (for stable operation) and a maximum of 20%. To test whether weeping occurs, we use the correlation by Lockett and Banik (1984): $Fr_{hole} > 2/3$. The method requires all liquid heights to be evaluated at weep rate conditions. This task is ignored for bubble-cap trays. The weep test is done at weeping conditions, with a weep factor at 60 % (this can be changed). Calculating liquid heights is done by adding various contributions with correlations from Lockett (1986) and Kister (1992), see Appendix A. If weeping occurs at the lower bound for the free area ratio, a flag is set for the final task to adapt the design.

The final task consists of evaluating all liquid heights at normal conditions and to do a number of checks:

- vapor distribution (for bubble-caps),

- weeping (for sieve/valve trays),
- hydraulic flooding,
- excessive liquid entrainment,
- froth height limit, and
- excessive pressure drop

If a check fails the design is adapted to correct the problem, according to the adjustments shown in Table 2.5 after which new areas are calculated with capacity correlations. Part of this task is also to keep the layout parameters that are adjusted within certain lower and upper bounds to maintain a proper tray design. Finally the number of iterations for the design method is checked against a maximum (default 30) to prevent a continuous loop.

The adjustment factors f_1 , f_2 , and f_3 are percentual in/decrements, normally set at 5, 2, and 1 %. These factors – together with all the default, lower, and upper settings that are used in the design routine – are stored in a “design file” that can be tailored to handle specific kinds of designs and columns. This allows the selection of different methods for capacity and hydrodynamic calculations as well. Also the fraction that the flows need to change before a re-design is issued can be changed in this manner together with other design criteria.

2.2.2 Packing Design: Fraction of flooding

For packed columns only the column diameter is a design parameter to be evaluated. Default packing data are used for all packing parameters that are not specified; values of 1” inch metal Pall rings for random packed sections and of Koch Flexipack 2 (316ss) for structured sections.

To determine the packed column diameter, the diameter that gives rise to the flooding pressure drop (as specified) is computed using the selected pressure drop model. The resulting diameter is corrected for the fraction of flooding and the system factor:

$$D_c = \frac{D_{c,flood}}{\sqrt{FF SF}} \quad (2.34)$$

If no pressure drop model is selected the Leva (1992) model is selected (which is only a function of the packing factor). If no pressure drop at flood is specified, it is estimated with Kister’s correlation (1992) (which is only a function of the packing factor). Thus, as long as the packing factor is known, this method will not fail.

Table 2.5: Tray design checks and adjustments

Problem	Test	Adjustments
Bubble cap vapor distribution	$h_{lg}/h_d > 0.5$	$p + f_1$, $h_{skirt} + f_2$, $h_{slot} + f_3$, $d_h - f_3$
Weeping	$Fr_h/(2/3) < 1 - f_a$ $f_{ree} < 0.05$ $A_b < A_{bf}$: else:	$A_b = A_{bf}$ $W_f + f_1$ $A_b - f_1$ $d_h - f_3$ $h_w - f_3$ $t_v + f_2$ (vt)
Hydrodynamic (downcomer) flooding)	$T_s < h_{db}/FF$	$T_s + f_1$ $A_d + f_1$ $h_w + f_2$ $h_c + f_3$
Excessive liquid entrainment		$A_b + f_1$ $T_s + f_1$ $d_h - f_2$ $h_w - f_3$
Froth height limit	$h_f > 0.75T_s$	$A_b + f_1$ $T_s + f_2$ $h_w - f_3$
Excessive pressure drop	$g\rho h_{wt} > \Delta p_{max}$	$A_b + f_1$ $h_w - f_1$ $d_h + f_2$ $p + f_1$ (bc) $h_{skirt} + f_2$ (bc) $h_{slot} + f_3$ (bc)
Excessive vapor entrainment		$A_d + f_1$

2.2.3 Pressure drop

Tray design on pressure drop works as discussed above but with a default fraction of flooding of 75 %. However, the specified pressure drop functions as a maximum allowed pressure drop per tray. No adjustment is done if the pressure drop is below this specified pressure drop.

Packing design automatically finds the diameter resulting in the specified pressure drop (with the selected pressure drop model). This is done by using a linear search technique as the different packing pressure drop correlations can behave quite irregularly. The maximum allowed pressure drop is the flooding pressure drop as specified or computed from Kister's correlation and the packing factor. If the pressure drop is specified to be very low the column diameter might converge to unrealistic diameters. A zero or larger than flooding pressure drop specification results in a 70 % fraction of flooding design.

Symbol List

a_d	Interfacial area density (m^2/m^3)
a^I	Interfacial area (m^2)
A_h	Hole area (m^2)
A_b, A_{bub}	Bubbling area (m^2)
A_d	Downcomer area (m^2)
c	Number of components, Molar concentration ($kmol/m^3$)
d_h	Hole diameter (m)
D	Binary diffusivity coefficient (m^2/s)
D_c	Column diameter (m)
D_e	Eddy dispersion coefficient (m^2/s)
e	Energy transfer rate (J/s)
f_{ij}	Component i feed flow to stage j ($kmol/s$)
f_1, f_2, f_3	Design adjustment factors
F_j	Total feed flow rate to stage j ($kmol/s$)
F_p	Packing factor ($1/m$)
F_s	F factor $F_s = U_v \sqrt{\rho_V}$ ($kg^{0.5}/m^{0.5}s$)
FF	Fraction of flooding
FP	Flow parameter $FP = M_L/M_V \sqrt{\rho_V^V/\rho_L^L}$
Fr	Froude number
g	Gravitational constant, 9.81 (m/s^2)
G	Interlinked flow rate ($kmol/s$)
h	Heat transfer coefficient ($J/m^2 K s$)
h_c	Clearance height under downcomer (m)
h_{cl}	Clear liquid height (m)

h_d	Dry tray pressure drop height (m)
h_{db}	Downcomer backup liquid height (m)
h_f	Froth height (m)
h_i	Liquid height at tray inlet (m)
h_{lg}	Liquid gradient pressure drop height (m)
h_l, h_L	Liquid pressure drop height (m)
h_{ow}	Height of liquid over weir (m)
h_r	Residual pressure drop liquid height (m)
h_{wt}	Wet tray pressure drop liquid height (m)
h_w	Weir height (m)
h_{udc}	Liquid height pressure loss under downcomer (m)
H	Molar enthalpy ($J/kmol$)
\bar{H}_i	Partial molar enthalpy of component i ($J/kmol$)
J	Molar diffusion flux ($kmol/m^2s$)
k	Binary mass transfer coefficient (m/s)
K_i	K-value or equilibrium ratio component i : $K_i = y_i/x_i$
L	Liquid flow rate ($kmol/s$)
Le	Lewis number ($Le = Sc/Pr$)
M	Mass flow rate (kg/s)
N	Mass transfer rate ($kmol/s$)
n	Number of stages
p	Hole pitch (m), Pressure (Pa)
Δp	Pressure drop (Pa)
ΔP_{max}	Maximum design pressure drop ($Pa/tray$ or Pa/m)
Pr	Prandtl number
Q	Heat input (J/s)
Q_L	Volumetric flow over the weir (m^3/s)
r	Ratio sidestream to internal flow
$[R]$	Matrix defined by (2.13) and (2.14)
Sc	Schmidt number
SF	System derating factor
t	Residence time (s)
t_v	Valve thickness (m)
T	Temperature (K)
T_s	Tray spacing (m)
V	Vapor flow rate ($kmol/s$)
We	Weber number
W_l	Weir length (m)
x	Liquid mole fraction
y	Vapor mole fraction
z	Mole fraction

Greek:

α	Fraction liquid in froth
β	Fractional free area $\beta = A_h/A_b$,
ϕ	Fractional entrainment
ρ	Density (kg/m^3)
σ	Surface tension (N/m)
η	Viscosity ($Pa\ s$)
$[\Gamma]$	Thermodynamic matrix
λ	Heat conductivity ($W/m/K$)

Superscripts:

I	Interfacial
L	Liquid
P	Phase P
V	Vapor

Subscripts:

$flood$	at flooding conditions
i	component i
j	stage j , component j
$spec$	specified
t	total
ν	from interlinking stage ν

References

P.E. Barker, M.F. Self, "The evaluation of Liquid Mixing Effects on a Sieve Plate using Unsteady and Steady-State Tracer Techniques", *Chem. Eng. Sci.*, Vol. **17** (1962) pp. 541.

S.D. Barnicki, J.F. Davis, "Designing Sieve-Tray Columns, Part 1: Tray Design", *Chem. Engng.*, Vol. **96**, No. 10, (1989) pp. 140–146.

S.D. Barnicki, J.F. Davis, "Designing Sieve-Tray Columns, Part 2: Column Design and Verification", *Chem. Engng.*, November, pp. 202–212 (1989).

W.L. Bolles, in B.D. Smith, *Design of Equilibrium Stage Processes*, Chap. 14, McGraw-Hill (1963).

F. Kastanek, "Efficiencies of Different Types of Distillation Plate", *Coll. Czech. Chem. Comm.*, Vol. **35** (1970) pp. 1170.

H.Z. Kister, *Distillation Design*, McGraw-Hill, New York (1992).

G.F. Klein, *Chem. Engng*, May 3, 81 (1982).

H.A. Kooijman, R. Taylor, "On the Estimation of Diffusion Coefficients in Multicomponent Liquid Systems", *Ind. Eng. Chem. Res.*, Vol **30**, No. 6, (1991) pp. 1217–1222.

R. Krishnamurthy, R. Taylor, "A Nonequilibrium Stage Model of Multicomponent Separation Processes. Part I: Model Description and Method of Solution", *AIChE J.*, Vol. **31**, No. 3 (1985), pp. 449–455.

M. Leva, "Reconsider Packed-Tower Pressure-Drop correlations", *Chem. Eng. Prog.* January, 65 (1992).

M.J. Lockett, *Distillation Tray Fundamentals*, Cambridge University Press (1986).

M.J. Lockett, S. Banik, "Weeping from Sieve Trays", AIChE Meeting, San Francisco, Nov. (1984).

O. Ogboja, A. Kuye, "A procedure for the design and optimisation of sieve trays", *Trans. I. Chem. E.*, Vol. 68, Part A, Sept. (1990) pp. 445-452.

R.H. Perry, D. Green, *Perry's Chemical Engineering Handbook*, 6th edition, section 18, Liquid-Gas System, 18-8 – 18-12 (1984).

B.D. Smith, *Design of Equilibrium Staged Processes*, McGraw-Hill, New York (1963)

J. Stichlmair, A. Mersmann, "Dimensioning Plate Columns for Absorption and Rectification", *Chem. Ing. Tech.*, Vol. **45**, No. 5 (1978) pp. 242.

R. Taylor, H.A. Kooijman, "Composition derivatives of Activity Models (for the estimation of Thermodynamic Factors in Diffusion)", *Chem. Eng. Comm.*, Vol. **102** (1991) pp. 87–106.

R. Taylor, H.A. Kooijman, J-S. Hung, "A second generation nonequilibrium model for computer simulation of multicomponent separation processes", *Comput. Chem. Engng.*, Vol. **18**, No. 3, pp. 205–217 (1994).

R. Taylor, R. Krishna, *Multicomponent Mass Transfer*, Wiley, New York (1993).

Chapter 3

Flow Models

Mass transfer models are developed that account for cross flow effects on large distillation trays while avoiding the pitfalls that can strike while employing overall mass transfer coefficients in the calculation of interphase mass transfer rates. New plug and dispersion flow models for the nonequilibrium column model are proposed and found to predict tray efficiencies in general agreement with FRI experimental data on large scale equipment. Several methods of evaluating binary mass transfer coefficients in distillation have been evaluated. Of the methods tested, that of Chan and Fair (1984) provides the best predictions of column performance.

Additional evidence that the Maxwell-Stefan equations should be used in the calculation of mass transfer rates in distillation is provided by comparing the predictions of the nonequilibrium model with the new flow and mass transfer models with a simpler model based on all components having an equal facility for mass transfer. Column designs obtained with the simple model can be very different (in terms of numbers of stages, optimal feed, sidestream and controller locations) from those obtained with the more rigorous approach.

3.1 Mass Transfer Modeling Inconsistencies

Consider transport across the gas/vapor - liquid interface. We shall denote the two bulk phases by “L” and “V” and the interface by “I”. Though the analysis below is developed for liquid-vapor transport the formalism is generally valid for all two-phase systems. Therefore, what follows applies equally to distillation, stripping, and absorption operations.

At the V/L interface we have continuity of the molar fluxes N_i^V and N_i^L , which include both diffusive

and convective contributions

$$N_i^V = J_i^V + y_i N_t^V = N_i = J_i^L + x_i N_t^L = N_i^L \quad (3.1)$$

where the diffusion fluxes J are given by

$$(J^V) = c_t^V [k^V] (y^V - y^I) \quad (3.2)$$

$$(J^L) = c_t^L [k^L] (x^I - x^L) \quad (3.3)$$

and we consider transfer from the “V” phase to the “L” phase as leading to a positive flux. The matrices of mass transfer coefficients are calculated with (2.11) from the $[\Gamma]$ (2.12) and $[R]$ matrices (2.13 and 2.14). The binary mass transfer coefficients for $[R]$ are estimated from empirical correlations as functions of column design and operational parameters and physical properties including the binary pair Maxwell-Stefan diffusion coefficients.

We also have continuity of the energy fluxes across the V/L interface

$$h^V (T^V - T^I) + \sum_{i=1}^c N_i^V \bar{H}_i^V = h^L (T^I - T^L) + \sum_{i=1}^c N_i^L \bar{H}_i^L \quad (3.4)$$

Correction factors that account for the effect of finite rates of mass transfer on both the mass and heat transfer rate equations have been ignored in writing the above expressions; our experience is that their influence is negligible in the type of operations considered here. To complete the model of interphase transport at a point, we assume equilibrium prevails at the interface and relate the interface compositions through the equilibrium relations.

Krishnamurthy and Taylor (1985) used a mixed flow model to represent the flow patterns on a cross-flow distillation tray. This means that the rates of mass transfer can be calculated directly from equations (3.1-3.4) with the bulk compositions and temperatures equal to those of the streams leaving the tray. This is the simplest possible model of a cross-flow tray but it must be said that, for all but some small laboratory and pilot scale columns, it is not a particularly accurate reflection of the true flow patterns on a real distillation tray. The mixed flow model predicts tray efficiencies that are much lower than they should be as shown in Figure 3.1 where we plot the Murphree tray efficiencies for a depropanizer operating at a pressure of 15 atm. Column design parameters are provided in Table 3.1. Efficiencies closer to, or even exceeding 100% would be expected for this sort of column. It must be emphasized that the nonequilibrium model does not use efficiencies; Figure 3.1 is created using efficiencies that are calculated from the results of a simulation. The reason for the low efficiencies is that in the mixed flow model the composition differences between the streams leaving a tray (the ones used in the calculation of the mass transfer rates) are the lowest on the tray.

A better (although still not perfect) description of the flow patterns on a distillation tray is to assume that the vapor rises in plug flow through a locally well-mixed liquid and that the liquid traverses the tray also in plug flow. These two assumptions are the key to the development of some tray efficiency prediction methods (see AIChE, 1958; Lockett, 1986). Other methods are based on a dispersion model for the liquid phase (Lockett, 1986).

Table 3.1: Column Design Parameters for Depropanizer

Stages	2-10	11-24
Sieve plate material	316SS	316SS
Column Diameter (m)	5.07	7.15
Total tray area (m^2)	20.2	40.2
Number of passes	5	5
Tray spacing (m)	0.5	0.5
Flow path length (m)	0.862	1.19
Active area (m^2)	16.5	31.5
Total hole area (m^2)	0.932	1.57
Total downcomer area (m^2)	1.81	4.25
Hole diameter (mm)	4.76	4.35
Hole pitch (cm)	1.90	1.85
Total weir length (m)	19.1	26.5
Weir height (cm)	5.08	4.64
Downcomer clearance (cm)	4.58	3.37
Tray thickness (mm)	2.54	2.54

All such developments, whether they be for binary systems or for multicomponent ones, are based on the well-known addition of resistances formula for the *overall* mass transfer coefficients. For multicomponent systems (see Toor, 1964; Taylor and Krishna, 1993)

$$(J^V) = c_t^V [K^{OV}] (y^V - y^*) \quad (3.5)$$

where (y^*) is the vector of mole fractions of a vapor in equilibrium with the *bulk* liquid and $[K^{OV}]$ is the matrix of overall mass transfer coefficients.

$$[K^{OV}]^{-1} = [R^{OV}] = [k^V]^{-1} + \frac{c_t^L}{c_t^V} [M] [k^L]^{-1} \quad (3.6)$$

The matrix $[M]$ is given by

$$[M] = \partial y_i^I / \partial x_j^I = [K] [\Gamma^L] \quad (3.7)$$

where $[K]$ is a matrix with the equilibrium ratios (K -values) on the main diagonal and zeroes everywhere else.

These relations were *not* used by Krishnamurthy and Taylor (1985) in their development of a nonequilibrium model; it is, however, straightforward to do so. The vapor phase diffusion fluxes J are calculated from (3.2) with $[K^{OV}]$ substituted for $[k^V]$ and the liquid phase rate equations are omitted. The equilibrium equations remain but use the bulk liquid mole fractions and the equilibrium mole fractions y^* .

There are, however, several assumptions built into equation (3.6) that limit its usefulness. The most important limitation is that the total molar flux must be zero. This assumption, which is common in the analysis of distillation operations, rests on two other assumptions:

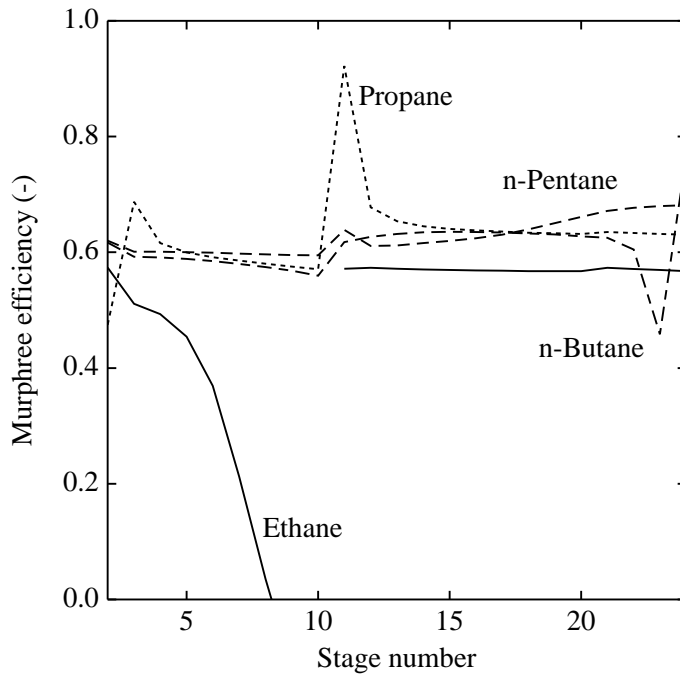


Figure 3.1: Murphree efficiencies for a depropanizer predicted by a nonequilibrium model assuming both vapor and liquid phases are completely mixed.

1. the differences between the partial molar enthalpies of vapor and liquid phases (essentially the latent heats of vaporization) must be the same for all components.
2. that there is no sensible heat transfer between the phases (see chapter 11 of Taylor and Krishna (1993) for a more detailed discussion).

Unequal latent heats can be accounted for quite easily by including the bootstrap matrices in the expression for the overall mass transfer coefficients (chapter 7 of Taylor and Krishna, 1993). However, no similar expression for the matrix of overall mass transfer coefficients can be derived if we retain the sensible heat transfer terms. We have encountered situations using equations (3.4), (3.5) and (3.6) where the heaviest component transfers from the liquid to the vapor phases when, in fact, exactly the reverse should take place. A graphic demonstration of this “phenomenon” can be seen in Figure 3.2 which shows the liquid phase mole fractions for the depropanizer used earlier. Note that the mole fraction of *n*-pentane actually decreases as the liquid approaches the feed tray. Figure 3.3 shows that the reason for this is that the mass transfer rate of *n*-pentane is negative for several trays above the feed, indicating that this particular component is being vaporized when, as the heaviest component in a chemically simple system, it should be condensing. In fact, the mole fraction of *n*-pentane on all the trays above the feed is much too high.

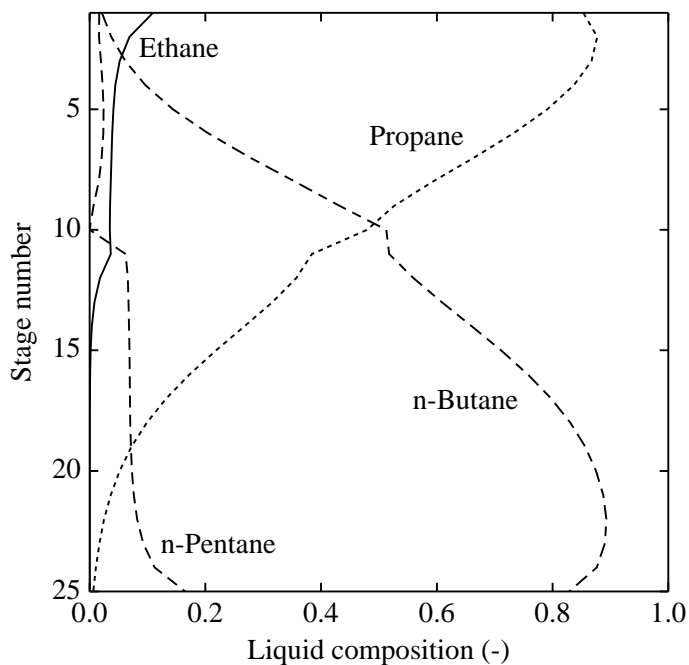


Figure 3.2: Liquid composition profiles for a depropanizer predicted by a nonequilibrium model with the molar fluxes calculated using overall mass transfer coefficients and the energy balance includes the sensible heat transfer terms.

The incorrect prediction of the *direction* of mass transfer for *n*-pentane has nothing to do with diffusional interaction effects modeled through use of the Maxwell-Stefan equations. The physical properties of the components in this system are sufficiently similar that multicomponent diffusional interactions can be discounted as an explanation for this problem. The situation occurs because we have created an inconsistent model in which mass transfer rates are evaluated using the overall mass transfer coefficients which pay no heed to sensible heat transfer together with the interfacial energy balance with the sensible heat terms included. Since the total flux in most distillations is almost always very small (but not zero), the sensible heat term is bound to be important since the energy balance involves the subtraction of two small numbers. Unfortunately, to force equimolar overflow by making the latent heats equal and the vapor, liquid, and interface have the same temperature (thereby making the sensible heat terms fall out of the model equations) necessarily leads to liquids that are (slightly) superheated and to vapors that are subcooled, possibly by significant amounts. Neither condition is likely to be encountered on every tray of a distillation column even though it can occur in some cases. Further, we cannot use this method for gas absorption where large temperature differences and significant departures from saturation are the order of the day.

Equation (3.5) serves as the starting point for the development of point (and tray) efficiencies in multi-component distillation and in the modeling of mass transfer in continuous contact devices (see chapters

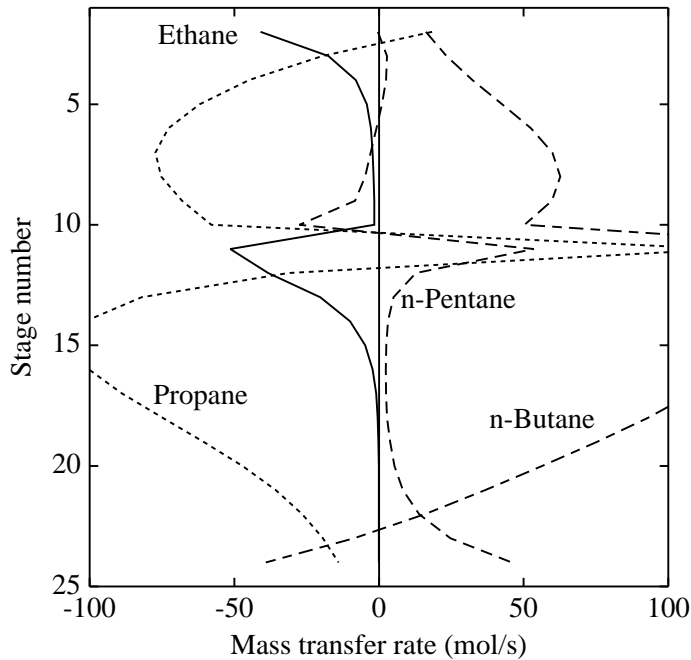


Figure 3.3: Interphase mass transfer rates for the depropanizer for the same combination of models used in Figure 3.2.

12 and 13 of Taylor and Krishna, 1993, Toor, 1964). The key assumptions are that the matrix of overall mass transfer coefficients can be considered constant and that the equilibrium vapor composition, y^* , varies only as the bulk liquid composition changes as it flows across the tray. However, this does not eliminate the inconsistencies noted above.

The same assumptions can be used to derive expressions for the average mass transfer rates (rather than the tray efficiency) for use in a nonequilibrium model. Taylor and Krishna (1993) give the expressions for a model based on plug flow of vapor through a well mixed liquid. This does not help either.

We are faced with a problem. If we ignore the sensible heat transfer terms, we may use the overall mass transfer coefficients (corrected only for unequal latent heats) but will suffer erroneous predictions of the bulk phase temperatures. If we include the sensible heat transfer term in the energy balance but omit its influence in the formula for the overall mass transfer coefficients (as we must) we run the much more serious risk of predicting the wrong *direction* of mass transfer for some components. On the other hand, the mixed flow model of tray hydrodynamics, which has none of these inconsistencies because the overall mass transfer coefficients are not needed, clearly is an inadequate representation of the flows on large trays leading to poor predictions of the tray efficiency. In an attempt to account for composition changes over the flow path Krishnamurthy and Taylor (1985) used arithmetic or logarithmic averages of the entering and leaving mole fractions. In this case predicted efficiencies *may* be larger than 100%.

However, although good results for tray columns can be obtained using this averaging procedure, it is fundamentally wrong.

A better model is needed which avoids as many of these inconsistencies as possible. Thus, one of the objectives of this paper is to develop methods of estimating the mass transfer rates on a cross flow distillation tray that do not use overall mass transfer coefficients. We do this by modeling the vapor and liquid phase mass transport processes independently. In the next section we develop the model for the vapor phase based on the assumption that the vapor rises in plug flow through the liquid phase. After this we develop plug flow and dispersion flow models for the liquid phase. The predictions of tray efficiencies obtained with the various models are compared to the methods we used before and to experimental data of Yanagi and Sakata (1979, 1981, 1982) in order to see if the predicted efficiencies are reasonable.

One of the other questions we shall address in this paper is to ask if there any significant differences between column simulation results obtained using the Maxwell-Stefan formulation for the mass transfer rates compared to a simpler approach that neglects interaction effects based on the assumptions that the binary Maxwell-Stefan diffusion coefficients in each phase may be considered equal (at some average value) and that the matrix of thermodynamic factors may be ignored. A related issue we shall investigate is what correlation for the binary (Maxwell-Stefan) mass transfer coefficients (of several that have been published) provides the “best” predictions of column performance.

3.2 Flow Models

In this section we develop flow models for cross flow distillation trays. We begin by developing the equations for plug flow in the vapor phase. We then turn our attention to the liquid phase and develop both plug flow and axial dispersion models.

3.2.1 Vapor Flow Model

As is commonly done in models of mass transfer on distillation trays we shall assume that the vapor rises in plug flow through the liquid. If v_i represents the molar flow rate of component i in the vapor phase, $V = \sum v_i$ the total vapor flow rate, a the interfacial area per unit volume of froth, h_f the froth height, and A_b the active bubbling area, then the component material balances for the vapor phase may be written as:

$$\frac{dv_i}{dh} = -N_i a A_b \quad (3.8)$$

where N_i is the molar flux of species i across the vapor-liquid interface. Summation of the component material balances gives

$$\frac{dV}{dh} = -N_t a A_b \quad (3.9)$$

where N_t is the total molar flux. Substituting $N_i = J_i^V + y_i N_t$ and writing $v_i = y_i V$ results in

$$V \frac{dy_i}{dh} + y_i \frac{dV}{dh} = -J_i^V a A_b - y_i N_t a A_b \quad (3.10)$$

The right members on both sides cancel each other and we obtain

$$V \frac{dy_i}{dh} = -J_i^V a A_b \quad (3.11)$$

In order to proceed further we need a model for the diffusion fluxes. In conventional treatments of distillation we use equation (3.5) and assume that the matrix of overall mass transfer coefficients and the equilibrium composition, y^* , is constant over the froth height. The assumption of constant y^* is equivalent to assuming the liquid is well mixed vertically and that the vapor-liquid equilibria may be adequately by a linear equation. For reasons explained above we do not want to use overall mass transfer coefficients. On the other hand we would like an analytical solution since numerical approximations to the above differential equations will dramatically increase the computational cost of this kind of simulation to the point where it might not be practical. We shall continue using equation (3.2) for the vapor phase diffusion fluxes and make the assumptions that the matrix of vapor phase mass transfer coefficients may be considered constant and that the interface composition, y^I , also may be assumed constant over the froth height. If the resistance to mass transfer is confined entirely to the vapor phase (an assumption often made in distillation calculations but one that is not always justifiable then our assumptions of constant $[k^V]$ and y^I are equivalent to the conventional assumptions of constant $[K^{OV}]$ and y^* . This gives us hope that our revised set of assumptions will provide acceptable results.

With the diffusion fluxes given by $(J^V) = c_t^V [k^V](Y)$ where the mole fraction differences are $(Y) = (y^V) - (y^I)$, we obtain

$$V \frac{d(Y)}{dh} = -c_t^V [k^V](Y) a A_b \quad (3.12)$$

With the above assumptions and the additional one that interfacial area per unit volume (a) is constant we may integrate (3.12) from $h = 0$ and $(Y) = (Y_{in})$ up to a height h and mole fraction difference (Y) :

$$(Y) = \exp \left[-\frac{c_t^V [k^V] a A_b h}{V} \right] (Y_{in}) = \exp[-\zeta N^V] (Y_{in}) \quad (3.13)$$

where $[N^V]$ is the number of transfer units for the vapor phase, and ζ is a dimensionless height h/h_f . The mass transfer coefficient matrix, $[k^V]$, is evaluated at the bulk compositions leaving the tray. The relation With (3.13) we relate the entering and leaving mole fraction differences:

$$(Y_{out}) = \exp[-N^V] (Y_{in}) \quad (3.14)$$

The average diffusion fluxes (\bar{J}^V) can be found from

$$(\bar{J}^V) = c_t^V [k^V] (\bar{Y}) \quad (3.15)$$

where (\bar{Y}) is the average mole fraction difference, given by

$$(\bar{Y}) = \int_0^1 (Y(\zeta)) d\zeta = [\exp[-N^V] - [I]] [-N^V]^{-1} (Y_{in}) = \Omega [-N^V] (Y_{out}) \quad (3.16)$$

$\Omega[M]$ is a matrix function defined as

$$\Omega[M] = [\exp[M] - [I]][M]^{-1}[\exp[M]]^{-1} = [\exp[-M] - [I]][-M]^{-1} \quad (3.17)$$

Finally, the average molar fluxes can be computed with

$$(\bar{N}^V) = (\bar{J}^V)aA_b + \bar{N}_t(\bar{y}^V) = (\bar{J}^V)aA_b + \bar{N}_t((y^I) + (\bar{Y})) \quad (3.18)$$

where it was necessary to neglect the covariance term $\overline{((N_t - \bar{N}_t)(y^V - \bar{y}^V))}$, anticipating that this term is negligible (because the total flux usually is very small, at least in distillation operations). The molar fluxes cannot be computed without this simplification. The average mass transfer rates are obtained by multiplying the above expression by $aA_b h_f$.

Figure 3.4 shows the efficiency profiles for our depropanizer calculated assuming the vapor passes in plug flow through a completely mixed liquid phase. Comparison with Figure 3.1 shows that the efficiencies are substantially higher than they were when we assumed both phases were completely mixed. However, we have not yet taken into account the effects of cross flow of the liquid.

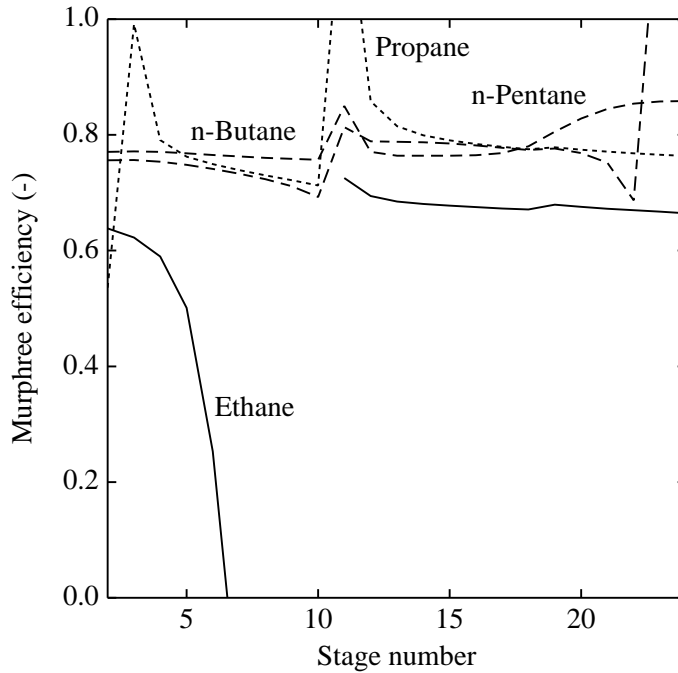


Figure 3.4: Murphree efficiencies for a depropanizer predicted by a nonequilibrium model assuming the vapor rises in plug flow through a well-mixed liquid phase.

3.2.2 Liquid Plug Flow Model

If we assume that the liquid flows across the tray in plug flow then we may derive the following expression for the mole fraction change in the liquid

$$L \frac{d(X)}{dz} = (J^L) a W h_f \quad (3.19)$$

where W is the weir length. We use equation (3.3) for the liquid phase diffusion fluxes $(J^L) = -c_t^L [k^L](X)$ where $(X) = (x_i^L) - (x_i^I)$ and obtain

$$L \frac{d(X)}{dz} = -c_t^L [k^L] a W h_f (X) \quad (3.20)$$

Note that the sign is negative (as the flux is defined positive for transfer to the liquid phase) but the same matrix function will be obtained in the solution. Integrating from $z = 0$ and $(X) = (X_{in})$ to z and mole fraction difference (X) we obtain

$$(X) = \exp \left[-\frac{c_t^L [k^L] a W h_f z}{L} \right] (X_{in}) = \exp[-\zeta N^L] (X_{in}) \quad (3.21)$$

where $[N^L]$ is the number of transfer units for the liquid phase, and ζ is a dimensionless length z/Z . The liquid diffusion flux is

$$(\bar{J}^L) = -c_t^L [k^L] \Omega [-N^L] (X_{out}) \quad (3.22)$$

and the molar fluxes follow from

$$(\bar{N}^L) = (\bar{J}^L) a A_b + \bar{N}_t ((x^I) + (\bar{X})) \quad (3.23)$$

The above expressions are based on the same sort of assumptions made in deriving the vapor plug flow model; constant matrix of liquid phase mass transfer coefficients, neglect of the covariance term in the average flux calculation and, perhaps most important of all, constant interface composition. The latter assumption is needed in order to separate the vapor and liquid mass transfer calculations.

Now, while it might be acceptable to assume constant interface composition in the vapor phase in order to integrate the vapor phase material balances at a single point on the tray, it is less reasonable to assume that the interface composition is the same everywhere on the tray, even assuming the vapor mixes completely in the disengagement zone and, therefore, enters the tray with a uniform composition. Thus, the vapor and liquid interface mole fractions, which are used in the equilibrium equations, represent calculated average compositions. At the very least the vapor interface mole fractions needs to be corrected. The correction must be a function of the degree of liquid mixing on the tray and be identically zero if the liquid is completely mixed. The correction of the vapor interface mole fraction can be related to the change in the liquid mole fraction with the help of the equilibrium matrix, $[M]$. The change in the bulk mole fraction serves as an estimate of the correction to be made to the interface mole fraction. We assume the correction is given by the following expression:

$$\Delta(y^I) = [M](\bar{X} - X_{out}) \quad (3.24)$$

which, on substituting for the liquid composition changes, becomes

$$\Delta(y^I) = [M][\Omega[-N^L] - [I]]X_{out} \quad (3.25)$$

This expression obeys all of our theoretical demands; the correction disappears for a completely mixed liquid (\bar{X} equals X_{out}). The correction also vanishes when $[M] = [0]$ as it should.

In practice the actual correction will be smaller than the above estimate since the change in interface mole fraction must be less than the change in the bulk mole fractions. How much less is uncertain. In the absence of a more soundly based model we use a multiplying factor of 0.75 to obtain a correction which results in good estimates for experimental efficiencies as will be shown later.

The efficiency profiles for our depropanizer assuming both phases travel in plug flow are shown in Figure 3.5. Notice a further increase in the component tray efficiencies, particularly those of the two key components, propane and *n*-butane, and that the tray efficiencies now may be greater than 100%, as is likely to be the case. Figure 3.6 shows the composition profiles and we see that the mole fraction of *n*-pentane above the feed is very low and does *not* show the strange behavior observed in Figures 3.2 and 3.3.

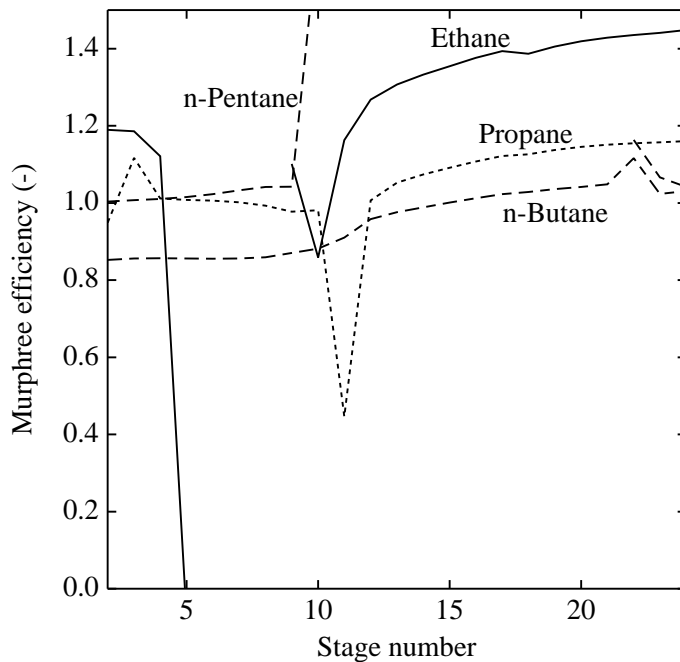


Figure 3.5: Murphree efficiencies for a depropanizer predicted by a nonequilibrium model assuming both vapor and liquid phases are in plug flow.

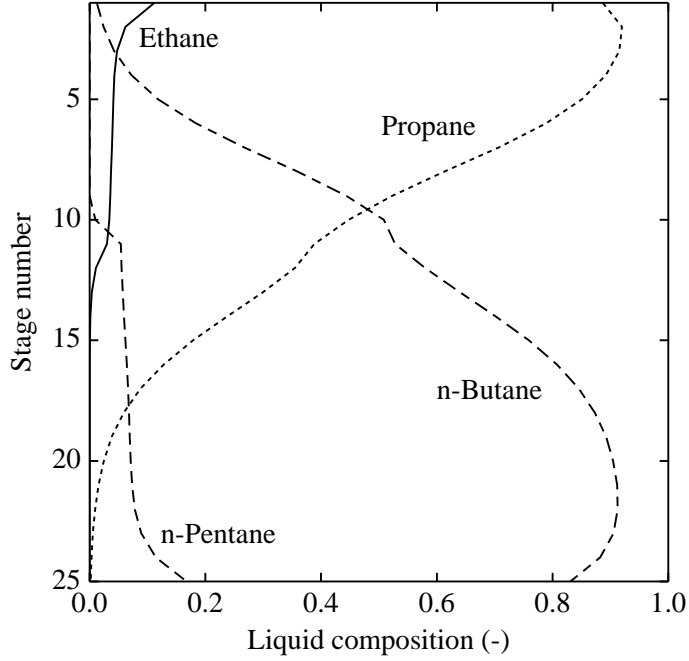


Figure 3.6: Liquid composition profiles for a depropanizer predicted by a nonequilibrium model with the molar fluxes calculated using the plug flow models derived in this paper.

3.2.3 Dispersion Flow model

The starting point for a liquid dispersion-flow model is the differential equation for plug-flow (3.20) expanded with a second derivative term which describes axial dispersion:

$$L \frac{d(X)}{dz} = D_e W h_{cl} c_t^L \frac{d^2(X)}{dz^2} - c_t^L [k^L] a W h_f(X) \quad (3.26)$$

Introducing the dimensionless length $\zeta = z/Z$ we obtain

$$\frac{D_e W h_{cl} c_t^L}{LZ} \frac{d^2(X)}{d\zeta^2} - \frac{d(X)}{d\zeta} - \frac{c_t^L [k^L] a A_b h_f}{L}(X) = 0 \quad (3.27)$$

By making the substitution $A = 1/Pe = D_e W h_{cl} c_t^L / LZ$, this becomes

$$A \frac{d^2(X)}{d\zeta^2} - \frac{d(X)}{d\zeta} - [N^L](X) = 0 \quad (3.28)$$

This second order differential equation can be solved analytically, using the substitutions $a = 1/2A$ and $[b] = a[2[N^L]/a + [I]]^{1/2}$ and the boundary conditions at $\zeta = 1$:

$$\frac{d(X)}{d\zeta} = 0 \quad (3.29)$$

$$(X) = (X_{out}) \quad (3.30)$$

to give (X) as the following function of ζ :

$$(X) = [[p] \exp[[m](\zeta - 1)] - [m] \exp[p](\zeta - 1)] [b]^{-1} \frac{(X_{out})}{2} \quad (3.31)$$

where we have defined $[p] = a[I] + [b]$ and $[m] = a[I] - [b]$. Integration over $\zeta = [0, 1]$ results in:

$$(\bar{X}) = [[p][\exp[m] - [I]][m]^{-1}[\exp[m]]^{-1} - [m][\exp[p] - [I]][p]^{-1}[\exp[p]]^{-1}] [b]^{-1} \frac{(X_{out})}{2} \quad (3.32)$$

which, using the Ω matrix function, is

$$(\bar{X}) = \frac{1}{2}[[p]\Omega[m] - [m]\Omega[p]][b]^{-1}(X_{out}) \quad (3.33)$$

Numerical evaluation of (3.33) for a binary system shows that for Peclet numbers going to zero we obtain $(\bar{X}) = (X_{out})$ corresponding to a completely mixed flow. For very large Peclet numbers, (10^3) say, $(\bar{X}) = \Omega[-N^L](X)$ (as already derived for plug flow). Of course, the computed average vapor interface composition needs to be corrected as described above for the liquid plug flow model.

3.3 Evaluation of Flow Models

We have already shown how the flow models influence the tray efficiency with the help of a hypothetical depropanizer. In this section we investigate the performance the flow models by comparing the predicted efficiencies with experimental data on “large” diameter trays.

Murphree efficiencies as a function of the fraction of flooding for eight data sets were obtained from FRI reports by Yanagi and Sakata (1979, 1981, 1982). Two systems were used in the FRI tests: the cyclohexane - *n*-heptane system at pressures of 28, 34, and 165 *kPa*, and the *i*-butane - *n*-butane system at pressures of 1138, 2056, and 2756 *kPa*. The experiments were carried out in sieve tray columns operated at total reflux. It is worth pointing out that this data is for binary systems; there is almost no published data for multicomponent systems on large scale equipment and what little is available usually contains insufficient data to allow us to attempt a simulation.

Nonequilibrium simulations were done for a column with the same tray design (the design parameters are summarized in Table 3.2) at a very high reflux ratio in order to closely approximate total reflux. The Murphree efficiencies were calculated for each component on each tray from the results of a simulation and averaged (over those trays not adjacent to condenser/reboiler). Simulations were done using four different combinations of flow model.

- Mixed vapor - Mixed liquid
- Plug flow vapor - Mixed liquid
- Plug flow vapor - Dispersion flow liquid
- Plug flow vapor - Plug flow liquid

Eddy diffusivities for use in the dispersion flow models were estimated using Zuiderweg's (1982) correlation (this model is recommended by Korchinsky, 1994). The mass transfer coefficients were estimated using the Chan and Fair (1984) correlations as also recommended by Korchinsky (1994) (see, also, the next subsection).

Simulations were carried out with flows that go from 20% to 100% of flooding. Results from some of our simulations are shown in Figures 3.7 and 3.8, where the experimental data is shown as points and the simulation results by lines. Limitations on space mean that only a small fraction of our results can be shown here; we have tried to show the most important trends by means of one figure per system. For the simulations in Figures 3.7 and 3.8 the Chan and Fair correlations were used to show the differences between the different flow models. The experimental efficiencies show a decline at low and high fractions of flooding, probably due to weeping and liquid entrainment. The Chan and Fair model includes a quadratic dependence of N^V on the fraction of flooding in order to account for the decrease in mass transfer at both low and fractions and high fractions of flooding. For this reason the Chan and Fair method usually describes the mass transfer (and hence, the efficiencies) better than the other mass transfer coefficient models. As we can see from Figure 3.8, the *i*-butane - *n*-butane system has high Murphree efficiencies with values over 100%. Both figures show that the Mixed-Mixed flow model underpredicts the efficiencies, as is true for the Plug flow vapor - Mixed flow liquid model. The performance of the Plug flow vapor - Dispersion flow liquid and the Plug-Plug flow model are very similar and model the experimental efficiencies quite well. This should not be too surprising as this data was actually used in the development of the Chan and Fair correlations. We are, however, using the correlations in a nonequilibrium model rather than in an efficiency calculation.

Only models including the dispersion or plug flow model for the liquid can predict efficiencies higher than 100% (such as for the *i*-butane - *n*-butane system). This points quite clearly to the need to use a liquid plug flow model with a correction added to the mole fraction difference.

3.4 Evaluation of Mass Transfer Coefficient Correlations

Four different methods for estimating the binary (Maxwell-Stefan) mass transfer coefficients for sieve trays are available:

- AIChE method, as described by the *AIChE Bubble Tray Design Manual* (AIChE, 1958, Gerster *et al.* 1958).

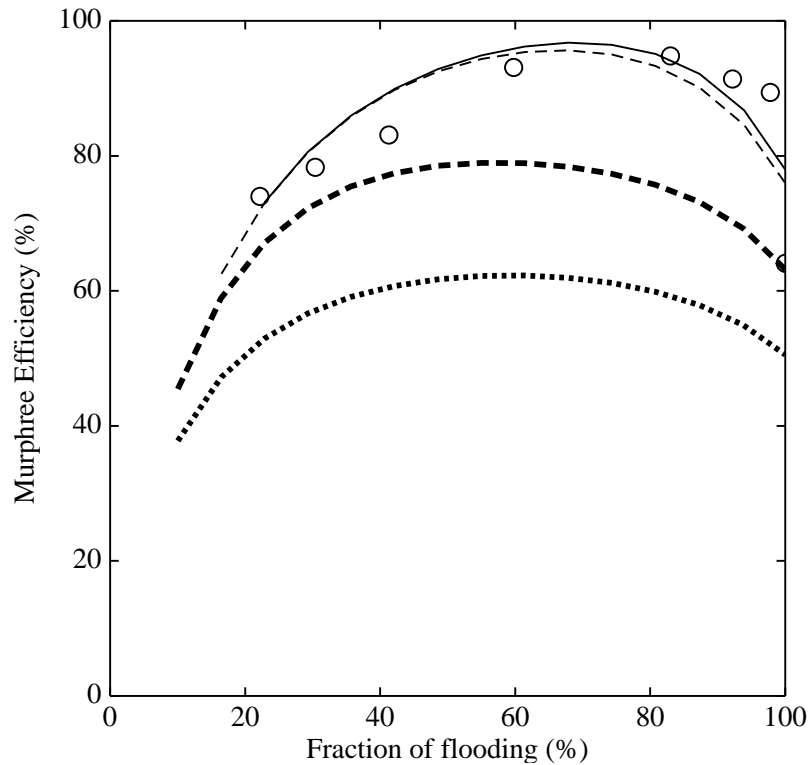


Figure 3.7: Murphree efficiencies for different flow models for a (8% hole area) sieve tray column with the cyclohexane - *n*-heptane system operating at 165 *kPa*. Mixed-Mixed flow (thick dotted line), Plug flow vapor - Mixed flow Liquid (thick dashed line), Plug flow vapor - Dispersion flow liquid (dashed line), and Plug-Plug flow (solid line). Mass transfer coefficients from the Chan and Fair correlation.

- Chan and Fair (1984).
- Zuiderweg (1982).
- Chen and Chuang (1994).

A summary of the specific equations used to calculate the binary mass transfer coefficients is given by Taylor and Krishna (1993).

Figures 3.9 and 3.10 show the behavior of the above mass transfer coefficient correlations, using the Plug flow vapor - Dispersion flow liquid models. In general, the AIChE and the Chan-Fair correlations behave in essentially the same way, except for the strong dependence on the fraction of flooding of the Chan-Fair model. This is not surprising since both use the same expression for the liquid mass

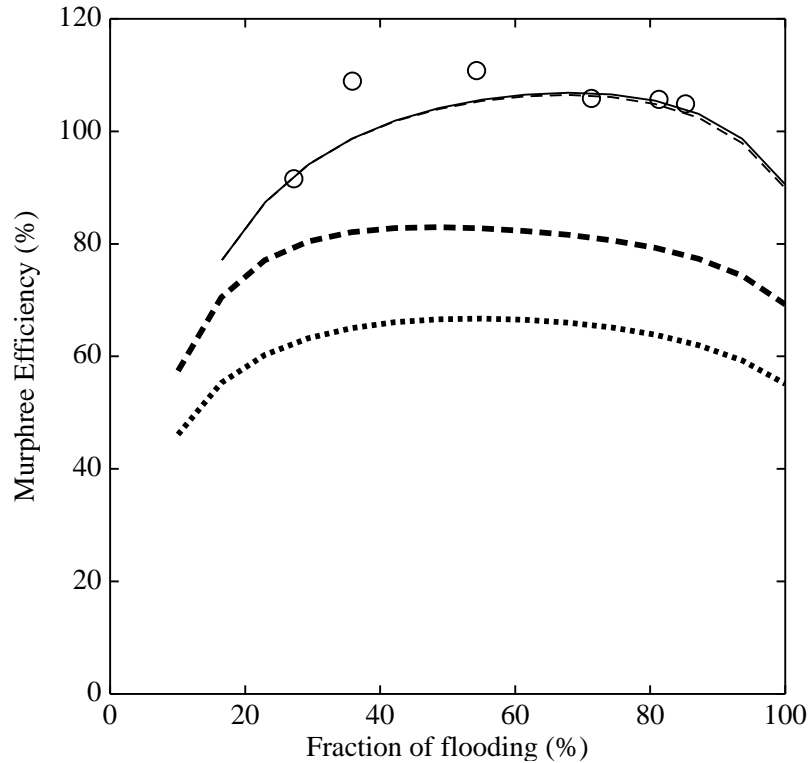


Figure 3.8: Murphree efficiencies for different flow models for a (8% hole area) sieve tray column with the *i*-butane - *n*-butane system operating at 2068 *kPa*. Mixed-Mixed flow (thick dotted line), Plug flow vapor - Mixed flow Liquid (thick dashed line), Plug flow vapor - Dispersion flow liquid (dashed line), and Plug-Plug flow (solid line), Mass transfer coefficients from the Chan and Fair correlation.

transfer coefficients. The Zuiderweg and Chen-Chuang models also behave in the same way in the sense that they predict higher efficiencies as they have higher values for the liquid number of transfer units than the first two correlations. This also makes the difference between mixed and plug liquid flow larger for these correlations. Overall, the Zuiderweg and Chen-Chuang models tend to overpredict the Murphree efficiencies (as is shown in Figure 3.10). The Chan-Fair correlation tends to describes the overall behavior of the Murphree efficiencies better than the other correlations.

In another recent study Korchinsky *et al.* (1994) recommended both the Chan and Fair method and set of correlations due to Stichlmair (1978). We did not include the Stichlmair correlations in this study as our experience is that this method does not extrapolate well to conditions beyond the range of parameter values for which the correlations are designed. While it might be argued that no correlation should be used beyond its published range, we believe that correlations should be developed that extrapolate in sensible ways and provide a reasonable numerical result when used outside its range. Stichlmair's cor-

Table 3.2: Sieve Plate Dimensions of FRI Column

Column diameter (<i>m</i>)	1.2
Tray spacing (<i>m</i>)	0.61
Sieve plate material	316SS
Plate thickness (<i>mm</i>)	1.5
Hole diameter (<i>mm</i>)	12.7
Hole pitch (<i>mm</i>)	30.2
Weir length (<i>m</i>)	0.94
Weir height (<i>mm</i>)	25.4,50.8
Downcomer clearance (<i>mm</i>)	22,38
Effective bubbling area (<i>m</i> ²)	0.859
Hole area (<i>m</i> ²)	0.118

relations fall short of this goal. The same criticism can also be levelled at the Chan and Fair correlations, mostly due to the built-in quadratic dependence on the fractional approach to flooding. The quadratic function in the Chan-Fair correlation for example, always has its maximum at a fraction of flooding of about 0.6 (depending on how the liquid height varies with the fraction of flooding). This limits the model to sieve trays only and to the range of fractions of flooding where the quadratic term is positive (the fraction of flooding must lie between 0 and 1.2). Presumably, the fall-off in tray performance at low and high fractions of flooding is due to increases in weeping or entrainment at these extreme flows. It is not clear to us that mass transfer coefficient correlations should account for these effects. It would be better to develop separate corrections which are applied to the mass transfer coefficients using the actual entrainment and weeping rates (see Lockett *et al.*, 1983, 1984). This would separate the influences of these phenomena from models that describe the mass transfer process. We have encountered situations where the Chan and Fair correlations provide negative mass transfer coefficients because the flows are outside this range. Not only are negative mass transfer coefficients physically meaningless, they prevent the program that implements our nonequilibrium model from converging to a solution! Despite this problem with the Chan and Fair method we think its limitations are less serious (from our perspective) than are the limitations of other methods and, for now, it is our method of choice.

The resistance to mass transfer in distillation operations often is assumed to reside entirely in the vapor phase although this is by no means a settled issue (see Lockett, 1986). The simulations carried out for this paper suggest that for the cyclohexane - *n*-heptane system the liquid phase contributes about 15% of the resistance. This figure rises to about 30% for the *i*-butane - *n*-butane system. Clearly, the resistance in the liquid phase is too large to be ignored.

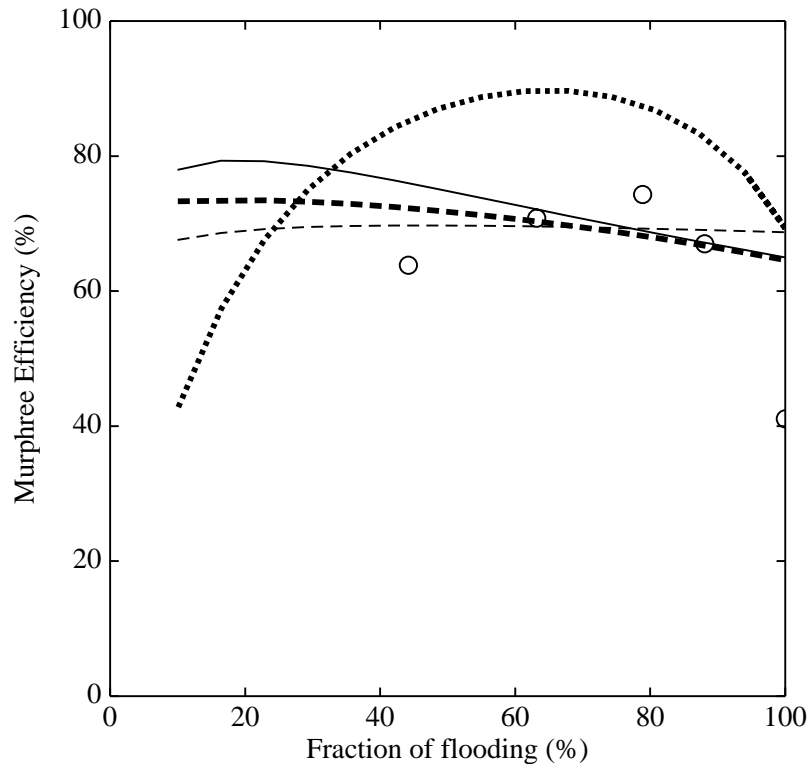


Figure 3.9: Murphree efficiencies for different Mass Transfer Coefficient models for a (14% hole area) sieve tray column with cyclohexane - *n*-heptane system operating at 34 *kPa*. Chan and Fair (thick dotted line), AIChE (thick dashed line), Zuiderweg (dashed line), and Chen and Chuang (solid line).

3.5 Maxwell-Stefan or Not?

There is no doubt that using the Maxwell-Stefan equations in order to calculate the matrix of multi-component mass transfer coefficients imposes a significant computational penalty on the use of mass transfer models of distillation. The penalty is not significant for the completely mixed flow models (of both phases) since the mass transfer rate equations can be written in a form that requires only a couple of matrix-vector multiplications. However, the plug flow vapor and liquid models require the evaluation of exponential matrices which is significantly more time consuming. Worst of all is the dispersion model which involves the computations of the square root of a matrix which cannot be evaluated anywhere near as efficiently (in general) as can the exponential matrix. For these latter models the computational penalty can be severe, especially for systems with many components. We pose the question: Should we, in fact, use the Maxwell-Stefan equations or should we be content with a simpler model that is based on identical mass transfer coefficients for all components. In this latter case, if we also neglect thermody-

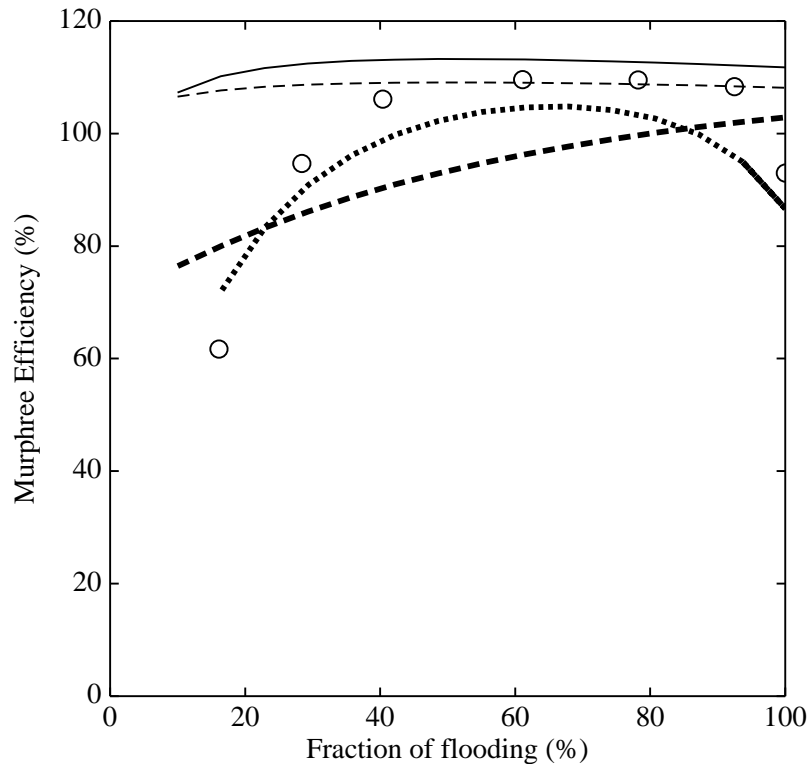


Figure 3.10: Murphree efficiencies for different Mass Transfer Coefficient models for a (14% hole area) sieve tray column with *i*-butane - *n*-butane system operating at 1138 *kPa*. Chan and Fair (thick dotted line), AIChE (thick dashed line), Zuiderweg (dashed line), and Chen and Chuang (solid line).

dynamic interactions in the mass transfer rate equations, all of the matrices involved are diagonal which means that no matrix function computations are required at all. The benefit is a significant decrease in the computer time requirements.

The answer is that there are a great many cases where we do not need the rigor of the Maxwell-Stefan equations but there are cases where it is essential to use them. Figures 3.11 to 3.13 provide two examples. In Figure 3.11 we show part of the liquid phase composition profile for an extractive distillation of an acetone - methanol binary using water as the extractive agent. The figure shows the profiles towards the bottom of the column with the multicomponent mass transfer coefficients computed using the Maxwell-Stefan equations and using a model in which all the diffusion coefficients are set equal to the average value and where thermodynamic interactions are ignored as well. Figure 3.12 shows the temperature profiles for the same system. While the profiles are qualitatively similar, there are significant quantitative differences between them in the sense that the mole fractions and temperatures on a given tray can be sufficiently different to influence both the design and operation of this column. McCabe-Thiele diagrams

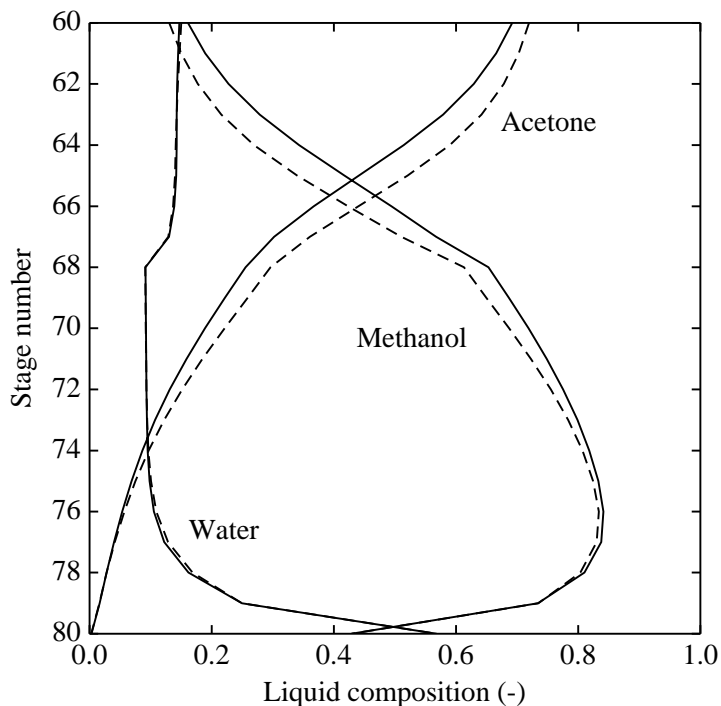


Figure 3.11: Liquid phase composition profiles for acetone - methanol - water extractive distillation column. Solid line - Maxwell-Stefan model, dashed line - equal diffusivity model.

(not shown here) show that for the calculations using the full Maxwell-Stefan model the feed stage is located in close to the optimal position. The same cannot be said for the calculations with the equal-diffusivity model; the McCabe-Thiele diagram for that case shows that the feed tray is several trays removed from its optimal location. A design carried out with the two different mass transfer models could provide quite different initial column configurations.

Some extractive and azeotropic distillation operations are controlled by knowing precisely where steep temperature and composition fronts exist. In these cases it is essential to know exactly where these fronts are located. An equal diffusivity mass transfer model might suggest that the controllers should be located on a tray different from that suggested using the Maxwell-Stefan equations as the basis for the design.

Figure 3.13 shows the composition profiles for a large column distilling ethanol - *t*-butanol - water. The profiles obtained with the Maxwell-Stefan model and the equal-diffusivity model are, as in the previous case, qualitatively similar. However, the apparently small differences between the mole fraction profiles translate into an enormous difference between the methods if we seek to design a column that can produce products of the required purity (see, also, Krishnamurthy and Taylor, 1985c). Different

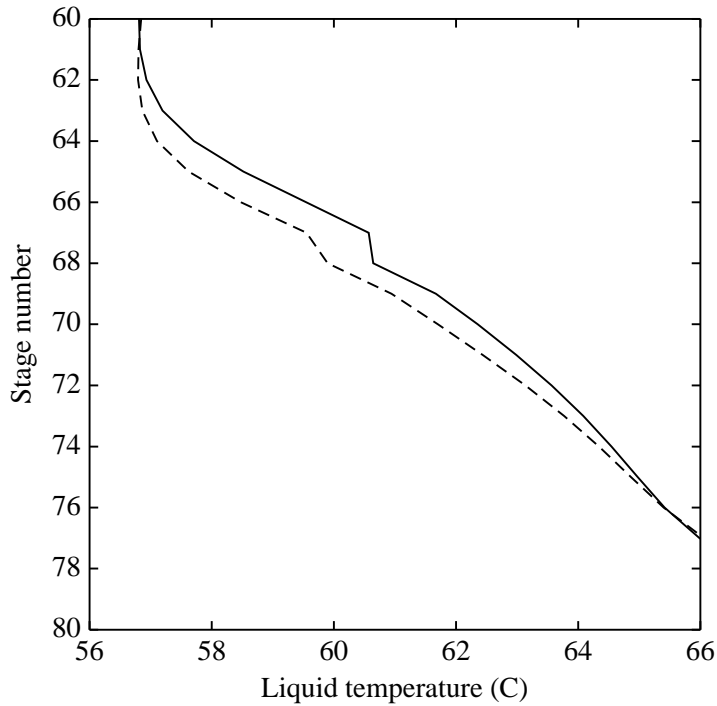


Figure 3.12: Liquid temperature profiles for acetone - methanol - water extractive distillation column. Solid line - Maxwell-Stefan model, dashed line - equal diffusivity model.

designs might be obtained using the two types of mass transfer model for distillation columns with a complicated configuration (multiple feeds and sidestreams). Another advantage of the Maxwell-Stefan formulation is that it becomes unnecessary to select a pair of key components on which to base the mass transfer coefficient calculation. All things considered we feel that the additional realism afforded by the Maxwell-Stefan formulation is worth the significant computational penalty associated with the model.

Symbol list

a	Interfacial area per unit volume (m^2/m^3)
a	Parameter = $Pe/2$
A_b	Bubbling area = $W Z$ (m^2)
$[b]$	Parameter matrix = $a[2[N^L]/a + [I]]^{1/2}$
c_t	Molar concentration ($kmol/m^3$)
D_e	Eddy diffusivity ($kmol/s m^2$)

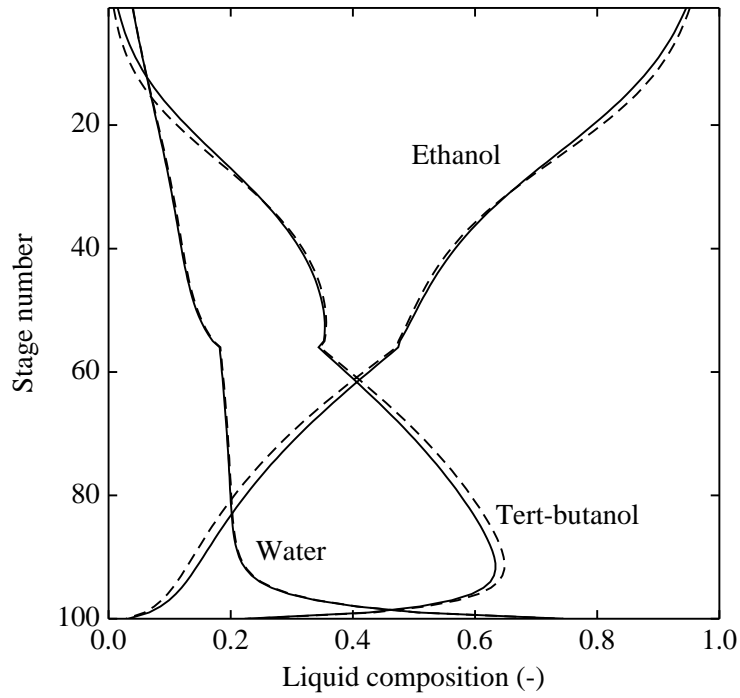


Figure 3.13: Liquid phase composition profiles for ethanol - *t*-butanol - water distillation column. Solid line - Maxwell-Stefan model, dashed line - equal diffusivity model.

h	Height (m), or Heat transfer coefficient (W/m^2K)
h_{cl}	Clear liquid height (m)
h_f	Froth height (m)
H	Molar enthalpy ($J/kmol$)
J	Diffusion flux ($kmol/s\ m^2$)
k	Mass transfer coefficient
$[K]$	Matrix of K-values (y^I/x^I on main diagonal)
L	Liquid flow rate ($kmol/s$)
$[M]$	$\partial y_i^I / \partial x_j^I$
N	Molar flux ($kmol/s$)
N	Binary matrix of Number of Transfer Units (NTU)
Pe	Peclet number = $DeW h_{cl} c_t^L / LZ$
T	Temperature (K)
V	Vapor flow rate ($kmol/s$)
W	Weir length (m)

x	Liquid mole fraction
X	Liquid mole fraction difference
y	Vapor mole fraction
Y	Vapor mole fraction difference
z	Path length (m)
Z	Total liquid flow path (m)

Greek:

Φ	Fractional flow,
Ω	Matrix function given by (3.17)
ζ	Dimensionless height or length

Superscript:

L	Liquid phase
V	Vapor phase
*	Equilibrium

Subscript:

i	Component i
e	Entrainment
t	Total
w	Weeping

References

AICHE, *Bubble Tray Design Manual: Prediction of Fractionation Efficiency*, AIChE, New York (1958).

J.L. Bravo, J.A. Rocha, J.R. Fair, "Mass Transfer in Gauze Packings", *Hydrocarbon Processing*, (January 1985) pp. 91–95.

G.X. Chen, K.T. Chuang, "Determining the Number of Gas-Phase and Liquid-Phase Transfer Units from Point Efficiencies in Distillation", *Ind. Eng. Chem. Res.*, Vol. **33** (1994) pp. 907–913.

H. Chan, J.R. Fair, "Prediction of Point Efficiencies on Sieve Trays", *Ind. Eng. Chem. Process Des. Dev.*, Vol. **23** (1984) pp. 814–819.

J.A. Gerster, A.B. Hill, N.N. Hochgraf, D.G. Robinson, *Tray Efficiencies in Distillation Columns*, AIChE, New York (1958).

H.A. Kooijman, R. Taylor, "A Nonequilibrium Model for Dynamic Simulation of Tray Distillation Columns", in press, *AIChE J.*, (1995).

W.J. Korchinsky, M.R. Ehsani, T. Plaka, "Sieve Plate point Efficiencies: 0.6 m Diameter Column", *Trans. I. Chem. E.*, Vol. **72**, Part A, (1994) pp. 465–471.

- W.J. Korchinsky, "Liquid Mixing in Distillation Trays: Simultaneous Measurement of the Diffusion Coefficient and Point Efficiency", *Trans. I. Chem. E.*, Vol. **72**, Part A, (1994) pp. 472–478.
- R. Krishnamurthy, R. Taylor, "A Nonequilibrium Stage Model of Multicomponent Separation Processes. Part I: Model Description and Method of Solution", *AIChE J.*, Vol. **31**, No. 3 (1985), pp. 449–455.
- R. Krishnamurthy, R. Taylor, "A Nonequilibrium Stage Model of Multicomponent Separation Processes. Part II: Comparison with Experiment", *AIChE J.*, Vol. **31**, No. 3 (1985b), pp. 456–465.
- R. Krishnamurthy, R. Taylor, "A Nonequilibrium Stage Model of Multicomponent Separation Processes. Part III: The Influence of Unequal Component Efficiencies in Process Design Problems", *AIChE J.*, Vol. **31**, No. 12 (1985c), pp. 1973–1985.
- R. Krishnamurthy, R. Taylor, "Simulation of Packed Distillation and Absorption Columns", *Ind. Eng. Chem. Process Des. Dev.*, Vol. **24** (1985d) pp. 513.
- R. Krishnamurthy, R. Taylor, "Absorber Simulation and Design Using a Nonequilibrium Stage Model", *Can. J. Chem. Eng.*, Vol. **64** (1986) pp. 1976.
- M. Lao, J.P. Kingsley, R. Krishnamurthy, R. Taylor, "A Nonequilibrium Stage Model of Multicomponent Separation Processes. Part VI: Simulation of Liquid-Liquid Extraction", *Chem. Eng. Commun.*, Vol. **86** (1989) pp. 73.
- M.J. Lockett, M.A. Rahman, H.A. Dhulesia, "The Effect of Entrainment on Distillation Tray Efficiency", *Chem. Eng. Sci.*, Vol. **38**, No. 5, (1983) pp. 661–672.
- M.J. Lockett, M.A. Rahman, H.A. Dhulesia, "Prediction of the Effect of Weeping on Distillation Tray Efficiency", *AIChE J.*, Vol. **30**, No. 3, (1984) pp. 423–431.
- M.J. Lockett, *Distillation Tray Fundamentals*, Cambridge University Press, New York (1986).
- J. Stichlmair, "Dimensionierung des gas/flüssigkeit kontaktapparates boden kolonne, Teil 1", *Chem. Ing. Tech.* **50**, 281–4; Teil 2, (1978) pp. 383–387.
- Taylor, R., M.F. Powers, M. Lao and A. Arehole, "The Development of A Nonequilibrium Model for Computer Simulation of Multicomponent Distillation and Absorption Operations", *I. Chem. E. Symp. Ser.*, Distillation and Absorption, No. 104, (1987) pp. B321.
- R. Taylor, R. Krishna, *Multicomponent Mass Transfer*, John Wiley and Sons, New York (1993).
- H.L. Toor, "Prediction of Efficiencies and Mass Transfer on a Stage with Multicomponent Systems", *AIChE J.*, **10**, (1964b) pp. 545–547.
- T. Yanagi, M. Sakata, "Performance of a Commercial Scale Sieve Tray", *I. Chem. E. Symp. Ser.*, No. 56, Bol. I, (1979).
- T. Yanagi, M. Sakata, "Performance of a Commercial Scale 14 % Hole Area Sieve Tray", Data tables of presentation at AIChE meeting, Houston, April (1981).
- T. Yanagi, M. Sakata, "Performance of a Commercial Scale 14 % Hole Area Sieve Tray", *Ind. Eng. Chem. Proc. Des. Dev.*, Vol. **21**, (1982) pp. 712–717.

F.J. Zuiderweg, "Sieve Trays – A View of the State of the Art", *Chem. Eng. Sci.*, Vol. **37** (1982) pp. 1441–1464.

Chapter 4

Dynamic Model Development

Dynamic nonequilibrium models for tray columns are developed. A full model with four holdup terms describing both froth and downcomer, as well as a two holdup model with only froth holdup terms, are introduced. The nonequilibrium models will be compared to corresponding conventional equilibrium models which are also described in this chapter. Finally, issues concerning the implementation and the integration of dynamic column models are discussed.

4.1 Nonequilibrium Model Assumptions

A schematic diagram of a general tray in a column is provided in Figure 4.1. Of central importance is the zone where vapor and liquid phases are brought into contact with each other in order to promote mass and energy transfer between the phases. A tray can operate in different flow regimes: spray, froth, emulsion, bubbling liquid, or foam. Here we will generally refer to the dispersion on the tray as the froth, although we do not limit our model to that regime. Above the froth is an area for vapor disengagement, to separate the phases to let them move countercurrently in the column. Similarly we have a downcomer for liquid disengagement. These disengagement areas are essential to the operation of a trayed column and certainly play a role in its performance.

What differentiates the dynamic model from the steady-state model (as described by Taylor *et al.*, 1994) is the use of holdup terms. For steady-state simulation holdup calculations are not required, however, in the dynamic model they represent the basic differential equations. For the general tray a number of distinct holdups can be identified:

- the liquid in the froth on a tray,
- the vapor dispersed in the froth on a tray,

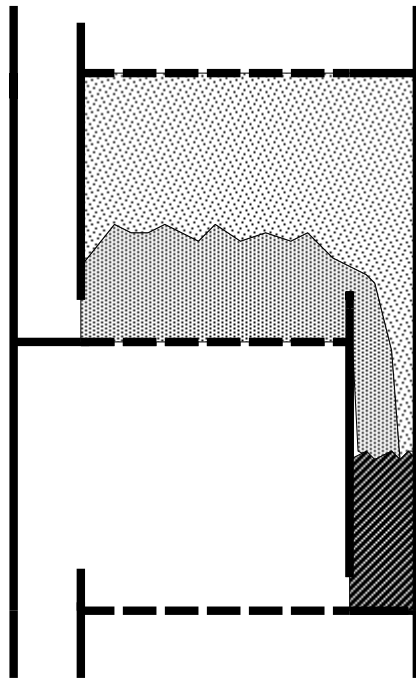


Figure 4.1: Schematic diagram of a general tray.

- the liquid in the downcomer below a tray,
- the vapor above the froth/downcomer on a tray.

The froth is modeled by two (or more, if multiple liquid phases are present) separate holdups. Figure 4.2 is a schematic diagram of these holdups and also shows the connecting flows between the different holdups. The following assumptions have been made in our dynamic nonequilibrium model:

- The trays are in mechanical equilibrium
- Thermodynamic equilibrium is assumed **only** at the interface between vapor and liquid phases on the tray. This is standard practice in the analysis of interphase mass transfer processes.
- Mass transfer occurs **only** between vapor and liquid on the tray, dictated by the transfer resistance in each phase
- Condenser and reboiler operate at equilibrium.

The dynamic model developed here uses all four holdups terms and avoids simplifications often made in other dynamic models such as constant holdups, neglecting energy derivatives, neglecting vapor

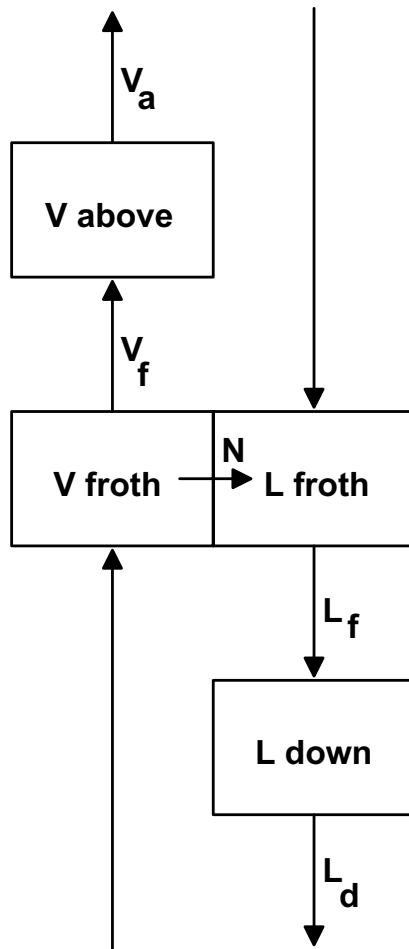


Figure 4.2: Schematic diagram of the holdups and connecting flows.

holdups, and constant (tray/component) efficiencies. To reduce the number of model equations the holdup terms for the vapor above the froth and in the downcomer can be lumped into the froth holdups or ignored (if it is desired to do so).

4.2 Nonequilibrium Model Equations

Component molar holdup terms are denoted with U_{ij}^{Pw} where P indicates the holdup phase type (V or L), w the place in the model (f for froth, d for downcomer, and a for above the froth), i the component, and j the plate number. Similarly, total molar holdups are denoted with U_{tj}^{Pw} and energy holdups with

E_j^{Pw} . Vapor and liquid holdup compositions are computed from

$$y_{ij}^w = \frac{U_{ij}^{Vw}}{U_{tj}^{Vw}} \quad (4.1)$$

$$x_{ij}^w = \frac{U_{ij}^{Lw}}{U_{tj}^{Lw}} \quad (4.2)$$

The interstage liquid and vapor flows on plate j are denoted with L_j^w and V_j^w where w indicates the holdup from which the flows originate (f , d , or a). Component molar feed flows are denoted similarly to molar holdups as F_{ij}^{Pw} . The mass transfer rates through the interface are positive from vapor to liquid and denoted by N_{ij}^w .

For a general stage (one not at the top or bottom of the column) the component molar balances over the four different holdups are:

$$\frac{dU_{ij}^{Vf}}{dt} = y_{i,j+1}^a V_{j+1}^a + F_{ij}^{Vf} - y_{ij}^f V_j^f - N_{ij}^f \quad (4.3)$$

$$\frac{dU_{ij}^{Lf}}{dt} = x_{i,j-1}^d L_{j-1}^d + F_{ij}^{Lf} - x_{ij}^f L_j^f + N_{ij}^f \quad (4.4)$$

$$\frac{dU_{ij}^{Va}}{dt} = y_{ij}^f V_j^f + F_{ij}^{Va} - y_{ij}^a V_j^a \quad (4.5)$$

$$\frac{dU_{ij}^{Ld}}{dt} = x_{ij}^f L_j^f + F_{ij}^{Ld} - x_{ij}^d L_j^d \quad (4.6)$$

These equations may be extended to include fractional entrainment (Φ_j^L , Φ_j^V), weep flow ratios (w_j), sidestream flow ratios (r_j), and interlinking flows ($G_{ij\nu}$). This is not done here (see, however, Taylor *et al.*, 1994). To correctly model the behavior of a column outside normal operational conditions the inclusion of entrainment and weep flows is essential.

The component molar holdups must sum to the total molar holdups:

$$0 = \sum_{i=1}^c U_{ij}^{Vf} - U_{tj}^{Vf} \quad (4.7)$$

$$0 = \sum_{i=1}^c U_{ij}^{Lf} - U_{tj}^{Lf} \quad (4.8)$$

$$0 = \sum_{i=1}^c U_{ij}^{Va} - U_{tj}^{Va} \quad (4.9)$$

$$0 = \sum_{i=1}^c U_{ij}^{Ld} - U_{tj}^{Ld} \quad (4.10)$$

The energy balances for each holdup are:

$$\frac{dE_j^{Vf}}{dt} = \frac{E_{j+1}^{Va}}{U_{t,j+1}^{Va}} V_{j+1}^a + \sum_{i=1}^c H_{ij}^{FVf} F_{ij}^{Vf} - \frac{E_j^{Vf}}{U_{tj}^{Vf}} V_j^f - \epsilon_j^{Vf} + Q_j^{Vf} \quad (4.11)$$

$$\frac{dE_j^{Lf}}{dt} = \frac{E_{j-1}^{Ld}}{U_{t,j-1}^{Ld}} L_{j-1}^d + \sum_{i=1}^c H_{ij}^{FLf} F_{ij}^{Lf} - \frac{E_j^{Lf}}{U_{tj}^{Lf}} L_j^f + \epsilon_j^{Lf} + Q_j^{Lf} \quad (4.12)$$

$$\frac{dE_j^{Va}}{dt} = \frac{E_j^{Vf}}{U_{tj}^{Vf}} V_j^f + \sum_{i=1}^c H_{ij}^{FVa} F_{ij}^{Va} - \frac{E_j^{Va}}{U_{tj}^{Va}} V_j^a + Q_j^{Va} \quad (4.13)$$

$$\frac{dE_j^{Ld}}{dt} = \frac{E_j^{Lf}}{U_{tj}^{Lf}} L_j^f + \sum_{i=1}^c H_{ij}^{FLd} F_{ij}^{Ld} - \frac{E_j^{Ld}}{U_{tj}^{Ld}} L_j^d + Q_j^{Ld} \quad (4.14)$$

where ϵ is the energy transport to/from the interface (see below). H_{ij}^{FPw} is the partial molar enthalpy of component i in the feed to the specified holdup and Q_j^{Pw} is the heat input into the specified holdup. The energy holdups E_j^{Pw} are related to the component molar holdups and the component enthalpies (H_{ij}^{Pw}) by

$$0 = \sum_{i=1}^c (H_{ij}^{Vf} U_{ij}^{Vf}) - E_j^{Vf} \quad (4.15)$$

$$0 = \sum_{i=1}^c (H_{ij}^{Lf} U_{ij}^{Lf}) - E_j^{Lf} \quad (4.16)$$

$$0 = \sum_{i=1}^c (H_{ij}^{Va} U_{ij}^{Va}) - E_j^{Va} \quad (4.17)$$

$$0 = \sum_{i=1}^c (H_{ij}^{Ld} U_{ij}^{Ld}) - E_j^{Ld} \quad (4.18)$$

Enthalpies are functions of the holdup temperature, T_j^{Pw} , pressure, p_j , and holdup molar compositions. The energy fluxes from the vapor to the interface and from the interface to the liquid on plate j are:

$$\epsilon_j^{Vf} = \sum_{i=1}^c N_{ij}^{Vf} H_{ij}^{Vf} + h_j^{Vf} a_j (T_j^{Vf} - T_j^I) \quad (4.19)$$

$$\epsilon_j^{Lf} = \sum_{i=1}^c N_{ij}^{Lf} H_{ij}^{Lf} + h_j^{Lf} a_j (T_j^I - T_j^{Lf}) \quad (4.20)$$

where T_j^I is the temperature of the interface on plate j . The energy balance over the interface equates these energy fluxes:

$$0 = \epsilon_j^{Vf} - \epsilon_j^{Lf} \quad (4.21)$$

The interface compositions x_{ij}^{If} and y_{ij}^{If} must sum to unity,

$$0 = \sum_{i=1}^c y_{ij}^{If} - 1 \quad (4.22)$$

$$0 = \sum_{i=1}^c x_{ij}^{If} - 1 \quad (4.23)$$

and obey the equilibrium relations ($i = 1 \dots c$) as well:

$$0 = K_{ij}^{If} x_{ij}^{If} - y_{ij}^{If} \quad (4.24)$$

The mass transfer rates N_{ij} from the vapor to the interface are equal to the mass transfer rates from the interface to the liquid. They are computed with the following rate equations:

$$(0) = (N_j) - N_{tj}(y_j^{Vf}) - c_j^{Vf} a_j [R_j^{Vf}]^{-1} [\Gamma_j^{Vf}] ((y_j^{Vf}) - (y_j^{If})) \quad (4.25)$$

$$(0) = (N_j) - N_{tj}(x_j^{Lf}) - c_j^{Lf} a_j [R_j^{Lf}]^{-1} [\Gamma_j^{Lf}] ((x_j^{If}) - (x_j^{Lf})) \quad (4.26)$$

where N_{tj} is the total mass transfer rate on plate j which equals to the sum of all the component mass transfer rates N_{ij} . c^{Vf} and c^{Lf} are the molar concentrations of the vapor and liquid phase of the froth. Note that only $c - 1$ fluxes, with c being the number of components, are independent and we will obtain $2(c - 1)$ rate equations. Also note that the rate equations are in matrix/vector form. The rate matrix $[R]$ is defined by (2.13, 2.14) and the thermodynamic factor matrix Γ by (2.12).

The pressure, p_j , is computed from the tray pressure drop and the pressure of the tray above. The pressure at the top of the column is specified (p_{spec}):

$$0 = p_1 - p_{spec} \quad (4.27)$$

$$0 = p_j - p_{j-1} - \Delta p_{j-1} \quad (4.28)$$

ΔP_{j-1} is the pressure drop for the specific type of column internals (computed empirically or theoretically, Taylor *et al.*, 1994).

The interholdup flow rates are determined through calculation of the total molar holdups. The total molar holdups can be computed from the height of the froth, h_j^f , the clear liquid height, h_j^{cl} , the tray spacing, h_j^{ts} , and the liquid height in the downcomer, h_j^d , of plate j :

$$0 = (h_j^f - h_j^{cl}) A_j^f c_j^{Vf} - U_{tj}^{Vf} \quad (4.29)$$

$$0 = h_j^{cl} A_j^f c_j^{Lf} - U_{tj}^{Lf} \quad (4.30)$$

$$0 = \{(h_j^{ts} - h_j^f) A_j^b + (2h_j^{ts} - h_j^d) A_j^d\} c_j^{Va} - U_{tj}^{Va} \quad (4.31)$$

$$0 = h_j^d A_j^d c_j^{Ld} - U_{tj}^{Ld} \quad (4.32)$$

The liquid heights are computed by empirical correlations or theoretical relations (see Appendix A). Note that each total holdup must be a function of the relevant flow rate (e.g. U_{tj}^{Ld} should be a function of L_j^d , etc.) to prevent higher index systems (more on this topic below). Since this is not the case for (4.31) we can replace it with

$$0 = V_j^f - V_j^a \quad (4.33)$$

to use a constant molar vapor holdup above the froth (usually the change in U_{tj}^{Va} is small). This assumption maintains the index of the system at one (instead of two) but violates the physical constraint of a fixed volume between the trays. For the correct dynamic simulation it is important that the liquid height correlations behave correctly besides being accurate (which is not required for steady-state simulation).

Alternatively, instead of computing the total holdups from liquid heights, which are computed from empirical correlations, the liquid and vapor flows could be computed directly from empirical or theoretical relations. Models describing the holdup or flow need to be accurate *and* have the correct behavior. Since the number of models which describe liquid heights and froth densities is much larger in comparison to models describing the flows, holdups are being calculated.

The variables and equations, as well as their number, type, and association, are summarized in Tables 4.1. The association is non-trivial as it determines the index of the resulting system of equations. Each variable must be represented (either directly or indirectly) in its associated equation to prevent the generation of a higher index DAE system. That is why the flow variables are matched up with the calculation of the molar holdups from the liquid heights (or directly from the calculation of the flows if that alternative is chosen). That is also why the mass transfer rates (N_{ij}) are somewhat strangely paired with the equilibrium (4.24), mass transfer rate (4.25, 4.26), and interface composition summation (4.22, 4.23) equations (together with the interface compositions y_{ij}^{If} , x_{ij}^{If}).

The total number of equations is $7c + 18$ per general stage where c represents the number of components in the system. Out of these, $4c + 4$ equations are ordinary differential equations while the rest ($3c + 14$) are algebraic equations. The feed flows (F), heat inputs (Q), top and condenser pressures (P_{spec} , P^c), and product streams (D , B) are functions of time. If they are constants we are solving a steady-state (SS) process, where all differential terms are set to zero. If they change over time we switch to dynamic simulation (DS) where we solve the resulting Differential-Algebraic system of equations until steady-state is reached (or until the variable changes are less than some specified small fraction). Of course, only during a steady-state simulation can we activate the *design-mode* which simultaneously corrects the column design to handle the process flows at hand. The resulting design can then be directly used for the dynamic simulation.

A simplification of this full tray model results from ignoring the vapor above the froth and the liquid in the downcomer. Equations 4.5, 4.6, 4.9, 4.10, 4.13, 4.14, 4.17, 4.18, 4.31, 4.32 are omitted from this model which has just $5c + 10$ variables. The neglected downcomer and vapor holdup could be optionally lumped into the liquid and vapor holdup equations (4.29, 4.30).

As mentioned before, the simplified model can (optionally) lump the downcomer liquid and/or vapor above the froth with the liquid or vapor froth holdup, respectively. Also, all holdups can be calculated at steady-state and kept constant during the dynamic simulation. However, lumping holdups, or keeping them constant, are not good representations of the real behavior of trays.

4.3 Reboiler and Condenser

Distillation columns also have various types of condensers and reboilers that usually have a significantly larger holdup than the holdup on any tray to give the column operational stability. It is these larger holdups that lead to differences in the transient behavior of various variables and, therefore, have a large

Table 4.1: Variables and equations for the full dynamic model

Variable(s)	Equation(s)	Number	Differential
$U_{ij}^{Vf}, U_{ij}^{Lf}, U_{ij}^{Va}, U_{ij}^{Ld}$	(4.3), (4.4), (4.5), (4.6)	4c	+
$E_j^{Vf}, E_j^{Lf}, E_j^{Va}, E_j^{Ld}$	(4.11), (4.12), (4.13), (4.14)	4	+
$U_{ij}^{Vf}, U_{ij}^{Lf}, U_{ij}^{Va}, U_{ij}^{Ld}$	(4.7), (4.8), (4.9), (4.10)	4	-
$V_j^f, L_j^f, V_j^a, L_j^d$	(4.29), (4.30), (4.31), (4.32)	4	-
$T_j^{Vf}, T_j^{Lf}, T_j^{Va}, T_j^{Ld}$	(4.15), (4.16), (4.17), (4.18)	4	-
T_j^I	(4.21)	1	-
N_{ij}	(4.25), (4.26)	c	-
x_{ij}^{If}	(4.26), (4.23), (4.24)	c	-
y_{ij}^{If}	(4.24), (4.22)	c	-
P_j	(4.27), (4.28)	1	-

effect on the column behavior. They also cause the system of equations to be very stiff.

The reboiler is modeled as a liquid holdup in the bottom of the column followed by a partial (equilibrium) reboiler. The holdup component molar balances (c) are:

$$\frac{dU_{ib}^L}{dt} = x_{in}L_n^d - x_{ib}L_b \quad (4.34)$$

where the liquid mole fraction is computed by:

$$x_{ib} = \frac{U_{ib}^L}{U_{tb}^L} \quad (4.35)$$

and the tray above the reboiler is tray n . The total holdup is computed by summing the component holdups:

$$0 = \sum_{i=1}^c U_{ib}^L - U_{tb}^L \quad (4.36)$$

Assuming a constant molar holdup we write the total molar balance (for dynamic state):

$$0 = L_n^d - L_b \quad (4.37)$$

We could also assume a more realistic constant volumetric holdup for the reboiler. At steady-state this equation is replaced by a direct specification of the molar (or possibly volumetric) holdup in the reboiler:

$$0 = U_{tb}^L - U_{tb,spec}^L \quad (4.38)$$

The energy holdup and energy relation are:

$$\frac{dE_b}{dt} = \frac{E_n^{Ld}}{U_n^{Ld}}L_n^d - \frac{E_b}{U_{tb}^L}L_b \quad (4.39)$$

Table 4.2: Variables and equations for the reboiler model

Variable(s)	Equation(s)	Number	Differential
U_{ib}^L	(4.34)	c	+
E_b	(4.39)	1	+
U_{tb}^L	(4.36)	1	-
L_b	(4.37) / (4.38)	1	-
T_b	(4.40)	1	-
P_b	(4.41)	1	-
V_r	(4.42)	1	-
y_{ir}	(4.43)	c	-
T_r	(4.44)	1	-
x_{ib}	(4.44), (4.45)	c	-
Q_r	(4.46)	1	-
B	(4.47)	1	-

$$0 = \sum_{i=1}^c (H_{ib}^L U_{ib}^L) - E_b \quad (4.40)$$

The pressure is determined from:

$$0 = p_b - p_n - \Delta p_n \quad (4.41)$$

For a partial reboiler we have total and component molar balances ($c + 1$), equilibrium relations(c), a summation equation for the vapor and liquid mole fractions (1), and an energy balance (1):

$$0 = L_b - V_r - B \quad (4.42)$$

$$0 = x_{ib} L_b - y_{ir} V_r - x_{ir} B \quad (4.43)$$

$$0 = K_{ir} x_{ir} - y_{ir} \quad (4.44)$$

$$0 = \sum_{i=1}^c (y_{ir} - x_{ir}) \quad (4.45)$$

$$0 = \frac{E_b}{U_{tb}^L} L_b + Q_r - H_r^V V_r - H_r^L B \quad (4.46)$$

where Q_r represents the reboiler duty, B the bottoms flow, and V_r the boilup vapor returned to stage n . Various reboiler specifications can be used, for example, the specification of the bottoms flow:

$$0 = B - B_{spec} \quad (4.47)$$

The ($3c + 9$) variables are U_{ib}^L , U_{tb}^L , E_b , T_b , L_b , P_b , V_r , y_{ir} , Q_r , T_r , x_{ir} , and B (see Table 4.2). In the case of a total reboiler with a *vapor* product, $x_{ir} B$ in the reboiler mole balance becomes $y_{ir} B$ and $H_r^L B$ in the energy balance becomes $H_r^V B$. For a total reboiler with a *liquid* product, $x_{ir} B$ in the reboiler mole balance becomes $x_{ib} B$ and $H_r^L B$ in the energy balance becomes $E_b B / U_{tb}^L$.

The condenser is modeled as a total condenser and reflux drum. The total condenser has the normal $(2c + 3)$ equations. The variables are the liquid product flow, L_c , the temperature, T_c , heat duty, Q_c , and the vapor and liquid mole fractions, x_{ic} and y_{ic} . The condenser equations are, respectively, a total molar balance, component molar balances (c), an energy balance, equilibrium relations (c), and a summation equation:

$$0 = V_2 - L_c \quad (4.48)$$

$$0 = y_{i2}V_2 - x_{ci}L_c \quad (4.49)$$

$$0 = H_2^V V_2 + Q_c - H_c^L L_c \quad (4.50)$$

$$0 = K_{ic}x_{ic} - y_{ic} \quad (4.51)$$

$$0 = \sum_{i=1}^c (y_{ic} - x_{ic}) \quad (4.52)$$

The pressure of the condenser, P_{cond} , is specified. Again, the ordering of these variables and equations is important to avoid index problems. The reflux drum has a vapor and a liquid holdup. Thus, we have c component molar holdups (U_i^{Ldrum}), a total molar holdup (U_t^{Ldrum}), and an energy holdup (E^{Ldrum}). We have a liquid distillate flow (D^L) and a returning liquid reflux (R). The molar component balances are:

$$\frac{dU_i^{Ldrum}}{dt} = x_{ic}L_c - x_i^{drum}(D^L + R) \quad (4.53)$$

with the total holdups:

$$0 = \sum_{i=1}^c U_i^{Ldrum} - U_t^{Ldrum} \quad (4.54)$$

The energy balances are:

$$\frac{dE^{Ldrum}}{dt} = H_c^L L_c - \frac{E^{Ldrum}}{U_t^{Ldrum}}(D^L + R) \quad (4.55)$$

The energy holdups are equated to the products of the molar holdups and enthalpies to determine the liquid drum temperature (T^{Ldrum}):

$$0 = \sum_{i=1}^c (U_i^{Ldrum} H_i^{Ldrum}) - E^{Ldrum} \quad (4.56)$$

We have a total of $c + 5$ equations and variables: U_i^{Ldrum} , U_t^{Ldrum} , E^{Ldrum} , T^{Ldrum} , R , and distillate rate D^L . Combined with the condenser this gives $3c + 8$ variables and $3c + 6$ equations. The extra equations needed are the condenser specification and constraint. For unsteady-state simulation the condenser constraint is a constant molar holdup:

$$0 = L_c - (D^L + R) \quad (4.57)$$

or constant volume holdup:

$$0 = \frac{L_c}{c_c^L} - \frac{(D^L + R)}{c_{drum}^L} \quad (4.58)$$

Table 4.3: Variables and equations for the condenser model

Variable(s)	Equation(s)	Number	Differential
L_c	(4.48)	1	—
x_{ic}	(4.49)	c	—
T_c	(4.51)	1	—
y_{ic}	(4.51), (4.52)	c	—
Q_c	(4.50)	1	—
U_i^{Ldrum}	(4.53)	c	+
E^{Ldrum}	(4.55)	1	+
U_t^{Ldrum}	(4.54)	1	—
T^{Ldrum}	(4.56)	1	—
R	(4.57) / (4.58) / (4.59) / (4.60)	1	—
D^L	(4.61)	1	—

Again, for the steady-state simulation this equation is replaced by the direct specification of the molar holdup:

$$0 = U_t^{Ldrum} - U_{t,spec}^{Ldrum} \quad (4.59)$$

or, the specification of the volumetric holdup:

$$0 = \frac{U_t^{Ldrum}}{c_{drum}^L} - V_{spec}^{drum} \quad (4.60)$$

Various steady-state condenser specifications can be used. For example, fixing the reflux ratio (RR) is represented by

$$0 = D^L RR - R \quad (4.61)$$

The variables and equations of the condenser are shown in Table 4.3. The vapor/liquid holdups in the connecting pipes between column and condenser/reboiler are neglected, but can be incorporated if necessary.

4.4 Equilibrium models

The nonequilibrium models developed above will be compared with the corresponding results from two equilibrium models which use a specified tray efficiency, ξ_j (assumed constant over the integration interval). The first model (EQL) neglects the vapor holdup and only the liquid holdup in the froth is included. This holdup can be computed by (4.30) or held constant (computed at steady-state or user specified). The set of equations for this model are:

$$\frac{dU_{ij}}{dt} = y_{i,j+1}V_{j+1} + x_{i,j-1}L_{j-1} + F_{ij} - y_{ij}V_j - x_{ij}L_j \quad (4.62)$$

Table 4.4: Variables and equations for the EQL model

Variable(s)	Equation(s)	Number	Differential
U_{ij}	(4.62)	c	+
U_{tj}	(4.63)	1	-
E_j	(4.65)	1	+
y_{ij}	(4.67)	c	-
V_j	(4.68)	1	-
L_j	(4.64)	1	-
T_j	(4.66)	1	-
P_j	(4.69)	1	-

$$0 = \sum_{i=1}^c U_{ij} - U_{tj} \quad (4.63)$$

$$0 = h_j^{cl} A_j^f c_j^{Lf} - U_{tj} \quad (4.64)$$

$$\begin{aligned} \frac{dE_j}{dt} = & \left(\sum_{i=1}^c y_{i,j+1} H_{i,j+1}^V \right) V_{j+1} + \left(\frac{E_{j-1}}{U_{t,j-1}} \right) L_{j-1} + \sum_{i=1}^c H_{ij}^F F_{ij} + Q_j \\ & - \left(\sum_{i=1}^c y_{ij} H_{ij}^V \right) V_j - \left(\frac{E_j}{U_j} \right) L_j \end{aligned} \quad (4.65)$$

$$0 = \sum_{i=1}^c H_{ij}^L U_{ij} - E_{ij} \quad (4.66)$$

$$0 = \xi_j K_{ij} x_{ij} - y_{ij} + (1 - \xi_j) y_{i,j+1} \quad (4.67)$$

$$0 = \sum_{i=1}^c y_{ij} - 1 \quad (4.68)$$

$$0 = p_j - p_{j-1} - \Delta P_{j-1} \quad (4.69)$$

where we have $c + 1$ differential equations. The tray pressures are computed with the tray pressure drops (the pressure of the tray at the top of the column specified). Table 4.4 lists the $2c + 6$ equations and variables.

If the vapor holdup is not neglected we obtain the following set of equations (model EQLV):

$$\frac{dU_{ij}^V}{dt} + \frac{dU_{ij}^L}{dt} = y_{i,j+1} V_{j+1} + x_{i,j-1} L_{j-1} + F_{ij} - y_{ij} V_j - x_{ij} L_j \quad (4.70)$$

$$0 = \sum_{i=1}^c U_{ij}^V - U_{tj}^V \quad (4.71)$$

$$0 = \sum_{i=1}^c U_{ij}^L - U_{tj}^L \quad (4.72)$$

$$0 = (h_j^f - h_j^{cl})A_j^f c_j^{Vf} - U_{tj}^V \quad (4.73)$$

$$0 = h_j^{cl} A_j^f c_j^{Lf} - U_{tj}^L \quad (4.74)$$

$$\begin{aligned} \frac{dE_j^V}{dt} + \frac{dE_j^L}{dt} &= \left(\frac{E_{j+1}^V}{U_{t,j+1}^V}\right)V_{j+1} + \left(\frac{E_{j-1}^L}{U_{t,j-1}^L}\right)L_{j-1} + \sum_{i=1}^c H_{ij}^F F_{ij} + Q_j \\ &\quad - \left(\frac{E_j^V}{U_j^V}\right)V_j - \left(\frac{E_j^L}{U_j^L}\right)L_j \end{aligned} \quad (4.75)$$

$$0 = \sum_{i=1}^c H_{ij}^V U_{ij}^V - E_{ij}^V \quad (4.76)$$

$$0 = \sum_{i=1}^c H_{ij}^L U_{ij}^L - E_{ij}^L \quad (4.77)$$

$$0 = \xi_j K_{ij} x_{ij} - y_{ij} + (1 - \xi_j) y_{i,j+1} \quad (4.78)$$

$$0 = p_j - p_{j-1} - \Delta P_{j-1} \quad (4.79)$$

$$(4.80)$$

with $c + 1$ differential equations and a total of $2c + 8$ equations and variables (U_{ij}^V , U_{ij}^L , U_{tj}^V , U_{tj}^L , E_j^V , E_j^L , V_j , L_j , T_j , and P_j). Again, neglected holdups could be lumped in as discussed previously.

4.5 Physical Property Models

So far only mathematical equations of the dynamic model have been discussed. However, the successful implementation of a column solver requires more than “just solving” the equations. A large and important part of a process simulator are the physical property models which supply the K-values, activity coefficients, binary diffusivities, densities, heat capacities, enthalpies, vapor pressures, viscosities, thermal conductivities, surface tensions, and binary mass transfer coefficients. A nonequilibrium model has a much higher demand for properties compared to an equilibrium model (Taylor *et al.*, 1994). Property models also impose a problem specially associated with dynamic simulation. Often, different correlations are used over different state variable ranges. When a switch between different correlations occurs due to a change in a state variable (such as temperature, pressure, or composition) it causes a discontinuity in the simulation. For the sake of consistency, properties need to be continuous and differentiable at or around any switching points. Depending on the solver used, proper handling of these discontinuities *may* require the physical property model/correlation switches to be signaled in some way. However, this is not (yet) done in the present implementation of the models described above. Rather, discontinuities of this kind are avoided as much as possible by using a single correlation for the whole integration. This has implications for the manner in which the model equations can be integrated.

4.6 Solving the Dynamic Nonequilibrium Model

The system of model equations consists of differential equations for the molar and energy balances and algebraic equations for all other relations. Therefore, we obtain a Differential-Algebraic system of Equations (DAE). A general form of a differential-algebraic system of m equations is:

$$\mathbf{F}(t, \mathbf{y}, \mathbf{y}') = \mathbf{0} \quad (4.81)$$

$$\mathbf{y}(t_o) = \mathbf{y}_o \quad (4.82)$$

where functions \mathbf{F} , variables \mathbf{y} and derivatives \mathbf{y}' are m dimensional vectors. The solution is traced over time (t) from the initial (at $t = t_o$) variable values \mathbf{y}_o . Typical DAE systems are large and sparse sets of stiff differential equations and nonlinear algebraic equations. Stiff differential equations mean that there are greatly differing time constants present, or, in other words, the eigen values of the Jacobian ($\partial\mathbf{F}/\partial\mathbf{y}$) are widely spread over the negative halfplane. This implies the use of implicit integration techniques which require derivative (Jacobian) information and thus, more calculations. The more nonlinear the equations are, the more the stepsize will be restricted since it will be limited by the more local character of the Jacobian information (which is used to "follow" the solution which is dictated by the algebraic constraints).

Two approaches are used to solve DAE systems. The procedural approach separates the algebraic equations from the differential equations, trying to solve the algebraic equations after each integration step for the differential equations. Although this might seem advantageous (the resulting two systems are of smaller dimension) it is not a rigorous method and may lead to obtaining a false transient. The other approach in solving a DAE system is to integrate the whole system of differential and algebraic equations simultaneously. There are two main types of such DAE solvers: those that employ Backwards Differentiation Formulae (BDF) and the one step (semi-) implicit methods (such as Runge-Kutta methods).

BDF methods replace the time derivative \mathbf{y}' by a difference formula approximation, by using previous variable values, resulting into systems of just algebraic equations which can be solved with a Newton type method. Generally only a few Newton iterations are applied, otherwise the stepsize will be reduced. For efficiency, instead of using a first order approximation for \mathbf{y}' , usually higher order BDF (limited to 15) are used. Selecting order and stepsize is automatized by the code through truncation error control. However, to switch order and stepsize at the same time makes this type of codes rather complicated.

The initial stepsize for BDF methods must be carefully chosen. If it is too small, we may fail to solve the system because the iteration matrix is very poorly conditioned, even though the problem might have been solved successfully given a better (larger) choice of initial stepsize. The method requires *consistent* initial derivative information to start, which must be either obtained through a one step algorithm or a specially supplied user routine. Unpleasant problems may occur if some derivatives are discontinuous. If we were to solve such a problem numerically, we would hope that the code could find the discontinuity and pass over it, or at least fail at the discontinuity. Instead, a code based on BDF with the usual error control mechanism is likely to fail not on the step which spans the discontinuity but on the subsequent

step. It is easily seen that these difficulties with the error estimate are not limited to problems whose solutions are discontinuous (see Petzold, 1982).

Other methods of solving DAE's are the so-called Runge-Kutta methods. The (semi-) implicit forms of these methods were originally developed for solving (very) stiff ODE systems. Efficient semi- or fully-implicit Runge-Kutta methods use one Jacobian evaluation and LU decomposition per step and solve one or more subsequent systems of linear equations.

The first publication on solving sets of differential algebraic equations (DAE's) was by Gear (1971), who solved them using adapted codes for solving ordinary differential equations (ODE's). His results were put into the code ODEPACK (Hindmarsh, 1983). Michelsen (1976) proposed a new implicit Runge-Kutta method; a Semi-Implicit Runge-Kutta (SIRK) method which was used by Holland and Liapis (1983) for dynamic column simulations. Petzold (1982) was the first to systematically describe and classify difficulties with DAE's according to the differential index of the system. This index equals the number of times the algebraic equations need to be differentiated (with respect to time) to obtain a set of only differential equations (thus, an ODE system is a DAE with index 0). The solution with higher index systems was analyzed for linear multistep methods such as the backward difference formulas (BDF). These methods are used in codes such as DASSL (Petzold, 1983) and LSODI (Hindmarsh, 1981).

For process systems Pantelides (1988) developed a structural approach for higher index problems and calculation of initial conditions. These concepts have been incorporated into the SPEEDUP dynamic simulator (Pantelides *et al.*, 1988). Some index two systems are solved by DASSL through modified error criteria to allow for more efficient stepsize algorithms. To handle index one problems that arise in process problems, Holl *et al.* (1988) developed the DIVA dynamic simulator. Finally, Bachmann *et al.* (1989) developed proper reformulation techniques and discussed numerical difficulties that arise if DAE systems are reformulated incorrectly. For simultaneous solution of Differential Algebraic Optimization Problems (DAOP), however, only self-starting methods (such as Runge-Kutta) can be considered. Petzold (1986) showed that some Runge-Kutta methods can suffer order reduction for index one problems. Brenan and Petzold (1987) extended this approach to consider the order, stability and convergence of Implicit Runge-Kutta (IRK) applied to higher index DAE systems. Burrage and Petzold (1988) further refined the convergence and stability properties of index one systems solved by IRK methods. Along with Brenan and Petzold (1987), they showed that orthogonal collocation on finite elements, an A-stable IRK method, is sufficiently stable and quite accurate for index one problems. Biegler gives a discussion on solving DAE's and DAOP. Roche (1989) applied the IRK methods for solving DAE systems as was done before with SIRK methods (Holland, 1983).

Disadvantages of BDF methods (in comparison with Runge-Kutta methods) are that they are not self starting (previous solutions are required), some iteration is required (with the inevitable chance of convergence failure), the code is more complicated, and the stepsize is not as simple to compute as it is for the Runge-Kutta methods. However, the advantages, such as a simple truncation error estimation, and a reduced number of function (and derivative) evaluations required per step (compared to RK methods) made the BDF methods more popular over the RK methods. However, for higher index problems or problems with discontinuities, only the RK methods are successful as most BDF codes will usually fail

(Gear and Petzold, 1984). It may also not be trivial to obtain initial values for all of the components of \mathbf{y} and \mathbf{y}' . As initialization is a problem for solving dynamic column simulations, together with the possible discontinuity problems caused by property routines, Runge-Kutta methods were selected in this work for integration. Order reductions for the RK methods have been found (Petzold, 1986) and care must be taken to avoid these situations. As mentioned earlier, general problems solving DAE systems are the error estimate problem and discontinuities. Furthermore, it is very important that sparsity is utilized for Jacobian calculations, since these tend to be computer time consuming.

The approach used here (referred to as BESIRK, see Appendix D) consists of a semi-implicit Runge-Kutta method developed originally by Michelsen (1976) but which is extended with an extrapolation technique (Bulirsch and Stoer, 1966) to improve the efficiency in solving DAE problems. This is similar to methods by Bader and Deuffhard (1983) and Deuffhard *et al.* (1987) as described in Hairer (1991,1994). One of the limitations of the BESIRK implementation is the fact that the differential terms must have constant coefficients. It is for this reason that molar holdups are used as model variables instead of molar compositions. The differential-algebraic system is rewritten in the form:

$$\mathbf{B}\mathbf{y}' = \mathbf{f}(t, \mathbf{y}) \quad (4.83)$$

where \mathbf{B} is a matrix of constant coefficients with a empty row for each algebraic equation. This also facilitates solving the steady-state problem since then the left hand side becomes the null vector and the Newton's method can use the same function vector \mathbf{f} .

The models are set up in a specific manner so that we can easily switch between solving steady-state and dynamic problems. This allows us to use the dynamic model as a relaxation method for solving steady-state problems (cf. Gani and Cameron, 1989). A dynamic simulation starts with a steady-state simulation using Newton's method. Special care must be taken for the Newton iterations to limit changes in specific variables (for example in preventing holdups to become negative). If the design mode was enabled, a second steady-state simulation is done upon convergence, but with a rationalized design. The results are saved and a perturbation is read from the input file. The dynamic simulation starts with all the variables initialized with the steady-state values. Certain perturbations restrict changes in some of the model variables in order to maintain the integrity of the DAE system (the algebraic equations must be satisfied, within tolerance). BESIRK is started and the system is integrated until the time of the following perturbation is reached, or, the variables do not change by more than a predefined fraction (here, 10^{-3}). If a new perturbation is present the dynamic simulation restarts at that time, otherwise a switch to the steady-state simulation is initiated after which the simulation terminates.

The system of model equations is sparse since each stage is usually only connected with the stage below and the stage above. To exploit this sparsity of the problem and to solve it efficiently we use the NSPIV sparse solver (Sherman, 1978). NSPIV does not save LU factors and cannot exploit the fact that multiple linear systems with the same matrix need to be solved. However, solving the sparse linear systems is isolated in one routine to easily switch to other sparse solvers.

To employ a BDF or (semi) implicit Runge-Kutta method we need the Jacobian of the right hand side of all the equations. This information is computed from analytical expressions with the exception of the enthalpies, heat transfer coefficients (4.19, 4.20), rate equations (4.25, 4.26), holdup equations (4.29-4.32),

and pressure drop derivatives (4.28). Obtaining an “analytical” Jacobian can be cumbersome but with a numerically computed Jacobian (by finite differencing) the integration becomes rather slow (even when exploiting the sparsity of the system). Furthermore, the accuracy of the Jacobian can be very important for SIRK methods and in finding the exact location of discontinuities. BESIRK updates the Jacobian for each integration but retains a copy of the Jacobian to use for each consecutive approximation in order to save Jacobian evaluations (see Appendix D).

The program keeps track of the index of the system of equations. This index indicates the number of times the algebraic constraints have to be differentiated with respect to the independent variable (time) to produce a system of only ordinary differential equations. Higher index problems are usually more difficult to solve. BESIRK signals a warning message when the index is higher than one (BESIRK tests if one of the derivatives $\partial f^y / \partial y$ is zero. If so, it tries to find substitutions from other algebraic equations that would make the derivative nonzero. If this is not possible the index is considered higher than one and Jacobian information is used to obtain an estimate of the index). BESIRK is successful in solving some systems of higher index.

Implementation of the model is done in a modular manner to allow for easy extension or modification of the equations. Each type of stage (condenser, tray, reboiler) has routines for:

1. Setting indices for variables and equations
2. Returning variable and equations identifiers
3. Initialization of variables (from the initial guess)
4. Obtaining results from variable vector
5. Setting matrix entries for the differential terms
6. Steady-state simulation variable updating
7. To return leaving stream variables with their indices
8. Function and Jacobian evaluations
9. Numerical evaluation of specific parts of the Jacobian
10. Adapting variables for perturbations

In addition there are routines for coordinating the exchange of stream information between stages. Only these routines, together with the main routine for function value evaluation need to be aware of all the different types of stages. This modular (or “object-oriented”) approach allows addition of different types of stages without requiring changes to the existing code.

In the dynamic simulator the condenser and reboiler have design routines similar to the trays. They design the molar holdup in the condenser and reboiler to equal 5 minutes of steady-state in-flow. Therefore, the size of the condenser and/or reboiler does not need to be specified.

In both steady-state and dynamic simulation the problem is solved as *one* system of equations as is done in equation oriented flowsheet solvers. Each routine only calculates stage sub-vectors of the variable vector and sub-matrices of the Jacobian. The sub-matrices are copied into the complete Jacobian matrix, which is stored as a sparse matrix.

At each report step during the integration the complete variable vector is copied to disk for later retrieval. Thus, a simulation which is stopped can also be continued from the simulation time at which it was interrupted. Routines returning the variable (and equation) identifiers facilitate in the reporting of the simulation as well as in providing debug facilities.

Symbol list

a	Interfacial area (m^2)
A	Area (m^2)
B	Bottoms flow rate ($kmol/s$)
c	Concentration ($kmol/m^3$)
	Number of components
D	Distillate flow rate ($kmol/s$)
E	Energy holdup ($J/kmol$)
F	Feed flow rate ($kmol/s$)
G	Interlinking flow rate ($kmol/s$)
h	Liquid height (m), Heat transfer coefficient ($W/m^2/K$)
H	Enthalpy ($J/kmol$)
k	Binary mass transfer coefficient ($kmol/m^2/s$)
K	Equilibrium constant = y/x
L	Liquid flow rate ($kmol/s$)
M	Molecular weight ($kg/kmol$)
N	Mass transfer rate ($kmol/s$)
n	Number of stages
p	Pressure (Pa)
Q	Heat input (J/s)
r	Sidestream flow ratio
R	Mass transfer rate matrix defined by (2.13,2.14), Reflux flow rate ($kmol/s$)
RR	Reflux Ratio = R/D
T	Temperature (K)
U	Molar holdup ($kmol$)
V	Vapor flow rate ($kmol/s$)
w	Weep flow ratio
x	Liquid mole fraction

y Vapor mole fraction

Greek:

Φ Fractional entrainment
 ϕ Fugacity coefficient
 ϵ Energy transfer rate (J/s)
 γ Activity coefficient
 Γ Thermodynamic matrix defined by (2.12)
 δ_{ij} Kronecker delta
 Δp Pressure drop (Pa)
 ξ Murphree vapor efficiency

Superscript:

a Holdup above froth and downcomer
 b Bubbling area plate
 cl Clear liquid
 d Holdup in downcomer,
Downcomer
 $drum$ Reflux drum
 f Froth
 I Interface
 L Liquid
 t Top
 ts Tray spacing
 V Vapor

SubScript:

b Bottom
 c Condenser
 i Component i
 j Stage j
 r Reboiler
 $spec$ specified
 t Total
 ν from interlined stage ν

Abbreviations:

DAE Differential-Algebraic-Equations
DS Dynamic Simulation/State
SS Steady-State

References

- R. Bachmann, L. Brull, Th. Mrziglod, U. Pallaske, "On Methods for Reducing the Index of Differential Algebraic Equations", *Comp. Chem. Engng.*, Vol. 14, No. 11 (1990) pp. 1271–1273.
- G. Bader, P. Deuffhard, "A semi-implicit mid-point rule for stiff systems of ordinary differential equations", *Numer. Math.*, Vol. 41, (1983) pages 373–398.
- K.E. Brenan, L.R. Petzold, "The Numerical Solution of Higher Index Differential/Algebraic Equations by Implicit Methods", *SIAM J. Numer. Anal.*, Vol. 26, No. 4, (1987) pp. 976–996.
- R. Bulirsch, J. Stoer, "Numerical treatment of Ordinary Differential Equations by Extrapolation Methods". *Num. Math.*, 8, (1966), pp. 1–13.
- K. Burrage, L.R. Petzold, "On Order Reduction for Runge-Kutta Methods Applied to Differential/Algebraic Systems and to Stiff Systems of ODE's", *SIAM J. Numer. Anal.*, Vol. 27, No. 2, (1988) pp. 447–456.
- P. Deuffhard, E. Hairer, J. Zugck, "One-step and extrapolation methods for differential-algebraic equations", *Numer. Math.*, Vol. 51, (1987) pp. 501–516.
- R. Gani, I.T. Cameron, "Extension of Dynamic Model of Distillation Columns to Steady-State Simulation", *Comp. Chem. Eng.*, Vol. 13, No. 3 (1989) pp. 271–280.
- C.W. Gear, "Simultaneous numerical solution of differential-algebraic systems", *IEEE Trans. Circ. Theory*, Vol. CT-18, No. 1, (1971) pp. 89–95.
- G.W. Gear, L.R. Petzold, "ODE Methods for the Solution of Differential/ Algebraic Systems", *SIAM J. Numer. Anal.*, Vol. 21, No. 4, (1984) pp. 716–728.
- E. Hairer, S.P. Norsett, G. Warner, *Solving Ordinary Differential Equations I. Nonstiff Problems*, 2nd Ed., Springer-Verlag, Berlin (1994).
- E. Hairer, G. Warner, *Solving Ordinary Differential Equations II. Stiff and Differential-Algebraic Problems*, Springer-Verlag, Berlin (1991).
- A.C. Hindmarsh, "LSODE and LSODI, Two New Initial Value Ordinary Differential Equation Solvers", *ACM Signum Newsletter*, 14, 4 (1980).
- A.C. Hindmarsh, "ODEPACK, a Systemized Collection of ODE Solvers", *IMACS Trans. Scient. Comp.*, 1, Ed. W.F. Ames, R. Vichnevetsky, North-Holland, Amsterdam, (1983) pp. 65–68.
- P. Holl, W. Marquardt, E.D. Gilles, "DIVA — A Powerfull Tool for Dynamic Process Simulation", *Comp. Chem. Eng.*, Vol. 12 (1988) pp. 421–426.
- M.L. Michelsen, "An Efficient General Purpose Method of Integration of Stiff Ordinary Differential Equations", *AIChE J.*, Vol. 22, No. 3, (1976) pp. 544.
- C.C. Pantelides, "SPEEDUP — Recent Advances in Process Simulation", *Comp. Chem. Eng.*, Vol. 12 (1988a) pp. 745–755.
- C.C. Pantelides, D. Gritsis, K.R. Morrison, R.W.H. Sargent, "The Mathematical Modeling of Transient

Systems using Differential-Algebraic Equations”, *Comp. Chem. Eng.*, Vol. **12**, No. 5 (1988b) pp. 449–454.

L.R. Petzold, “Differential/Algebraic Equations are not ODE’s”, *SIAM J. Sci. Stat. Comput.*, Vol. **3**, No. 3, (1982) pp. 367–384.

L.R. Petzold, “A Description of DASSL: a Differential/Algebraic System Solver”, *IMACS Trans. Scient. Comp.*, **1**, Ed. W.F. Ames, R. Vichnevetsky, North-Holland, Amsterdam, (1983) pp. 65–68.

L.R. Petzold, “Order results for implicit Runge-Kutta methods applied to differential/algebraic systems”, *SIAM J. Numer. Anal.*, Vol. 23, No. 4, (1986) pp. 837–852.

M. Roche, “Implicit Runge-Kutta Methods for Differential/Algebraic Equations”, *SIAM J. Numer. Anal.*, Vol. **26**, No. 4, (1989) pp. 963–975.

A.H. Sherman, “NSPIV, a FORTRAN subroutine for sparse gaussian elimination with partial pivoting”, *ACM Trans. Math. Software*, Vol. **4** (1978) pp. 391–398.

R. Taylor, H.A. Kooijman, M.R. Woodman, “Industrial Applications of a Nonequilibrium Model of Distillation and Absorption Operations”, *I.Chem.E. Symp. Ser.*, No. 128, Birmingham UK (1992) pp. A415–427.

R. Taylor, H.A. Kooijman, J-S. Hung, “A Second Generation Nonequilibrium Model for Computer Simulation of Multicomponent Separation Processes”, *Comp. Chem. Eng.*, Vol **18**, No. 3, (1994) pp. 205–217.

Chapter 5

Simulation Results

This chapter contains simulation results with the previously discussed dynamic models. Nonequilibrium model results indicate that the equilibrium model should not be used for the dynamic simulation. It cannot predict the changes in individual component efficiencies of nonideal separations, neither predict the changes in separation accompanied with operation close to flooding or below the weep point, nor simulate columns where the vapor and liquid might differ in temperature.

Using multicomponent diffusion calculations influences the steady-state simulation results but they do not affect the dynamic behavior of columns. This is in contrast to the use of different mass transfer coefficient correlations which have differing dynamic characteristics. Dynamic studies might actually be used to provide insight in the fundamental basis of the mass transfer coefficient correlations as well as that for interfacial areas.

Tray layout parameters may have a profound effect on the dynamic performance of the column. The effects of different tray design parameters on the mass transfer can only be modeled with a nonequilibrium model. Equilibrium model simulations can only take tray hydrodynamics into account, but the influence of the hydrodynamics on the tray performance is not accounted for.

Attempts to reduce the computer time by neglecting certain derivative information is shown to be counter-productive.

5.1 Steady-State Simulations

It is important to recognize that steady-state results for the dynamic nonequilibrium model described in the previous chapter are the same as the those from the steady-state implementation by Taylor *et al.* (1994) of Chapter 2, even though the model equations differ in form and number. This served as a check

Table 5.1: BTX Distillation Column Specifications

	Steady-State	$t = 0s$	$t = 600s$
Feed (mol/s):			
benzene	40	40	30
toluene	40	40	30
p-xylene	20	20	15
Reflux ratio	3	3	4
Reboil ratio	3	4	4

for the correctness of the new model equations. Steady-state results can be obtained by solving the dynamic model using Newton's method and setting the derivative terms to zero **or** by finding the final state of a dynamic simulation when none of the variables is changing.

Since the dynamic model uses full Jacobian evaluations with respect to all of the variables – in contrast to the steady-state implementation which only used composition derivatives of the rate equations – convergence usually improved in terms of number of iterations. However, more time per iteration is required for the evaluation of the Jacobian (due to the numerical evaluation of parts of the Jacobian and the increased number of variables). The use of holdups as variables also complicates finding the steady-state solution somewhat since the sum of the component holdups and the total holdup have to be equal. In the case where the initial guess is not very good this might cause problems and the changes in the holdups must be constrained.

The results of the two different dynamic equilibrium models (EQL and EQLV) are very similar, as the holdup of the vapor in the froth usually is small compared to that of the liquid (the differences show at higher pressures). Therefore, we have only included simulations of the EQLV model in order to use the same number and type of holdups when comparing the equilibrium and the nonequilibrium model.

5.2 Design mode

To illustrate the combination of a steady-state column design and a dynamic simulation with multiple perturbations a 28 valve tray column separating benzene, toluene and p-xylene is simulated. The feed is introduced at the middle of the column. UNIFAC and Antoine correlations were used to model the liquid thermodynamics and the Peng-Robinson equation of state for the vapor, including the excess enthalpies. Table 5.1 lists the steady-state feed flows, boilup ratio, and reflux ratios used to design the valve tray column. The column is initially perturbed by a change in the reboiler boilup ratio and after ten minutes by an increment of the reflux ratio in combination with a decrease of the total feedflow (to prevent the column from flooding). No difficulties were encountered with the integration of this example.

The column condenser operated at 1.2 *bar*, and the pressure drop in the column was calculated. The

feed pressure was 1.4 *bar* and the compositions were kept constant. The only mass transfer coefficient model available for valve trays is the AIChE model. The steady-state simulator automatically sized the column stripping and rectification sections as well as the total condenser and the partial reboiler. The column tray design was based on a fraction of flooding of 75%, resulting in a two pass 2.3 *m* column in the rectification section and a three pass 2.7 *m* column in the stripping section (with flowpath lengths of about 1 *m*).

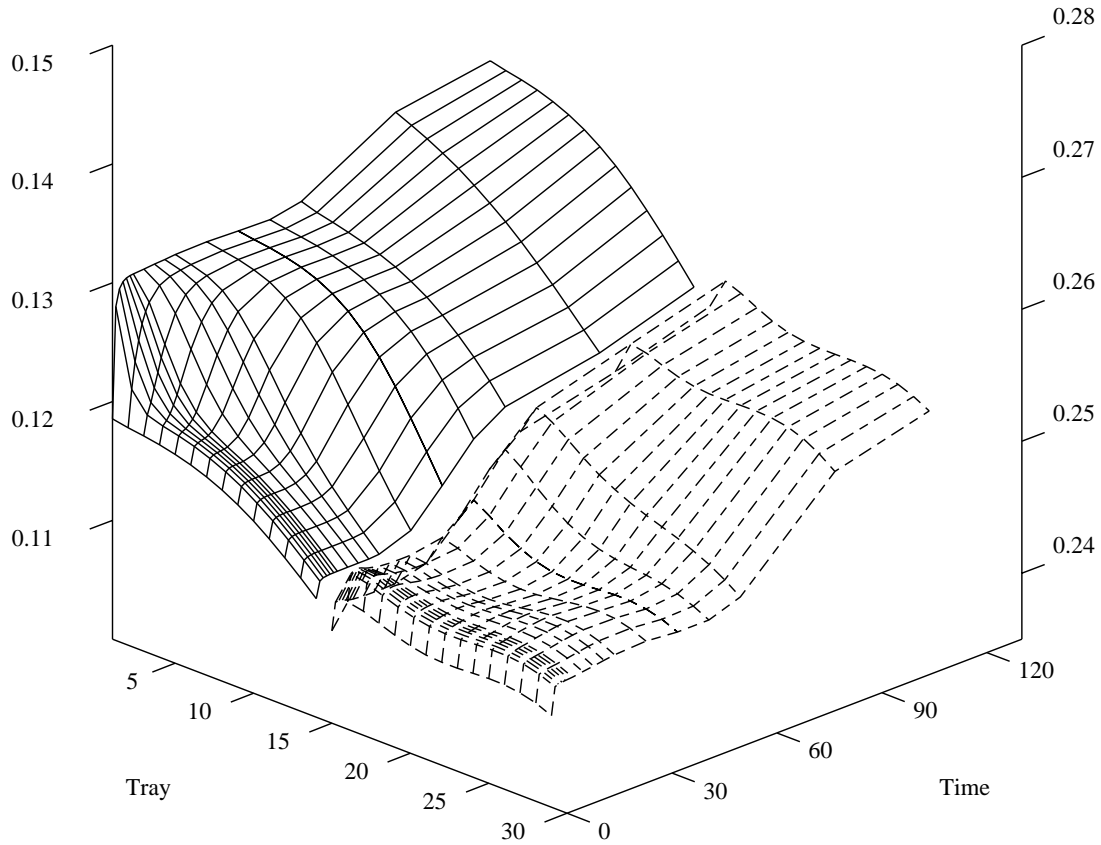


Figure 5.1: BTX distillation column internal liquid flows (kmol/s) as function of time (s) after increasing the boilup ratio. Flows in the rectification section (solid lines) use the left axis and the flows in the stripping section (dashed lines) use the right axis.

Internal liquid flows from the initial disturbance are plotted in Figure 5.1. The liquid flow profiles have been split into two parts, since the feed is a saturated liquid resulting in higher liquid flow rates in the stripping section of the column. The sudden increase of boilup ratio causes an increase in the vapor flow leaving the reboiler. This disturbance reaches the condenser very quickly as the vapor residence time on the trays is very short. Because the reflux ratio is fixed, the liquid reflux flow starts to increase. The residence time of the liquid on the trays is much higher and it takes about a minute for the increased liquid flows to reach the reboiler where it causes a new increase in the reboiled vapor flow. This, in turn, causes another increase in the vapor condensed in the condenser and refluxed to the column. But by that time, the perturbation has become smoother and after some time it disappears.

After 10 minutes the reflux ratio is increased and the total feed flow is reduced at the same time. Initially, this causes the refluxed liquid from the condenser to increase immediately and in turn the liquid flows in the rectification section. Because the feed is a saturated liquid the decrease of the total feed flow decreases the liquid flows in the stripping section. These changes work their way down the column. At the time the reboiler receives less liquid the vapor flows decrease as well. The vapor flow change reaches the condenser very quickly and the refluxed liquid flow rate starts to decrease as well. It continues to decrease until the increased liquid flow created by the initial reflux ratio change reaches the bottom of the column and gets vaporized. The result is several oscillations in the internal liquid and vapor flows which die out quickly.

5.3 Equilibrium Versus Nonequilibrium

Here we explore the differences between the dynamic results of equilibrium models and those of nonequilibrium models. Three examples have been simulated, an extractive distillation column, an acetone absorber, and a debutanizer adapted from Gani (1986). For comparison purposes the EQLV equilibrium model and the NEQ2H nonequilibrium models were used unless stated otherwise.

5.3.1 Extractive Distillation

Our first example is an extractive distillation column which separates n-heptane and toluene using phenol as extractive agent. Temperature sensors often are used to control this kind of extractive distillation column. Thus, we are interested in the differences in temperature profiles between equilibrium and nonequilibrium simulations of this type of column.

The simulated column has 29 sieve plates, a partial reboiler, and a total condenser. The column has a 50/50 mol% feed of toluene and n-heptane at stage 20 (counting from the top, including the condenser as the first stage) and a phenol feed at stage 10 which is three and a half times larger than our original feed. The phenol makes the n-heptane more volatile than the toluene and the distillate purity is about 98.5 mole%. The tray design was automatically generated by the nonequilibrium model (based on a design criterion of 75% fraction of flooding). The same sieve tray design was taken for all the simulations to

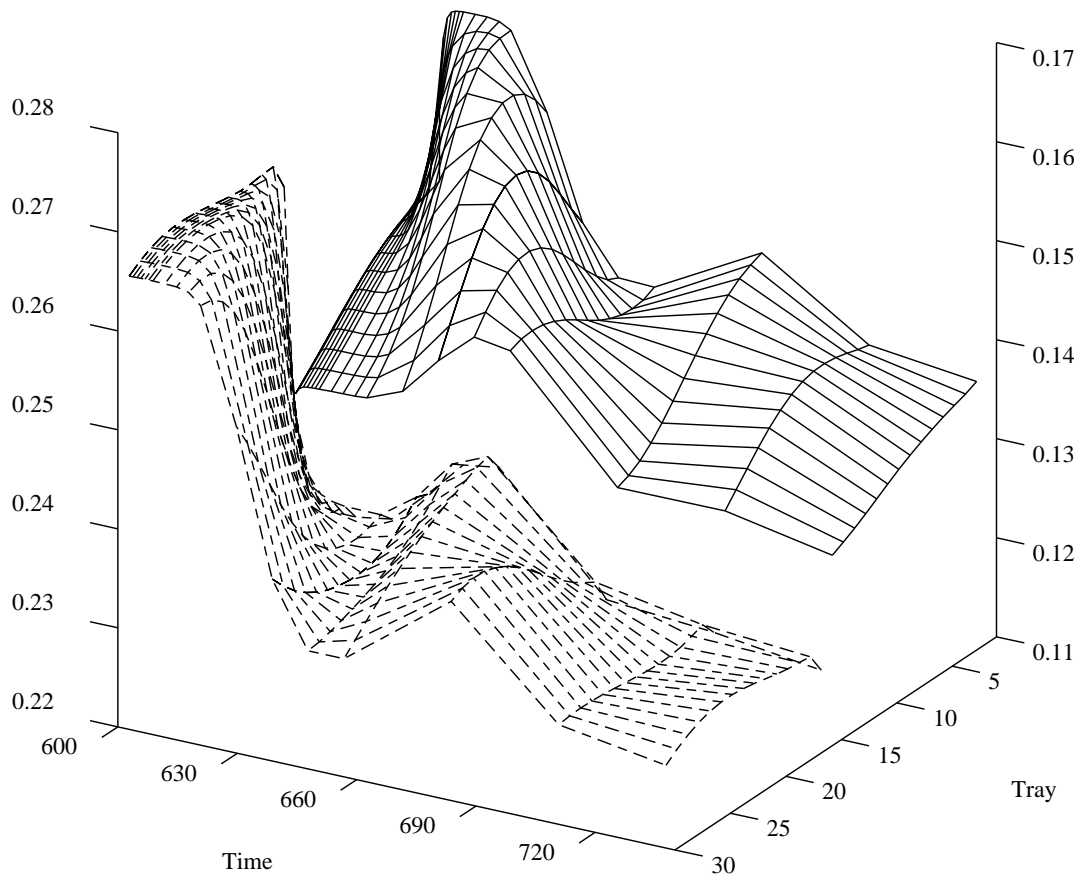


Figure 5.2: BTX distillation column internal liquid flows ($kmol/s$) after increasing the reflux ratio and decreasing the feed flow simultaneously. Flows in the rectification section (solid lines) use the right axis and the flows in the stripping section (dashed lines) use the left axis.

compare the results for the various models. The AIChE model was used for calculation of the mass transfer coefficients. The condenser and reboiler holdup were set to account for a liquid holdup of about 5 minutes (at a reflux ratio of 5). See Table 5.2 for a summary of the specifications.

To compare the two types of simulation it is necessary to use a Murphree tray efficiency for the equilibrium model which is a back-calculated average from the nonequilibrium simulation. This is needed to

Table 5.2: Extractive Distillation Column Specifications

DECHEMA K model			
UNIQUAC model (parameters by UNIFAC)			
Antoine Vapor pressure			
Excess Enthalpy			
Condenser pressure 2.0 (<i>bar</i>)			
Top pressure 2.0 (<i>bar</i>)			
Estimated pressure drop			
Feed stage	10		20
Vapor fraction			0
Temperature ($^{\circ}C$)	170		
Component flows (<i>mol/s</i>)			
n-heptane	0		25
toluene	0		25
phenol	175		0
Total Condenser (stage 1):			
Reflux ratio = 5.0			
Molar holdup = 45.0 (<i>kmol</i>)			
Partial Reboiler (stage 31):			
Bottom product flow rate = 200.0 (<i>mol/s</i>)			
Molar holdup = 90.0 (<i>kmol</i>)			
Section	1	2	3
First stage	2	10	20
Last stage	9	19	30
Column diameter (<i>m</i>)	2.57	2.09	2.17
Total tray area (m^2)	5.19	3.43	3.70
Number of flow passes	3	2	2
Tray spacing (<i>m</i>)	0.5	0.5	0.5
Liquid flow path length (<i>m</i>)	0.717	0.778	0.753
Active area (% total)	86.8	82.0	77.8
Total hole area (% active)	12.1	9.8	9.6
Downcomer area (% total)	6.6	9.0	11.1
Hole diameter (<i>m</i>)	0.00476	0.00476	0.00476
Hole pitch (<i>m</i>)	0.0130	0.0144	0.0144
Weir length (<i>m</i>)	6.23	3.56	3.67
Weir height (<i>m</i>)	0.0508	0.0508	0.0508
Downcomer clearance (<i>m</i>)	0.0381	0.0381	0.0381
Deck thickness (<i>m</i>)	0.00254	0.00254	0.00254

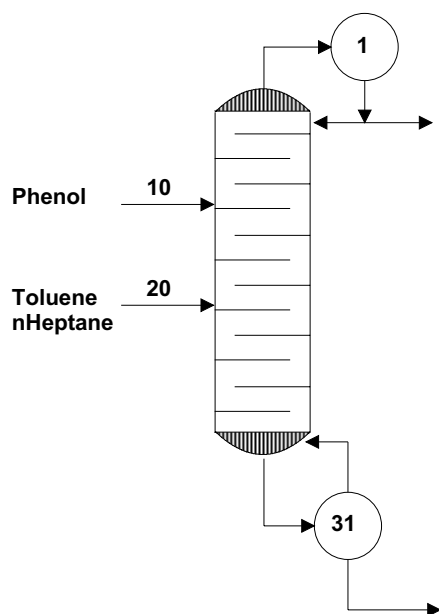


Figure 5.3: Extractive Distillation Column Configuration

obtain an equilibrium simulation with the same number of trays, and therefore, a comparable dynamic behavior. An equilibrium model with constant Murphree efficiency of 55 % for all the components gave similar products as those obtained in a nonequilibrium simulation.

The computed steady-state component Murphree efficiencies are shown in Figure 5.4. Notice that the component efficiencies are generally unequal and can vary outside the range from zero to one. Here, the efficiencies change radically and are very different from their average value, especially around the phenol feed. This is due to the fact that the phenol feed is subcooled (by about $40^{\circ}C$) for better separation, but it is still hotter than the internal flows at the feed tray. Therefore, the nonequilibrium model has a higher liquid temperature on the feed tray than the equilibrium model due to limited heat transfer with the vapor. This phenomena cannot be seen with the equilibrium model which assumes unlimited heat transfer.

The column was perturbed by decreasing the phenol feed temperature from 170° to $140^{\circ}C$. Computed Murphree efficiencies of the steady-state after this perturbation are shown in Figure 5.5. Note the differences with Figure 5.4. Since the efficiencies change over time the dynamic results computed with constant efficiencies in the equilibrium model become an approximation to the actual dynamic behavior.

The changes in the temperature profiles as a function of time for the equilibrium and nonequilibrium model are shown in Figure 5.6. There we can observe that the difference between the lines of the equi-

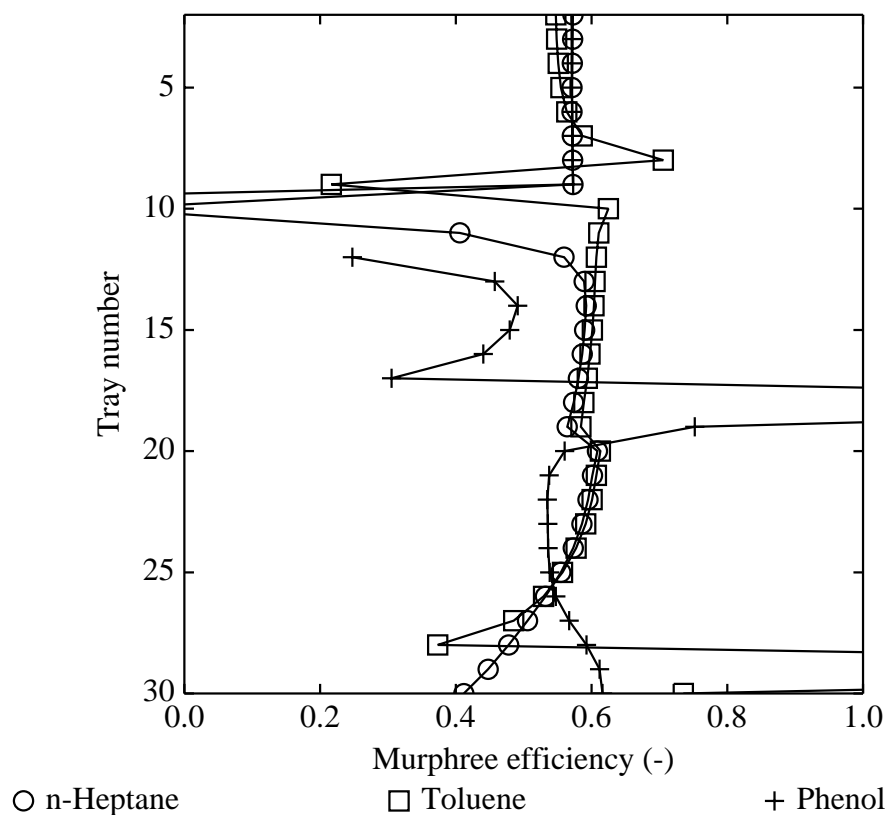


Figure 5.4: Murphree efficiencies backcalculated from nonequilibrium simulation for the extractive distillation of n-heptane and toluene with phenol.

librium model (dashed) and the nonequilibrium model (solid) can vary in a nonlinear fashion with time. This implies that the dynamic response for the temperatures on these plates is quantitatively and qualitatively different, with obvious implications for any control strategies derived from the simulations. The temperatures for the nonequilibrium model seem to fluctuate much less than those for the equilibrium model since mass and heat transfer limitations dampen the changes quicker. The fluctuations are due to the sudden increase in a cooler liquid flow going down the column, which will result in extra vapor being condensed below the phenol feed. When this extra liquid reaches the reboiler the vapor flow quickly rises (because the bottoms flow is constant) and so the internal liquid flow decreases. The vapor is condensed and partially returned to the column (since a reflux ratio was specified, and the condenser

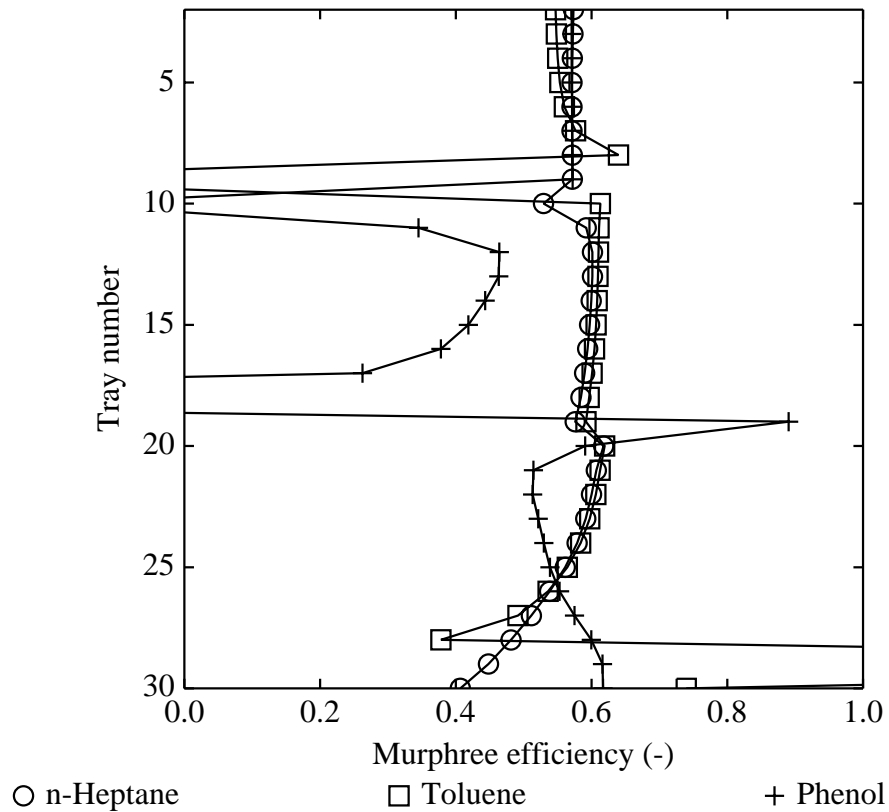


Figure 5.5: Murphree efficiencies backcalculated from nonequilibrium simulation for the extractive distillation after a drop in phenol feed temperature.

holdup is constant). This will send another wave of increased liquid flow down the column, but one that is smaller than the original one.

The liquid and vapor flows have been plotted as a function of time in Figures 5.7 and 5.8, respectively. Of course, with variable condenser and reboiler holdups the oscillations in the internal flows would be less pronounced or suppressed. But the initial wave of liquid down the column from the feed flow causes a nonlinear response which is quite different for both the models.

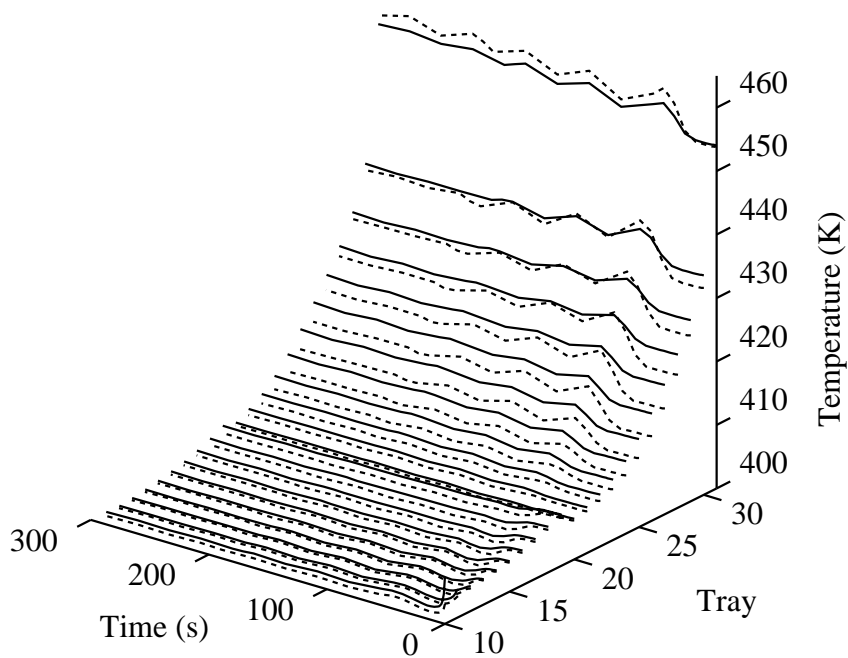


Figure 5.6: Temperatures (K) of trays 10 through 30 and the reboiler for the extractive distillation column as a function of time.

5.3.2 Acetone Absorber

The second example consists of a 30 sieve tray absorber in which acetone is to be absorbed in water from a vapor stream (specifications are given in Table 5.3). The column is perturbed by increasing the vapor feed temperature from 25 to 100°C. The column was simulated first with the nonequilibrium model (using the AIChE model for mass transfer coefficients) in design mode to obtain a suitable sieve-tray design and a back-calculated average Murphree efficiency (of 0.34) for the equilibrium simulation.

Initially the nonequilibrium model temperature profile (Figure 5.9) shows the typical bulge (of 2 to 3 °C)

Table 5.3: Acetone Absorber Specifications

DECHEMA K model		
NRTL Activity coefficient		
Antoine Vapor pressure		
Excess Enthalpy		
Top pressure 1.01325 (<i>bar</i>)		
Estimated pressure drop		
Feed stage	1	30
Pressure (<i>atm</i>)	1.0	1.0
Temperature (<i>°C</i>)	24.9	25.0
Component flows (<i>mol/s</i>)		
Nitrogen	0.0	10.0
Acetone	0.0	1.0
Water	40.0	0.0
First stage		1
Last stage		30
Column diameter (<i>m</i>)		0.42
Total tray area (<i>m</i> ²)		0.139
Number of flow passes		1
Tray spacing (<i>m</i>)		0.5
Liquid flow path length (<i>m</i>)		0.301
Active area (% total)		83.2
Total hole area (% active)		24.3
Downcomer area (% total)		8.4
Hole diameter (<i>m</i>)		0.00476
Hole pitch (<i>m</i>)		0.00907
Weir length (<i>m</i>)		0.373
Weir height (<i>m</i>)		0.0508
Downcomer clearance (<i>m</i>)		0.0381
Deck thickness (<i>m</i>)		0.00254

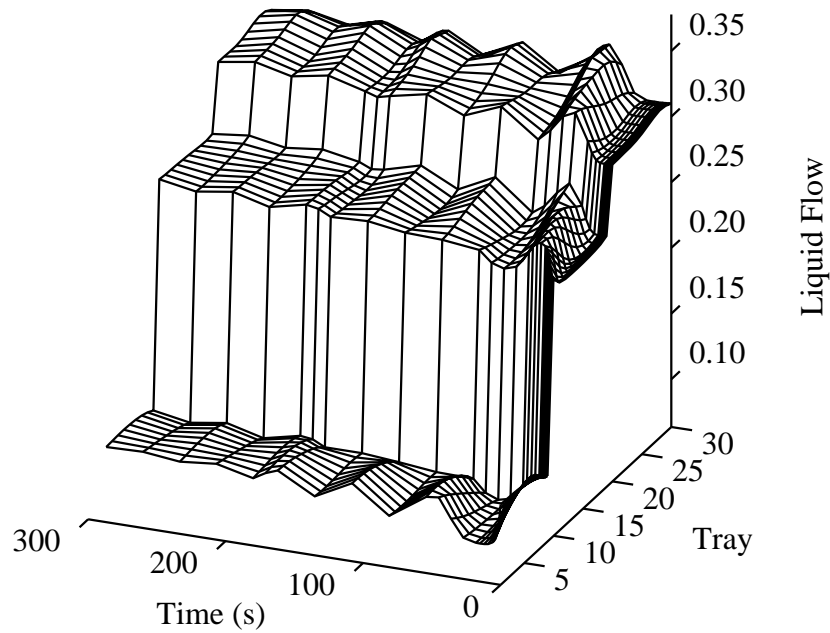


Figure 5.7: Internal liquid flows for the extractive distillation column.

caused by the heat of absorption of acetone in water and the evaporation of water in the bottom. After the vapor feed temperature increase the liquid temperatures in the column rise as well. The equilibrium model initially predicts a very similar temperature bulge at about the same tray (Figure 5.10). However after perturbation we see that the liquid temperature on the bottom tray quickly rises to a higher value than any of the tray above it. This is due to the assumptions that the temperature of the leaving flows on a tray have to be the same. Therefore, the model predicts that the vapor entering the bottom of the column, which has a temperature much higher than that of the liquid, is cooled down to the temperature of the liquid immediately. No heat transfer limitations are considered. The larger the difference in temperature between the vapor entering and the liquid leaving the column, the less appropriate is the assumption of thermal equilibrium between phases.

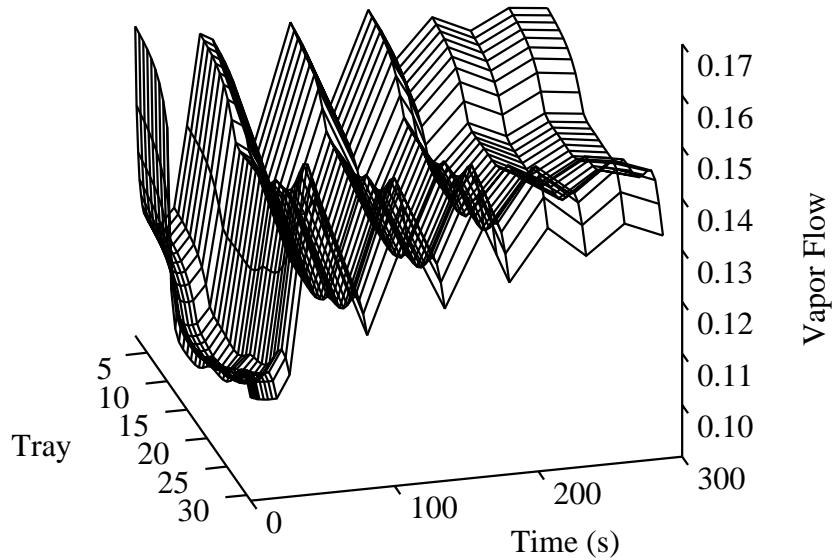


Figure 5.8: Internal vapor flows for the extractive distillation column.

Figure 5.11 shows the effects of the vapor temperature change for the concentration of acetone in the vapor leaving the column. Due to the lower temperatures in the column the change in acetone concentration is much less for the equilibrium model than that for the nonequilibrium model. Note that the response time is also different. Dynamic modeling of absorption columns like this can be important to ensure that environmental constraints are met at times even during temporary changes in vapor flow, temperature, and contamination levels. This can't be modeled with an equilibrium model if heat transfer plays an important role in the operation of the column. Furthermore, the nonequilibrium model has greater potential for modeling columns with trace components since mass transfer effects have a large influence on the efficiency of the trace components.

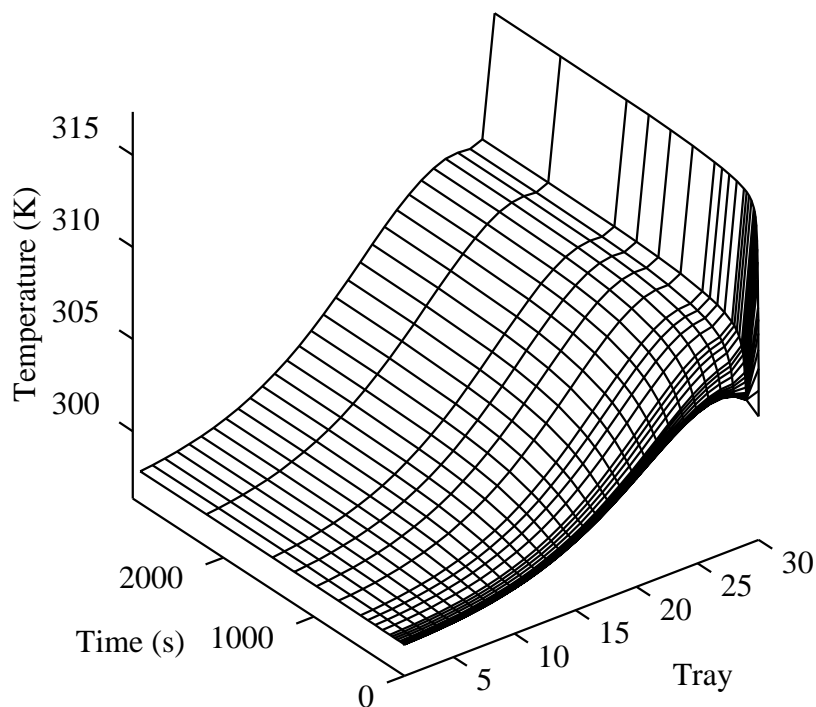


Figure 5.9: Temperature profiles for the acetone absorber simulated with the equilibrium model.

5.3.3 Debutanizer

This third example is an industrial debutanizer taken from Gani *et al.* (1986); it is their only example where sufficient tray design details and steady-state information are available to allow simulation with a nonequilibrium model. The valve tray column is 1.67 meter in diameter and they used a constant efficiency for all trays. The efficiencies, backcalculated from a steady-state nonequilibrium simulation, vary from 0.62 to 0.67 for the rectifying section and range from 0.68 to 0.77 in the stripping section. This compares very well with the average tray column efficiency of 0.7 reported by Gani *et al.* The column was perturbed with a 5 % increase in reflux rate keeping the reboiler duty constant. The simulated bottoms pressure corresponds very well with that reported by Gani (within 0.5 kPa). In Figure 5.12

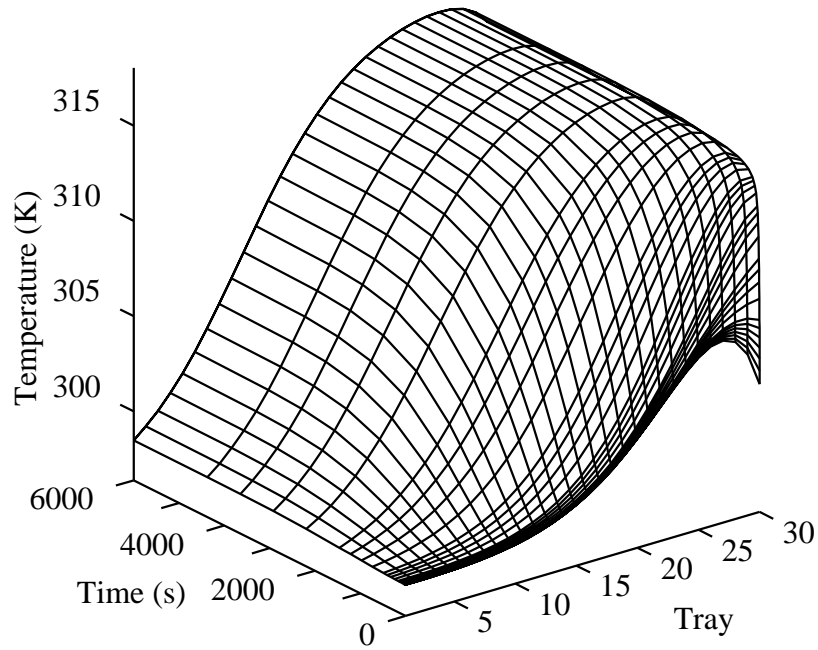


Figure 5.10: Temperature profiles for the acetone absorber simulated with the nonequilibrium model.

the liquid flows in the column are shown as a function of the time for both the nonequilibrium and the equilibrium model (comparable to the model of Gani *et al.*). The increased liquid flow perturbation moves down the column and passes the feed tray after about 3 minutes. From the tray profiles one can observe how the perturbation in the liquid flow becomes smoother as it moves down the column. The results of the two models are very similar in this case.

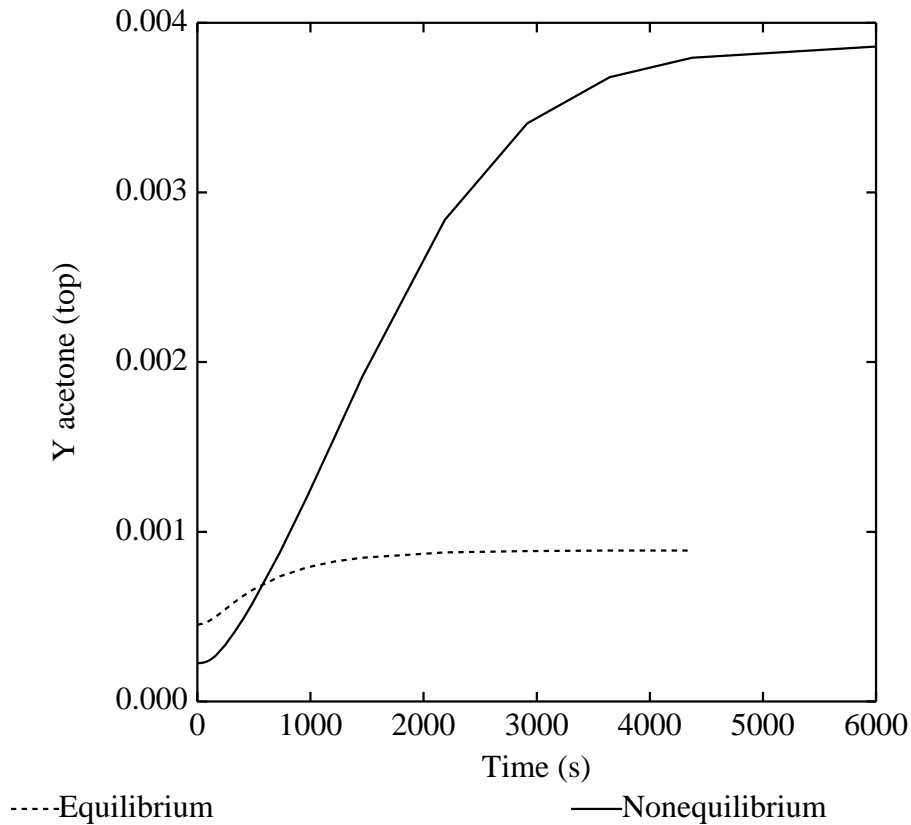


Figure 5.11: Molefraction of acetone of absorber off-gas as a function of time for the equilibrium (dashed line) and nonequilibrium (solid line) model.

5.4 Different Holdup Models

The different holdup models discussed in the previous chapter have different dynamic behavior. To illustrate this we use a depropanizer example taken from Taylor *et al.* (1994). A depropanizer column operates at a pressure of 15 *bar*, and shows the effects of the vapor holdups at high pressure. At these pressures the vapor holdups on and above the froth may be considerable and have to be properly modeled. Vapor holdup above the froth can be up to half as large as the combined liquid holdups on the tray and in the downcomer. Vapor holdup in the froth tends to be less than a tenth of the total liquid holdup and is less important. The downcomer liquid holdup varies with the size of the downcomer and

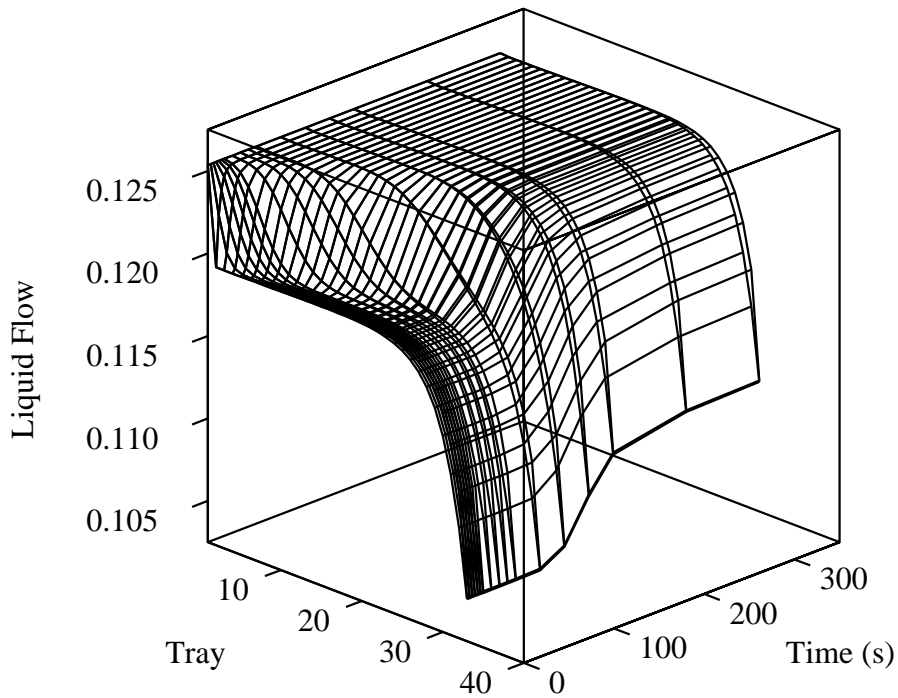


Figure 5.12: Liquid flows in Debutanizer

can be up to 50% of the liquid holdup on the tray. For this column the bottom flow rate is specified and the reflux ratio is increased from 2.5 to 4 at the start of the dynamic simulation. To check the effect of the inclusion of the vapor holdup above the froth two nonequilibrium simulations have been run, one with all the 4 holdups modeled separately and one with two holdups but with the downcomer liquid holdup lumped into one with the liquid holdup on the tray. The mass transfer is not influenced by this lumping (calculation of mass transfer coefficients and interfacial area are computed independent of the holdup). Figure 5.13 shows the temperatures on three trays (12, 15, and 18) as a function of the time (the solid lines are for the 4 holdup model). Note the logarithmic time scale. It is apparent that the inclusion of the vapor holdup above the froth is significant as the transients converge slower towards the steady-state values (as they should with more total holdup in the column). Naturally, this has consequences for the

time constants of the column and controller parameters derived from open-loop simulations.

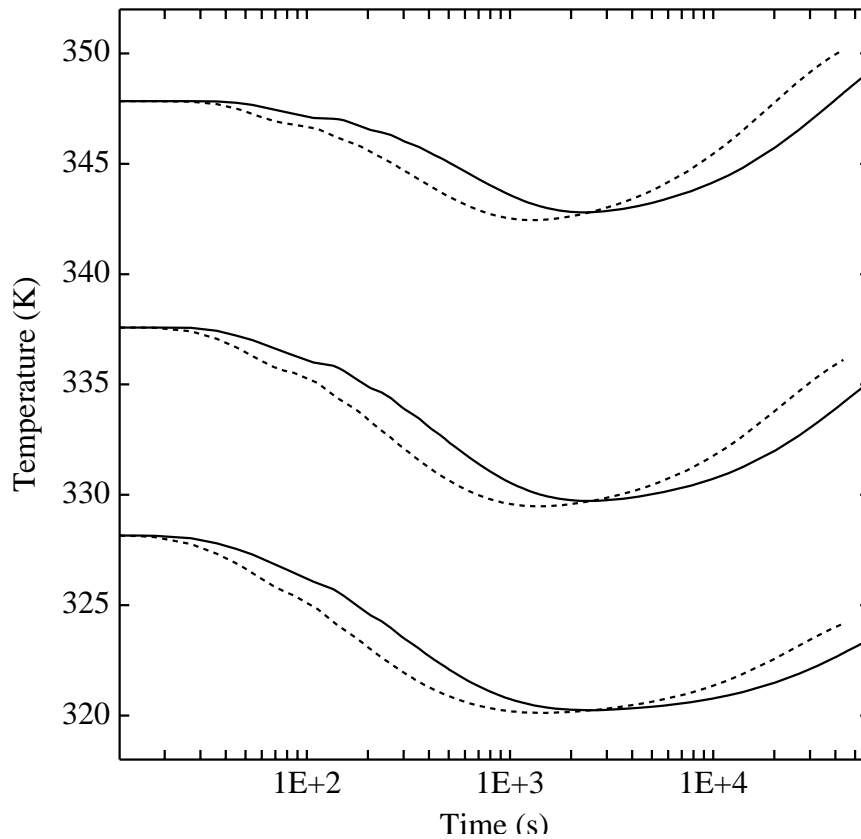


Figure 5.13: Temperatures of trays 12, 15, and 18 in a depropanizer modeled by the nonequilibrium model with 2 holdups (dashed lines) and the 4 holdup model (solid lines), after an increase in the reflux ratio.

The effects on the n-butane concentration in the distillate and that of propane in the bottoms is shown in Figure 5.14 and 5.15. The mole fractions are plotted for the equilibrium model without lumping and with lumping the liquid in the downcomer as well as for the nonequilibrium model with two and four holdups (with downcomer liquid lumping or constraining the vapor holdup above the froth, respectively). For all holdup models the steady-state values are the same at the begin and end, and for models with lumped holdups the mole fractions lag behind those of the non-lumped models. The figures also

show quantitative differences in the transients of equilibrium and nonequilibrium models. In both cases the equilibrium model predicted higher mole fractions for the impurities. Figure 5.15 shows that the nonequilibrium transient of propane mole fraction in the bottoms of the two holdup model differs qualitatively from that of the four holdup model. For the two holdup model we see first an increase in the mole fraction followed by a decrease to the new steady-state value, in contrast to the four model holdup which decreases monotonically. The difference between the two models is that the four holdup model does take into account the vapor holdup above the froth. Apparently, it is wrong to neglect to model the vapor above the froth at high pressures, as in this case. Note that transient of the four holdup model which constrains the vapor holdup above the froth to remain constant is quite different from the transient of the model which allows it to vary. The nonequilibrium model takes longer to reach steady-state than the equilibrium model, and the four holdup model takes longer than the two holdup model.

5.5 Mass Transfer Coefficients Models

In chapter 3 we saw that different Mass Transfer Coefficient (MTC) correlations can predict different column performances. Here we investigate their effects on the column dynamics of a nonideal separation with an example from Krishnamurthy and Taylor (1985), with the mixture methanol/i-propanol/water (see Figure 5.16, and Table 5.4). The final steady-state solution is the same as in their paper, but it is initiated from a steady-state with an i-Propanol feed mole fraction of 0.006 while the total feed flow is kept constant.

The four mass transfer models of chapter 3 are used to simulate the side-draw column where the feed flowrate of propanol is increased from 1 to 1.5 $kmol/s$. The results are shown in Figure 5.17 where the propanol mole fraction on the 25th tray are plotted as unction of the time. Initial and final steady-state concentrations are different for each model, as is to be expected. However, the dynamic behavior is quite similar. Only the Chan-Fair model shows some difference in its transient.

5.6 Mass Transfer Sensitivity

Mass transfer coefficients and interfacial area's are not (yet) very accurately known, which has led to some criticism of the use of nonequilibrium models. To investigate the effects of variations in the mass transfer coefficients and interfacial area, we multiply these with constants what can be varied. We look at the effects on the transients of the mole fraction propanol on the 25th tray of the propanol side-draw column using the Chan-Fair model. Naturally, the steady-state values change if we vary the constants. To compare the results, we scale the change so that the initial and final values coincide.

In Figure 5.19a and b the interfacial area is decreased, respectively increased by 50%, and the transients are correspondingly slower and faster. Similarly in Figure 5.20a/b both vapor and liquid mass transfer coefficients are decreased/increased by 50%. In Figure 5.21a and b the vapor respectively liquid mass

Table 5.4: Methanol/i-propanol/water Column Specifications

DECHEMA K model		
UNIQUAC Q'		
Antoine Vapor pressure		
Excess Enthalpy		
UNIQUAC parameters	Aij	Aji
Methanol-Isopropanol	-49.38165	62.04005
Methanol-Water	-102.9364	191.4061
Isopropanol-Water	431.6771	23.03152
Column pressure 1.0 (bar)		
	Initial	New
Feed stage	13	13
Pressure (bar)	1.0	1.0
Vapor fraction	0.0	0.0
Component flows (mol/s)		
Methanol	3.333	3.333
Isopropanol	0.05	1.667
Water	4.95	3.333
Total Condenser (stage 1):		
Reflux ratio = 5.0		
Molar holdup = 6.0 (kmol)		
Partial Reboiler (stage 31):		
Reboil ratio = 5.0		
Molar holdup = 6.696 (kmol)		
First stage		2
Last stage		29
Column diameter (m)		0.586
Total tray area (m ²)		0.27
Number of flow passes		1
Tray spacing (m)		0.55
Liquid flow path length (m)		0.467
Active area (% total)		88.9
Total hole area (% active)		19.1
Downcomer area (% total)		5.3
Hole diameter (m)		0.00476
Hole pitch (m)		0.0104
Weir length (m)		0.513
Weir height (m)		0.0508
Downcomer clearance (m)		0.0381
Deck thickness (m)		0.00254

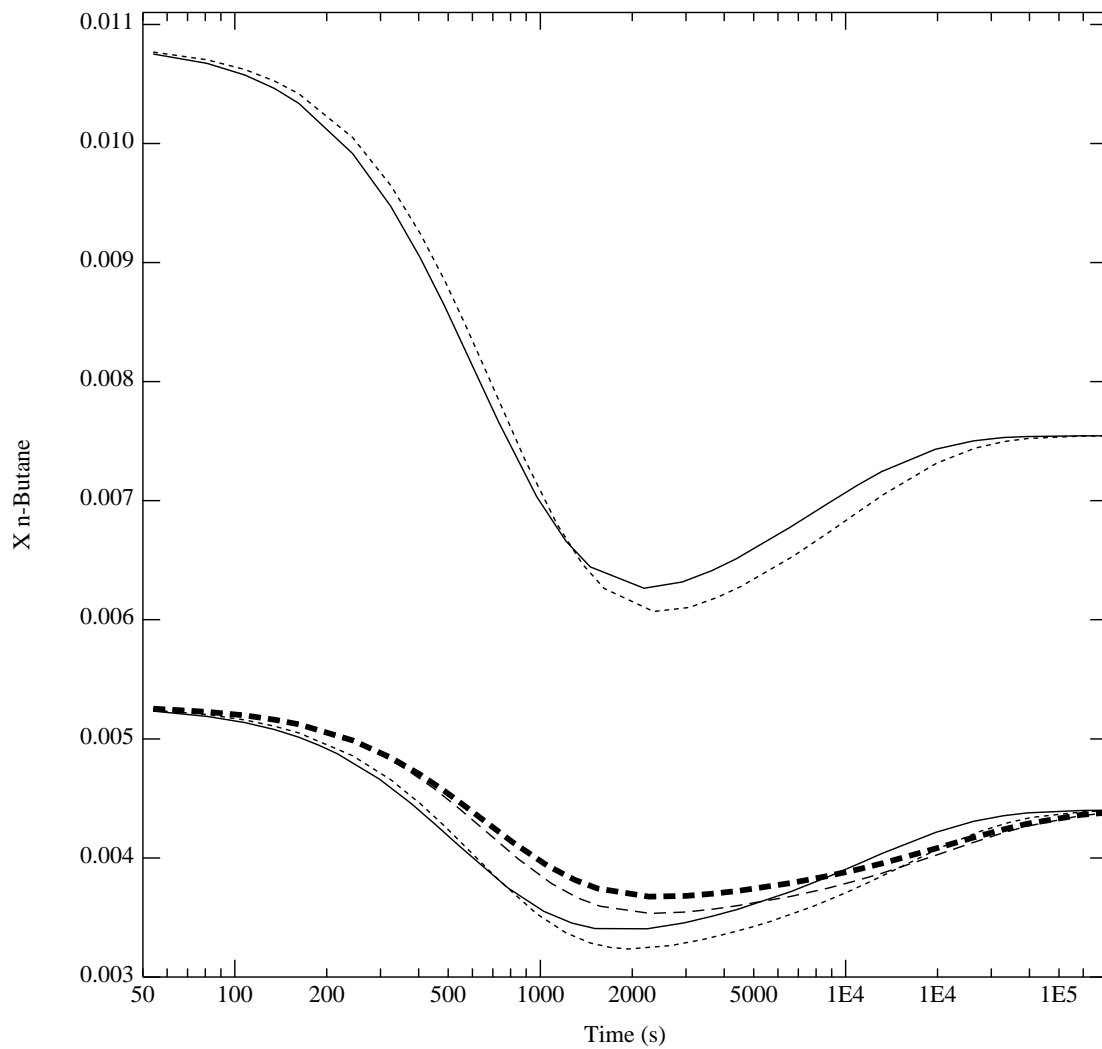


Figure 5.14: n-Butane composition in the distillate of the depropanizer. The equilibrium model predicts high concentration transients: the EQLV model (solid line), and the EQLV model with lumped downcomer liquid (dashed lines). The nonequilibrium model has low concentration transients: the NEQ2H model (solid line), the NEQ2H model with the lumped downcomer liquid (dotted line), the NEQ4H model (dashed line), and the NEQ4H model with constant vapor volume above the froth (thick dashed line).

transfer coefficients are increased by 100%. Increasing the vapor mass transfer coefficients has more influence than increasing the liquid MTC's since the mass transfer resistance is higher in the vapor phase

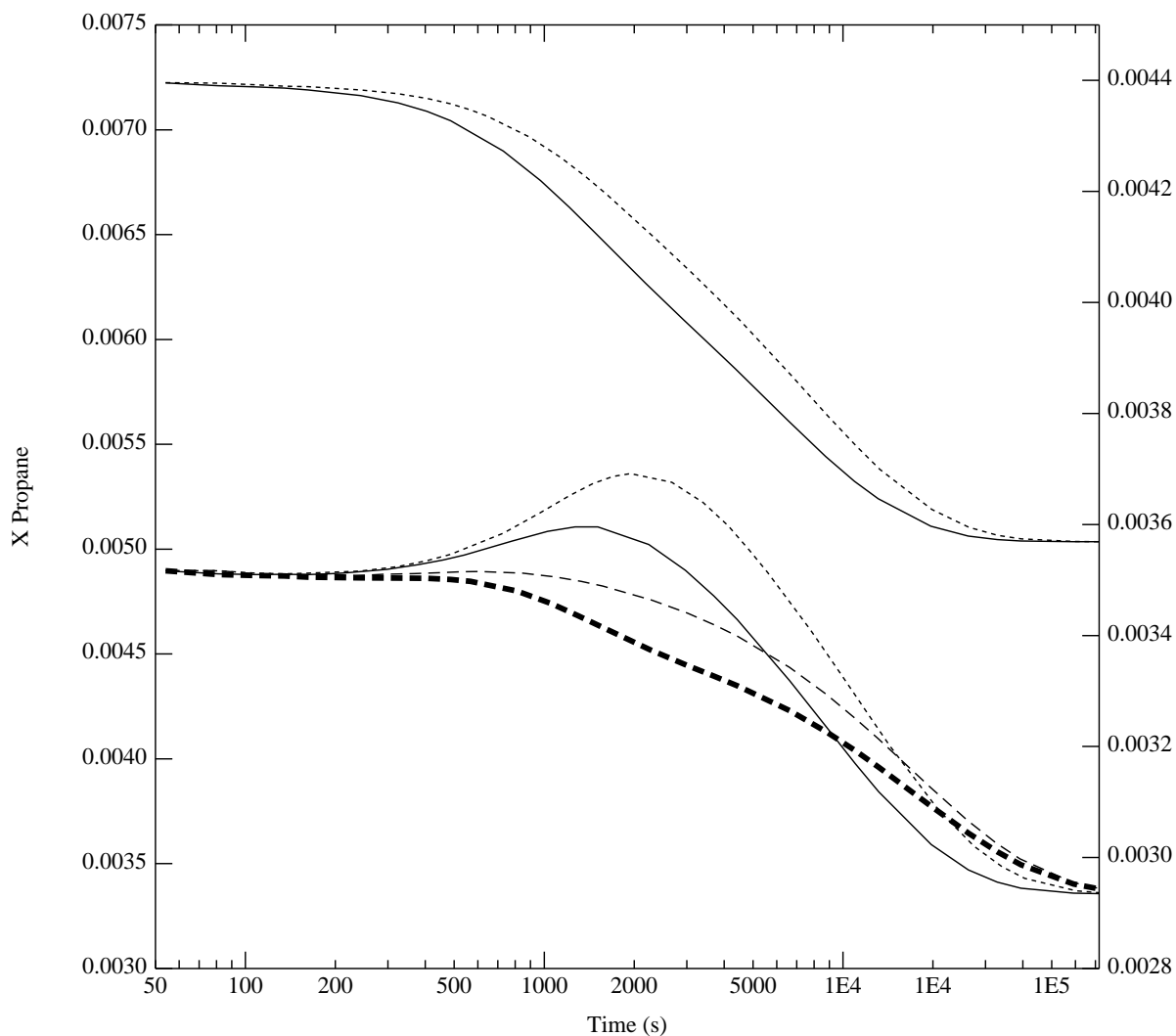


Figure 5.15: Propane composition in the bottoms of the depropanizer. The equilibrium model predicts high concentration transients (and uses the left axis): the EQLV model (solid line), and the EQLV model with lumped downcomer liquid (dashed lines). The nonequilibrium model has low concentration transients (and uses the right axis): the NEQ2H model (solid line), the NEQ2H model with the lumped downcomer liquid (dotted line), the NEQ4H model (dashed line), and the NEQ4H model with constant vapor volume above the froth (thick dashed line).

for this example (which is usually the case).

It is clear that the mass transfer coefficients as well as the interfacial area have a large influence on the

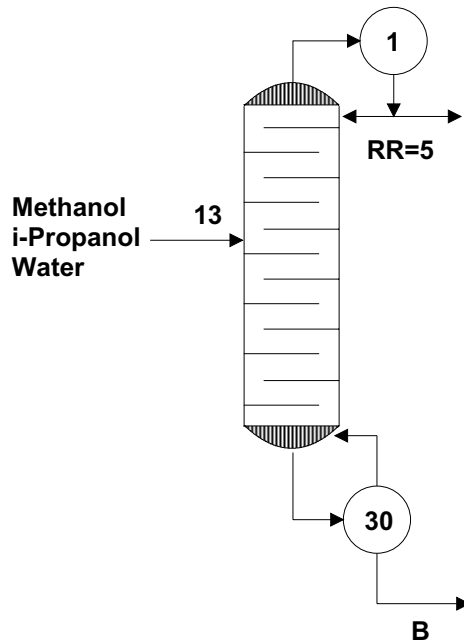


Figure 5.16: Methanol/i-propanol/water column configuration.

column dynamic transients. This means that through comparing experimental dynamic transients with model simulations we can discriminate between different mass transfer coefficient correlations as well as for correlations predicting the amount of interfacial area. Not only will initial and final steady-state values be different but the transients will differ as well. Since there is a large variance in predictions of the mass transfer coefficient correlations available from literature as was observed above and in chapter 3, we feel that more (fundamental) research is warranted.

5.7 Multicomponent and Effective Diffusivity

In chapter 3 the different steady-state column profiles were calculated by using the full matrix diffusivity model and by the using effective diffusivity method. However, it is unclear whether there is also a difference in the column dynamics. Here we use a nonideal example which comes from the production of ethanol. Ethanol produced by fermentation results in a ethanol-water mixture which also contains traces of other components. These traces must be removed to (very) low levels because of their smell. Here we discuss the removal of propanol using a side drawoff. A complete separation cannot be obtained since ethanol and water form an azeotrope. Therefore, the top product is close to the azeotrope (at about a mole fraction of 0.89, depending on the pressure), whereas the bottom is almost pure water. The feed

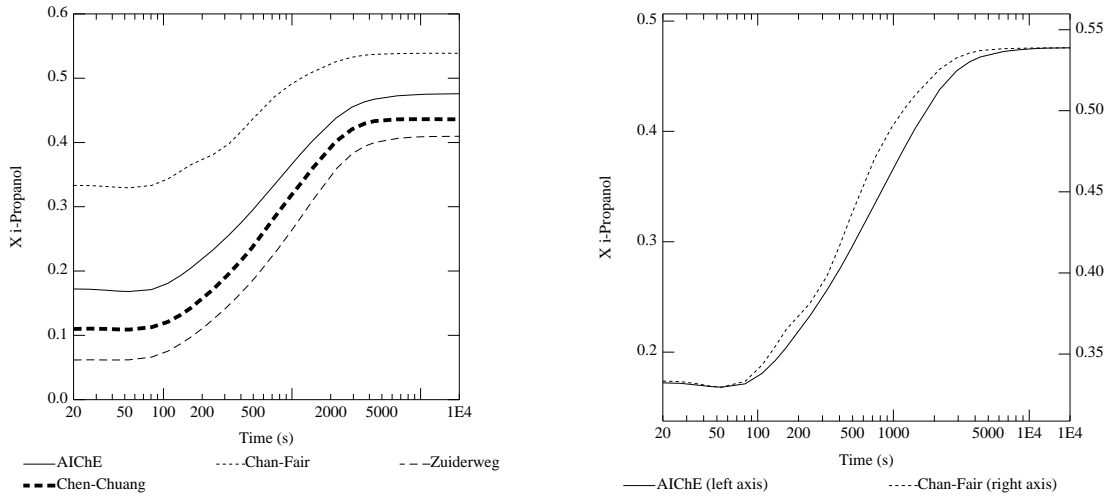


Figure 5.17: Dynamics of various mass transfer model for the methanol/i-propanol/water column.

also contains some 1-propanol, which has a higher boiling point than ethanol. Propanol forms an almost ideal solution with ethanol. Thus, in the top of the column where we have predominantly ethanol, it tends to go down. However, propanol in water is a quite volatile component, due to its high activity coefficient in water ($\gamma^\infty \approx 15$). The result is that in the bottom of the column propanol is pushed up and it will accumulate (over time) in the middle of the column. To prevent this build-up from causing problems it must be removed with a side drawoff as shown in Figure 5.22 (for specifications see Table 5.5). Simulations were run in sieve tray design mode using the AICHe MTC-model. The perturbation consisted of an increase in the n-propanol feed flow of 50%.

Figure 5.23 shows the i-propanol mole fraction as function of the time for the full and effective diffusivity model. Although the two column profiles are different the column dynamics are very similar and steady-state is reached at the same time for both models. This can be explained by the fact that the two models predict different individual mass transfer rates but the total mass transfer rates are not very different. Thus, only in the case where the total mass transfer rate is dominated by an individual component mass transfer rates the two models would show different column dynamics.

The same column (using the designed sieve tray layout) was used to investigate the buildup of the n-propanol in the column. The feed for the starting steady-state did not contain any n-propanol, just ethanol and water. Then the feed of 1 mol/s n-propanol was introduced. Column profiles are shown

Table 5.5: Propanol Side-draw Column Specifications

DECHEMA K model		
UNIFAC		
Antoine Vapor pressure		
Excess Enthalpy		
Column pressure 1.0 (<i>atm</i>)		
	Initial	New
Feed stage	45	45
Pressure (<i>atm</i>)	1.0	1.0
Vapor fraction	0.0	0.0
Component flows (<i>mol/s</i>)		
n-Propanol	1.0	1.5
Ethanol	10.0	10.0
Water	89.0	89.0
Sidestream stage	35	35
Phase	Liquid	Liquid
Flow (<i>mol/s</i>)	5.0	5.0
Total Condenser (stage 1):		
Reflux ratio = 4.0		
Molar holdup = 4.2 (<i>kmol</i>)		
Partial Reboiler (stage 50):		
Bottom product flow rate = 86.0 (<i>mol/s</i>)		
Molar holdup = 25.8 (<i>kmol</i>)		
Section	1	2
First stage	2	45
Last stage	44	49
Column diameter (<i>m</i>)	0.967	0.824
Total tray area (<i>m</i> ²)	0.734	0.533
Number of flow passes	1	1
Tray spacing (<i>m</i>)	0.53	0.5
Liquid flow path length (<i>m</i>)	0.8	0.603
Active area (% total)	91.2	83.5
Total hole area (% active)	17.4	16.5
Downcomer area (% total)	4.17	8.0
Hole diameter (<i>m</i>)	0.00476	0.00476
Hole pitch (<i>m</i>)	0.0109	0.0112
Weir length (<i>m</i>)	0.836	0.738
Weir height (<i>m</i>)	0.0508	0.0508
Downcomer clearance (<i>m</i>)	0.0381	0.0381
Deck thickness (<i>m</i>)	0.00254	0.00254

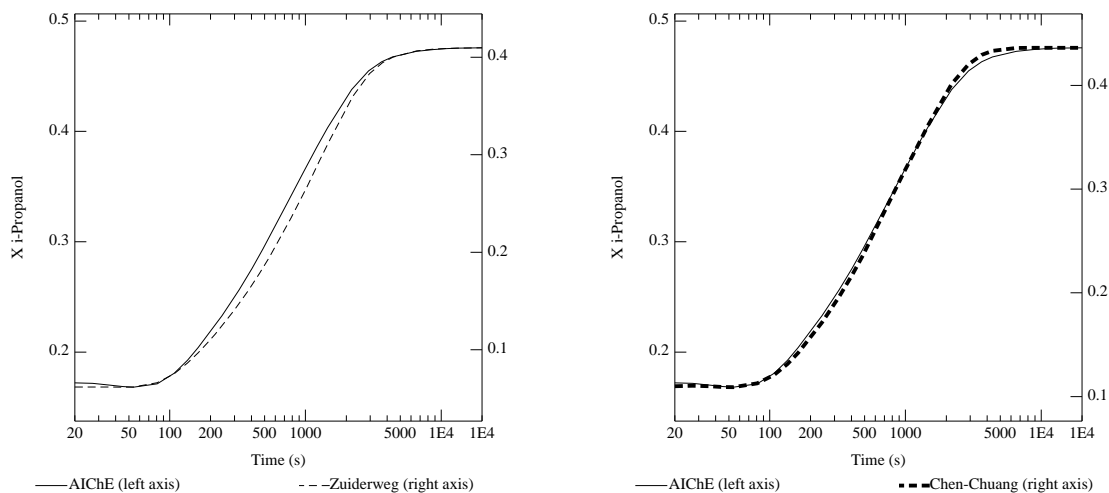


Figure 5.18: Dynamics of various mass transfer model for the methanol/i-propanol/water column.

Figure 5.24 for n-propanol, for both approaches. After scaling the mole fractions no differences in the column dynamics between the two approaches are observed. We see that the n-propanol concentration builds up in an hour or so. If the feed flow of n-propanol is much lower than 1 mol/s compared to the 99 mol/s ethanol and water, the time it takes for the column to reach steady-state can become quite long indeed (a general problem with the removal of these traces).

The differences between the two approaches are important as the mole fraction values *are* different. This is obvious from the concentration of n-propanol in the distillate where a difference of a factor two can be observed between the effective and the full diffusivity approach. It can also be seen for the methanol/i-propanol/water example of Krishnamurthy and Taylor (1985), where Figure 5.25 shows the column profiles of i-propanol as function of the time for the two different approaches.

5.8 Tray Layout and Operation

Tray layout parameters influence the hydrodynamics of trays. This has a natural influence on the column dynamics. For example a tray with a lower weir height has less holdup, and therefore faster dynamics. Similarly a tray with multiple passes has a faster transients than the same tray which only has a single

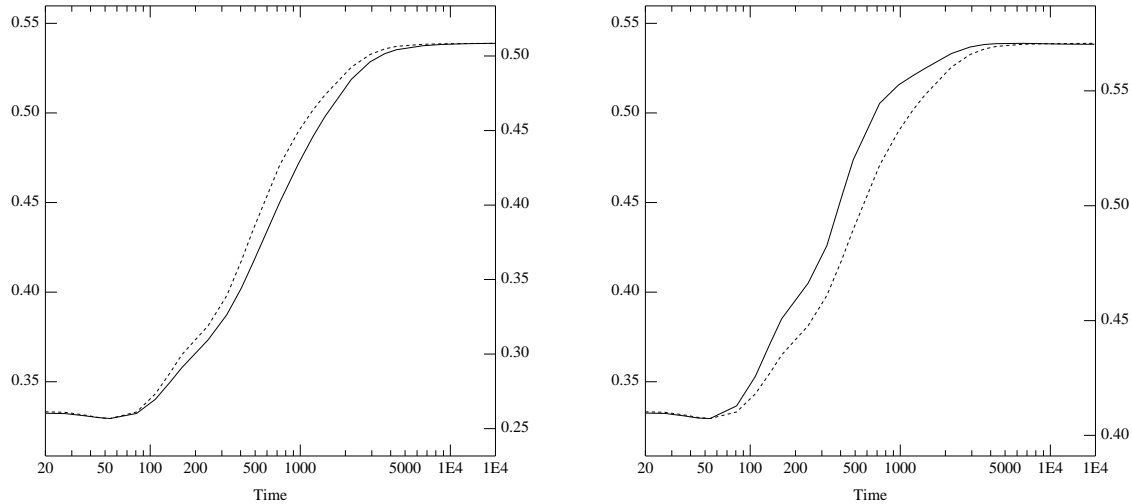


Figure 5.19: Propanol mole fraction transient on the 25th tray. The interfacial area is decreased (a, left) or increased (b, right) by 50% (right axis). The normal transient is shown with a dotted line (left axis).

pass. But also the column operation changes the hydrodynamics. Close to the flooding point as well as below the weep point the hydrodynamics will be different from those at normal operation. Therefore, the tray hydrodynamics must be included in any dynamic column model.

However, the tray hydrodynamics have an influence on the tray performance as well. This is where the difference between the equilibrium model and the nonequilibrium model becomes more apparent. The equilibrium model has no (consistent) manner in which to account for the influence of the hydrodynamics on tray performance in contrast to the nonequilibrium model where tray hydrodynamics is affecting the mass transfer coefficients.

We used the methanol/*i*-propanol/water example where we simulated the column with single pass trays and double pass sieve trays. Figure 5.26 shows the internal liquid flows for both the equilibrium (solid lines) and the nonequilibrium (dotted lines) for the double pass column simulations. Initially, the internal liquid flows initially increase and there are only small differences between both models. However, the transient for the nonequilibrium model dampens off earlier but takes longer to reach the steady-state values, compared to the those for the equilibrium model.

However, differences in internal flows translate into interesting results for the distillate mole fractions. In Figure 5.27 the *i*-propanol mole fraction in the distillate is plotted as function of the time, for the two

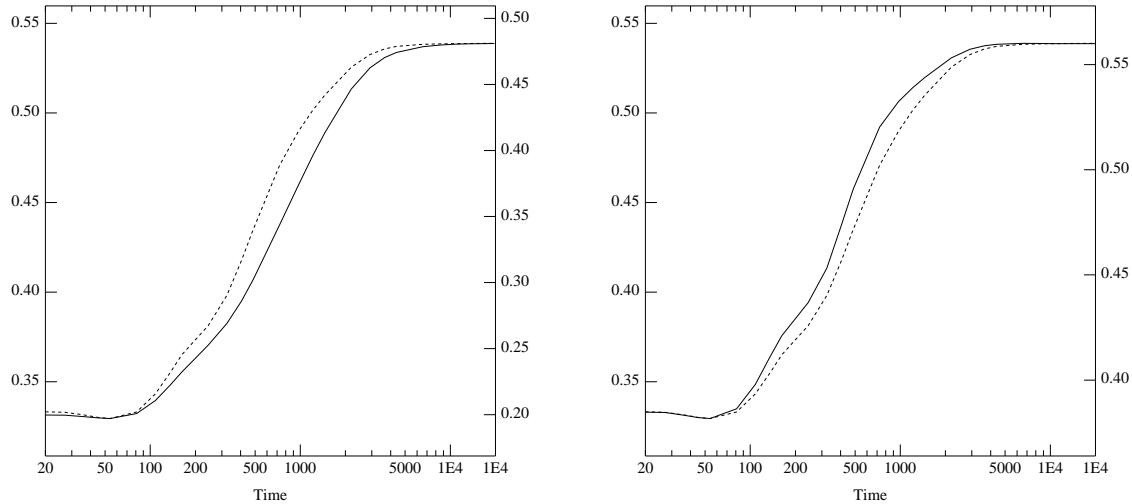


Figure 5.20: Propanol mole fraction transient on the 25th tray. The vapor and liquid mass transfer coefficients are decreased (a, left) or increased (b, right) by 50% (right axis). The normal transient is shown with a dotted line (left axis).

different models as well as for single and double pass trays. The dynamic behavior of the equilibrium model is quite different from that of the nonequilibrium model. Since the equilibrium model uses the same hydrodynamic routines the difference must be caused by the influence of the tray hydrodynamics on the separation. Observe that there is little difference between the one and two pass equilibrium simulations, but not so for the nonequilibrium simulation. The two pass column has a reduced liquid residence time. Since the perturbation introduces an increase in the internal liquid flowrate, it reaches the reboiler faster in a two pass tray column than in a single pass tray column. The different internal flows influence the separation. The *i*-propanol mole fractions for the condenser and first 24 trays are plotted in Figure 5.28.

Similar results may be obtained by varying other tray layout parameters. In Figure 5.29 the distillate *i*-propanol mole fraction is plotted as a function of time. Dashed lines correspond to one inch weir simulations where the solid lines use the (normal) two inch weir heights. As can be seen from the figure, initial and final steady-state values are identical for the equilibrium model (the thin lines). The distillate concentration in the simulation using weirs of one inch is changing first, but also takes a little longer to converge. The dynamic transients are very similar. However, although the initial values for the nonequilibrium model (the thick lines) are almost the same, the final values differ by more than 20%.

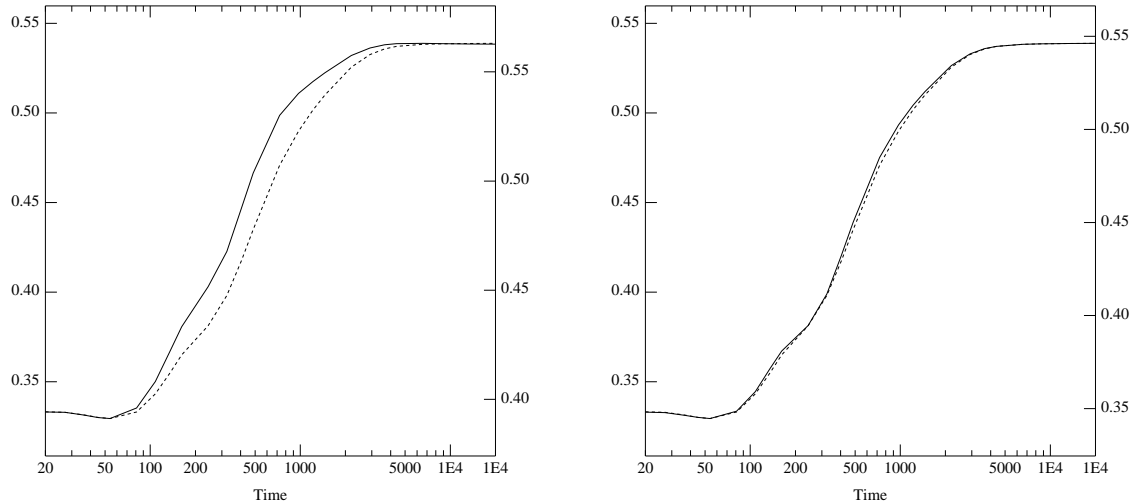


Figure 5.21: Propanol mole fraction transient on the 25th tray. The vapor mass transfer coefficients are increased by 100% (a, left) or the liquid mass transfer coefficients are increased by 100% (b, right), using the right axis. The normal transient is shown with a dotted line (left axis).

The dynamic behavior is also different, implying an effect of the hydrodynamics on the mass transfer which changed the transients. Other tray layout parameters, for example the free area ratio, have an influence on the column dynamics as well.

The influence of the tray hydrodynamics are even more important at column operation outside the normal range, in other words close to column flooding or with liquid weeping through the holes of the trays. We illustrate this with the methanol/*i*-propanol/water column using a different perturbation. Instead of changing the feed composition we increase the reflux ratio of the condenser from 5 to 6. Initially the trays operate at a fraction of flooding of around 75%, but after increasing the reflux ratio they operate at 90% and several trays in the top operate at 95% of flooding. Since the Chan-Fair was used to model this column, the average efficiency decreases due to the increase of the fraction of flooding (see Appendix A for the dependence of the mass transfer coefficients on the fraction of flooding). The transients for the *i*-propanol in the distillate for the equilibrium and nonequilibrium model are plotted in Figure 5.30. Besides the difference in the values for the *i*-propanol concentration in the distillate, the dynamic behavior is completely different. The equilibrium model predicts a decreased distillate concentration due to the constant efficiency (of 60%) and higher reflux. However, the nonequilibrium model predicts an *increasing* distillate concentration when the reflux is increased. Since it is impossible to predict

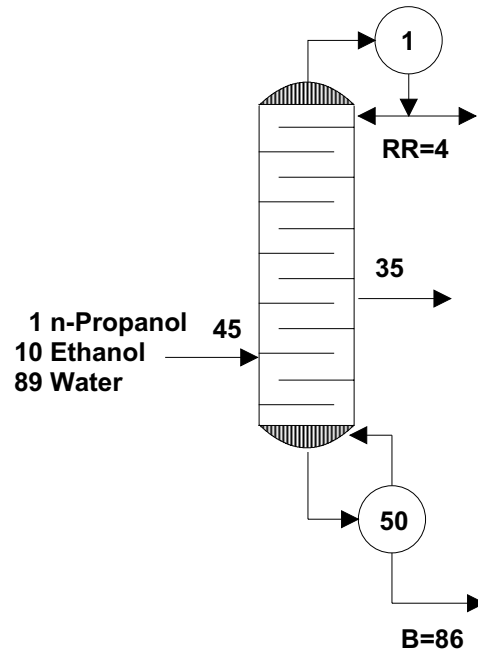


Figure 5.22: Ethanol/water column with side-draw for the removal of propanol.

the decremental effect of the tray hydrodynamics on individual component efficiencies the equilibrium model is unsuitable for this kind of dynamic simulations.

5.9 Neglecting Jacobian Terms

The evaluation of the numerical derivatives of the mass transfer rates with respect to all the variables is quite expensive. It is possible to neglect the change in the physical properties (such as densities, viscosities, etc.) during the finite differencing to obtain derivatives of the rate equations. Although this decreased the time required for the Jacobian evaluation, stepsize control of the integrator limited the stepsize to smaller steps to keep the errors within the specified tolerance. This resulted in actually requiring more computer time in comparison to integration using the complete derivative information. It shows that accurate Jacobians are required to obtain accurate dynamic results. Thus, it seems more useful to spend time on obtaining analytical derivatives of the mass transfer rate equations (possibly with the use of symbolic math packages) than on devising schemes which neglect or approximate Jacobian terms.

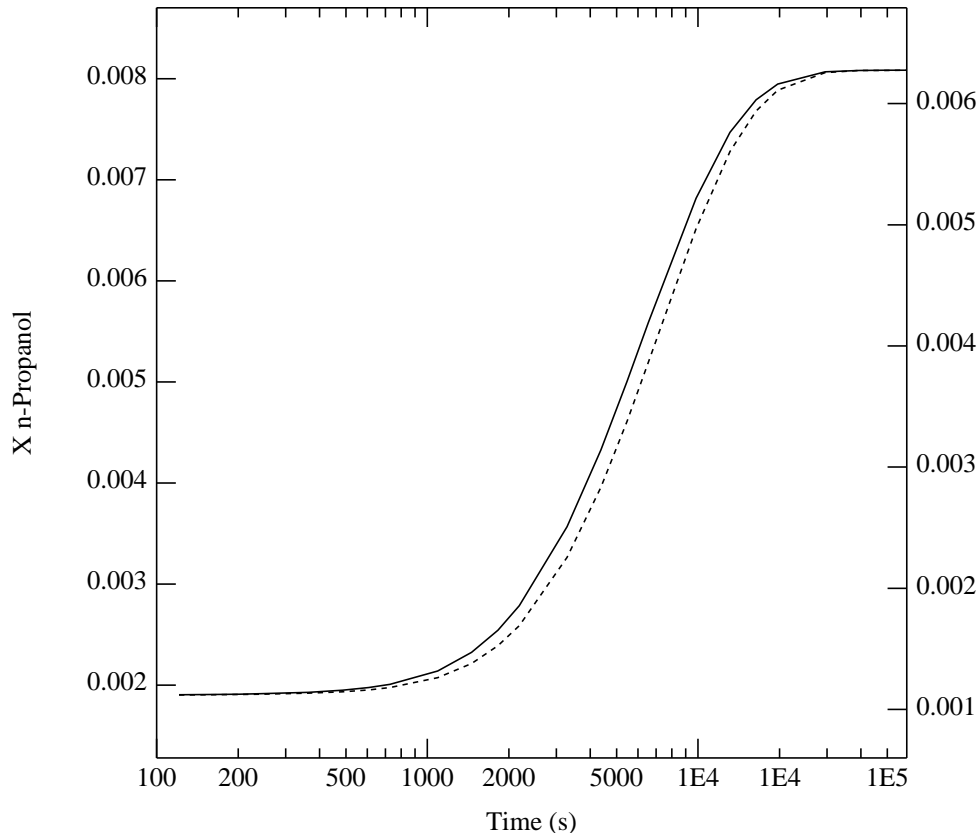


Figure 5.23: Mole fraction of n-propanol as function of the time using the full Maxwell-Stefan matrix diffusivity approach (solid line, left axis) and the effective diffusivity approach (dotted line, right axis).

References

- R. Gani, C.A. Ruiz, I.T. Cameron, "A Generalized Model for Distillation Columns I – Model Description and Applications", *Comp. Chem. Eng.*, Vol. **10**, No. 3 (1986) pp. 181–198.
- R. Krishnamurthy, R. Taylor, "A Nonequilibrium Stage Model of Multicomponent Separation Processes. Part III: The Influence of Unequal Component Efficiencies in Process Design Problems", *AIChE J.*, Vol. **31**, No. 12 (1985c), pp. 1973–1985.
- R. Taylor, H.A. Kooijman, J-S. Hung, "A Second Generation Nonequilibrium Model for Computer

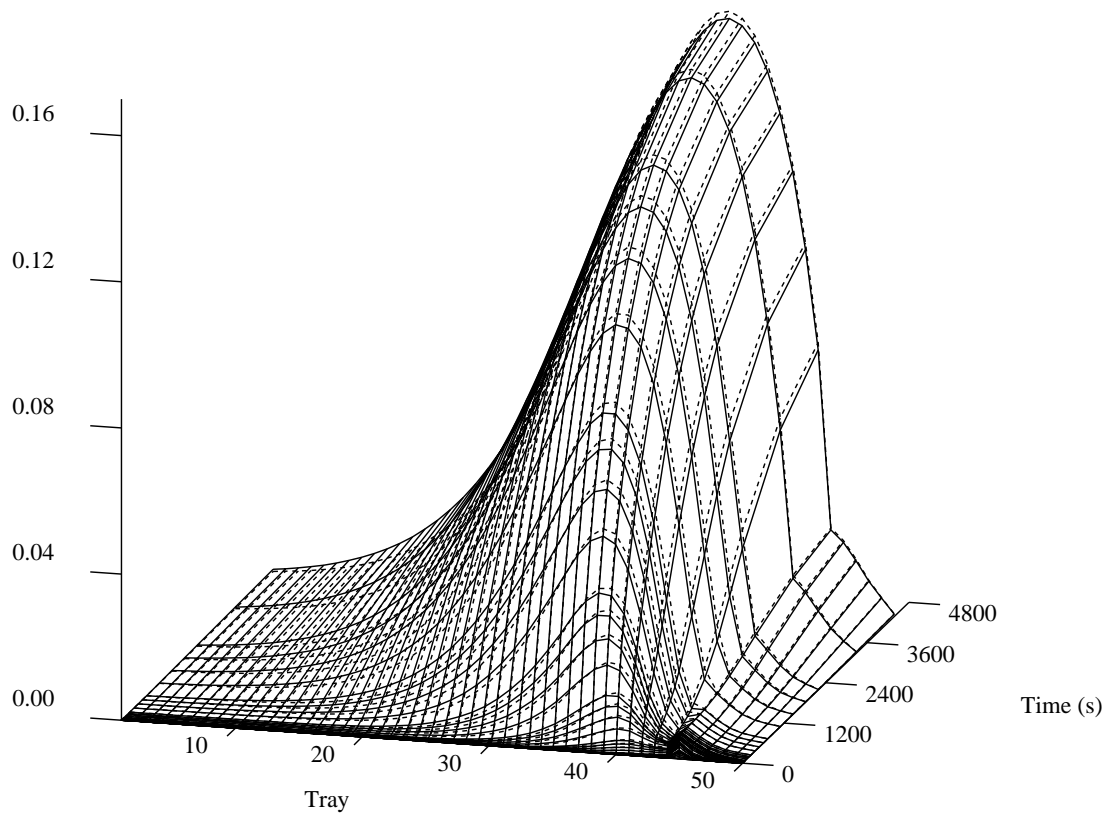


Figure 5.24: Mole fraction of n-propanol as function of time using the full Maxwell-Stefan approach (solid line) and the effective diffusivity approach (dotted line).

Simulation of Multicomponent Separation Processes”, *Comp. Chem. Eng.*, Vol **18**, No. 3, (1994) pp. 205–217.

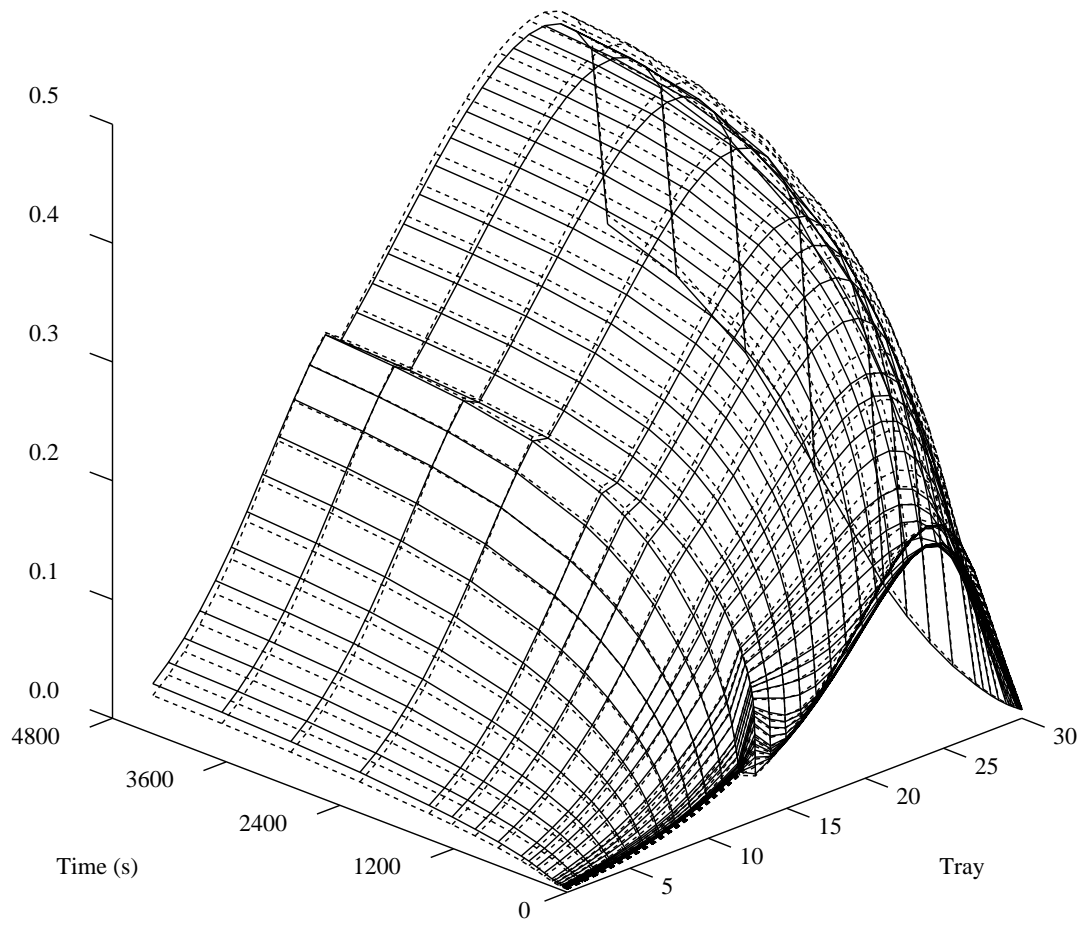


Figure 5.25: Mole fraction of i-propanol as function of time using the full Maxwell-Stefan approach (solid line) and the effective diffusivity approach (dotted line).

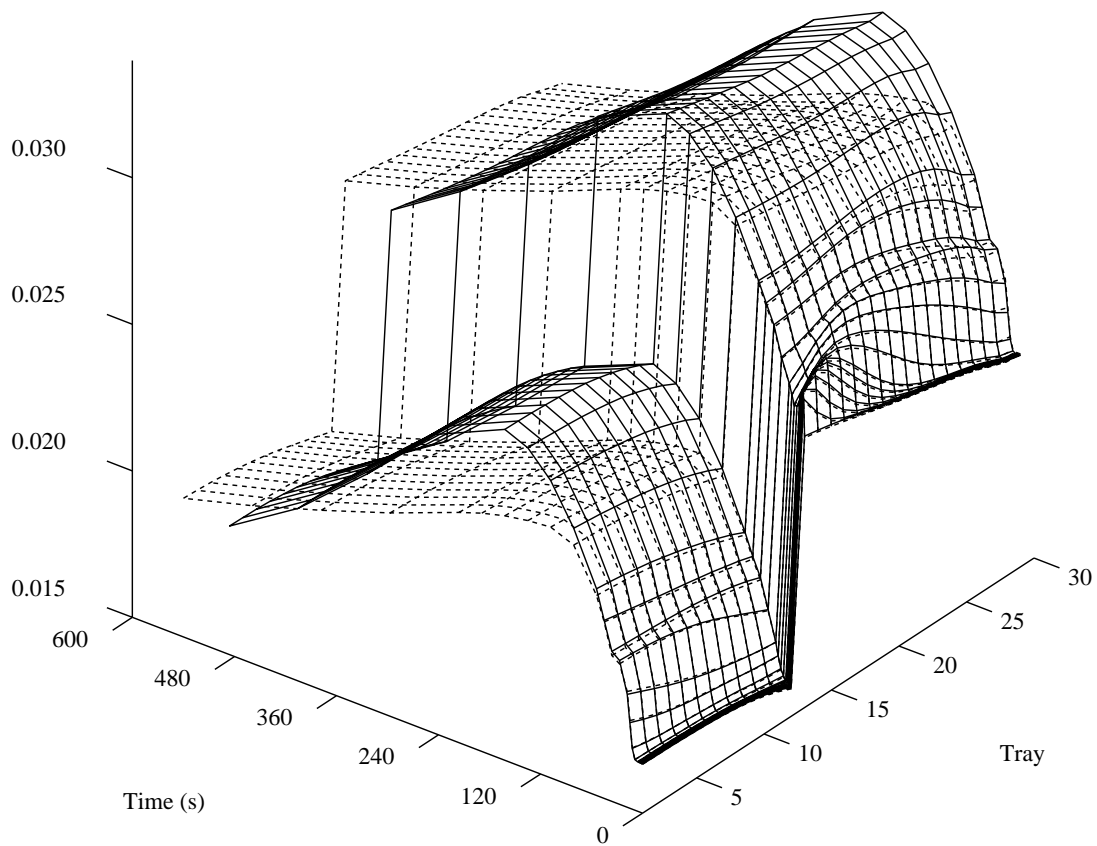


Figure 5.26: Internal liquid flow profiles ($kmol/s$) as function of time for the equilibrium (solid lines) and nonequilibrium (dotted lines) models using a double pass sieve tray.

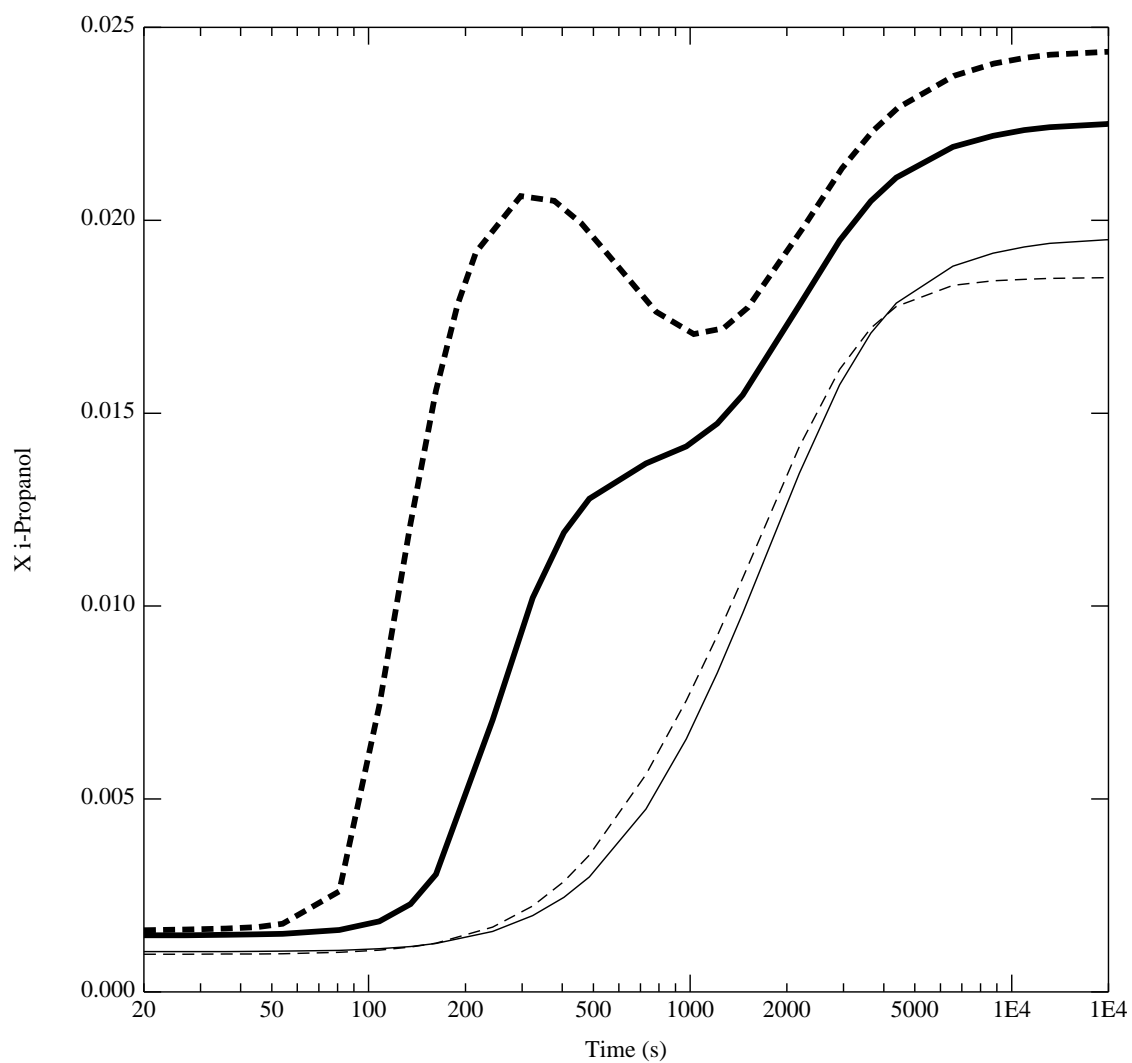


Figure 5.27: Mole fraction of i-propanol in the distillate as function of the time for the equilibrium (thin lines) and nonequilibrium (thick lines), using single pass sieve tray (solid lines) and double pass sieve trays (dashed lines). The methanol/i-propanol/water column was simulated with the Chan-Fair model.

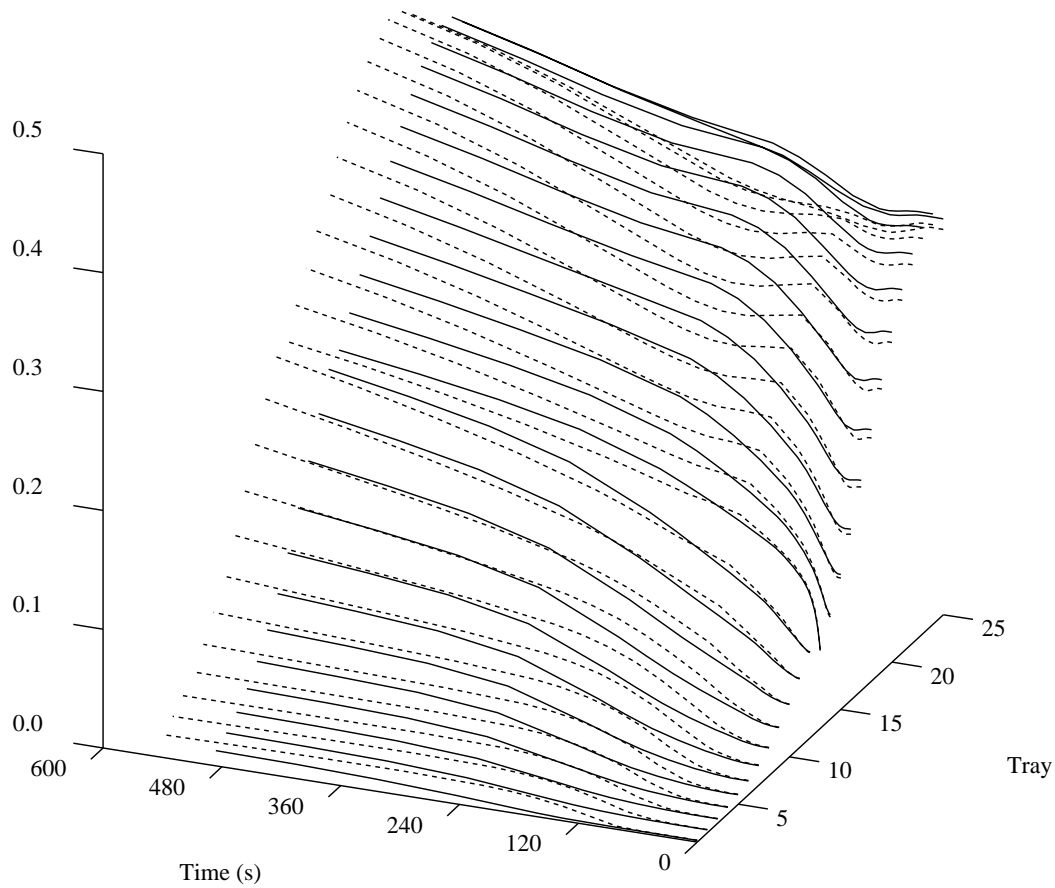


Figure 5.28: i-Propanol mole fractions as function of the time simulated with the nonequilibrium model for single (solid lines) and two pass (dotted lines) sieve trays.

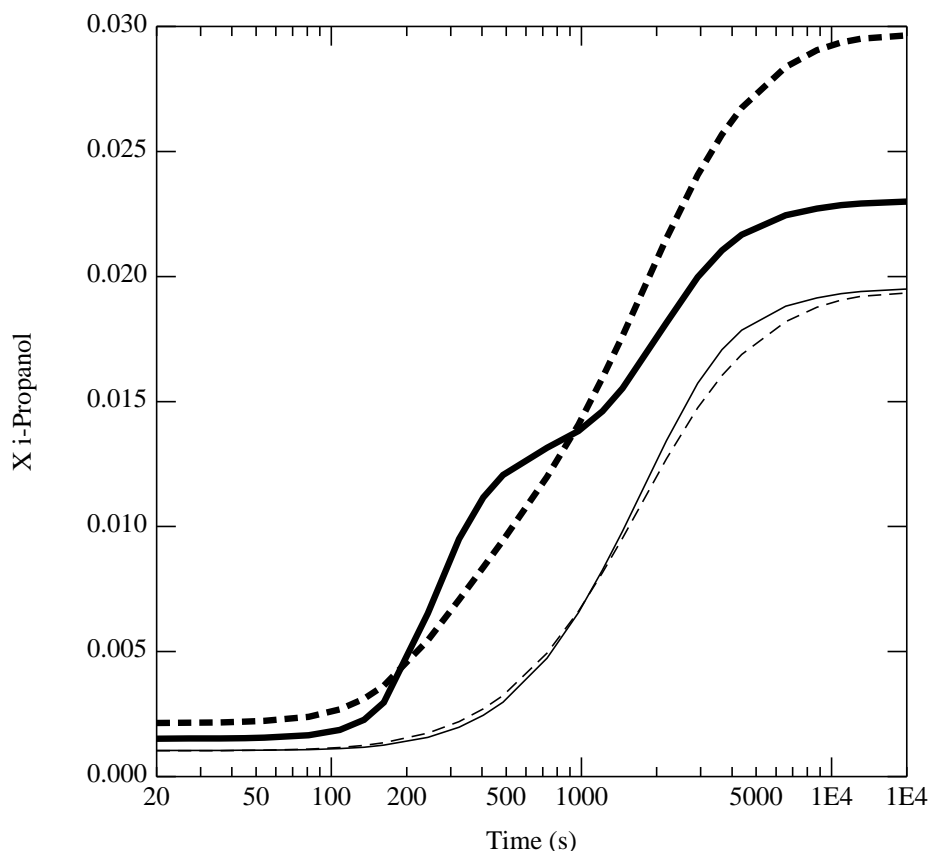


Figure 5.29: Distillate i-propanol mole fractions as function of the time simulated with the equilibrium (thin lines) and the nonequilibrium model (thick lines) with two different weir heights; one inch (dashed lines) and two inch (solid lines).

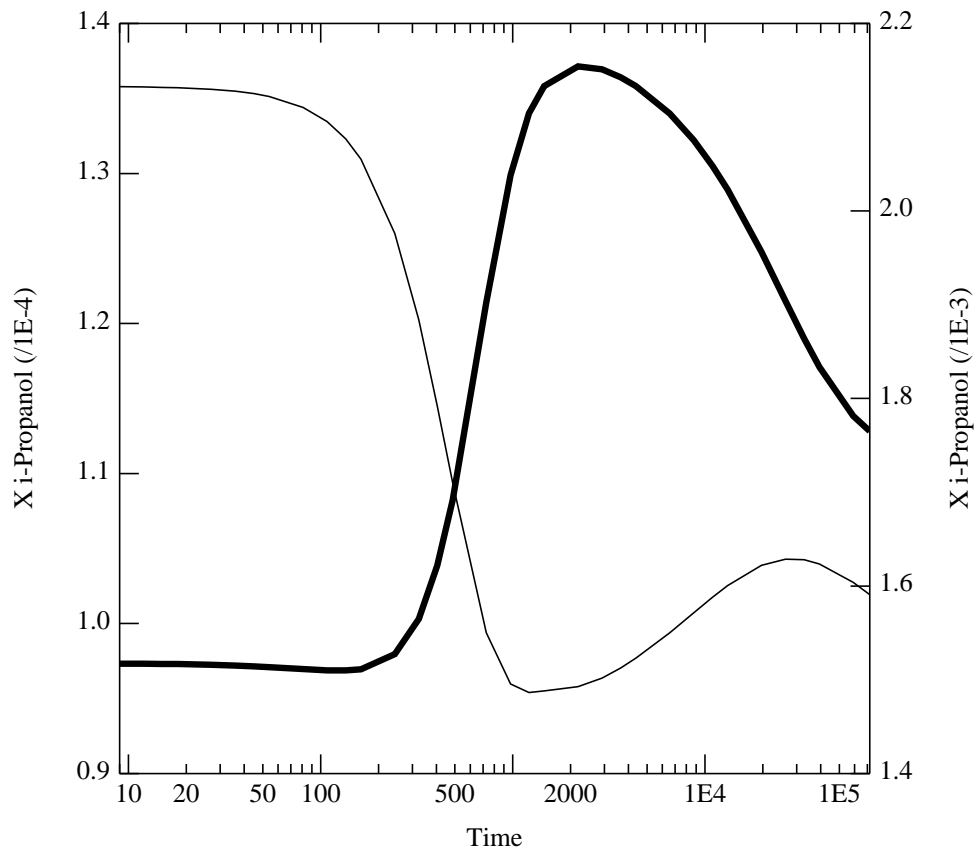


Figure 5.30: Distillate i-propanol mole fractions as function of the time after increasing the reflux ratio simulated with the equilibrium (thin lines, left axis) and the nonequilibrium model (thick lines, right axis).

Chapter 6

Conclusions

A rigorous nonequilibrium model has been developed where each phase in the froth and disengagement zone is considered as a separate, variable, completely mixed holdup and only mechanical equilibrium is assumed (equal pressure over the tray). Mass transfer occurs between the vapor and liquid in the dispersion on the tray. The nonequilibrium model includes tray sizing parameters and mass transfer models and it is observed that these have a direct and significant influence on the column dynamics. Thus, the nonequilibrium model has the potential to include tray sizing parameters as part of the column design, control, and optimization. Without efficiencies the model is predictive, no estimates were needed to describe the performance of an existing industrial column, just tray design layout and operational specifications. Tray layout specifications are not required for a nonequilibrium simulation, they can be generated by using the design-mode during a steady-state simulation.

Nonequilibrium simulations show that the (back-calculated) component Murphree tray efficiencies for multicomponent systems are unequal and can become completely different given a small change in specifications. If the component efficiencies are unequal and they change with respect to specifications then they cannot be used in dynamic column simulations since no model is available to rigorously compute the efficiencies. The difference between equilibrium with a constant efficiency and nonequilibrium simulation transients can be pronounced, both qualitatively and quantitatively. These differences are due to both mass and heat transfer limitations which the equilibrium model ignores. There are also significant differences in dynamic behavior of columns at higher pressures simulated with models that include or ignore the vapor holdup above the froth. In general, it also takes longer to reach a new steady-state for the nonequilibrium column simulation compared to the equilibrium simulation.

Mass transfer models are developed that account for cross flow effects on large distillation trays while avoiding the pitfalls that can strike while employing overall mass transfer coefficients in the calculation of interphase mass transfer rates. New plug and dispersion flow models for the nonequilibrium column model are proposed and found to predict tray efficiencies in general agreement with FRI experimental data on large scale equipment. Several methods of evaluating binary mass transfer coefficients in dis-

tillation have been evaluated. Of the methods tested, that of Chan and Fair (1984) provides the best predictions of column performance.

Additional evidence that the Maxwell-Stefan equations should be used in the calculation of mass transfer rates in distillation is provided by comparing the predictions of the nonequilibrium model with the new flow and mass transfer models with a simpler model based on all components having an equal facility for mass transfer. Column designs obtained with the simple model can be very different (in terms of numbers of stages, optimal feed, sidestream and controller locations) from those obtained with the more rigorous approach. However, there is little difference in the dynamic behavior of columns. This is in contrast to the use of different mass transfer coefficient correlations which have differing dynamic characteristics. Dynamic studies might provide insight on the fundamental basis of the mass transfer coefficient correlations as well as that for interfacial areas.

Tray layout parameters may have a profound effect on the dynamic performance of the column. Effects of different tray layout parameters on the mass transfer can only be modeled with a nonequilibrium model. Equilibrium model simulations will show no difference in performance other than those affecting the hydrodynamics of the tray layout. The free area ratio influences both the mass transfer and the hydrodynamics on the tray and is one of the most important parameters.

Future work on the dynamic nonequilibrium column model must include the extension to packed columns, which is rather simple if accurate and correctly behaving holdup correlations for structured and random packings are available. Recent advances in modeling packed columns have given rise to models of a more fundamental basis which also include the pressure drop over the packing.

As mentioned above, more fundamental research is needed to determine better methods to estimate mass transfer coefficients in the vapor and liquid phase, as well as the total interfacial area available for mass transfer. This remains an important area for improvement. Dynamic nonequilibrium simulations of experimental data might actually help to discriminate between various models and provide the actual relations between vapor and liquid resistances.

The influence of entrainment and weeping flows on the tray hydrodynamics and the mass transfer parameters is little understood, and not yet incorporated in a proper manner in the nonequilibrium model. To do so will allow the nonequilibrium model simulation of columns that operate outside the normal operation conditions. This is important for the simulation of the start-up and shut-down of column processes.

More models for the condenser and reboiler should be developed, including equations that model control units normally utilized in column operations. These models can become much more advanced and include the heat transfer process taking place or even the mass transfer process of condensing or evaporation. Extension of the models will allow more specifications.

Another interesting subject is the dynamic interaction of multiple interlinked columns, simulated with nonequilibrium models, for example those encountered in extractive distillation. Possibly dynamic nonequilibrium liquid-liquid column simulations are possible by extending the current steady-state

nonequilibrium implementation of this operations.

The design mode can be further enhanced by using an optimizing algorithm that would optimize the tray layout for minimum cost or pressure drop, maximum flexibility or mass transfer, or a combination of these.

Appendix A. Correlations

To use the dynamic nonequilibrium column model we have to evaluate the liquid holdups on a tray, the tray pressure drop, the binary mass transfer coefficients, and the interfacial area. Correlations for these properties are discussed here.

Tray pressure drop estimation

The liquid heights on the trays are evaluated from the tray pressure drop calculations. The wet tray pressure drop liquid height is calculated with:

$$h_{wt} = h_d + h_l \quad (\text{A.1})$$

where h_d is the dry tray pressure drop liquid height and h_l the liquid height:

$$h_l = h_{cl} + h_r + \frac{h_{lg}}{2} \quad (\text{A.2})$$

The clear liquid height, h_{cl} , is calculated with

$$h_{cl} = \alpha h_w + h_{ow} \quad (\text{A.3})$$

where the liquid fraction α is computed with the Barker and Self (1962) correlation:

$$\alpha = \frac{0.37h_w + 0.012F_s + 1.78Q_L/W_l + 0.024}{1.06h_w + 0.035F_s + 4.82Q_L/W_l + 0.035} \quad (\text{A.4})$$

The choice of correlation for the liquid fraction turns out to be important as certain correlations are dynamically unstable. The height of liquid over the weir, h_{ow} , is computed by various correlations for different types of weirs (see Perry) and a weir factor (F_w) correction (see Smith, pp. 487) is employed. For example for a segmental weir:

$$h_{ow} = 0.664F_w \left(\frac{Q_L}{W_l} \right)^{2/3} \quad (\text{A.5})$$

$$w = \frac{W_l}{D_c} \quad (\text{A.6})$$

$$F_w^3 = \frac{w^2}{1 - (F_w w (\frac{1.68 Q_L}{W_l^{2.5}})^{2/3} + \sqrt{1 - w^2})^2} \quad (\text{A.7})$$

where Q_L is the volumetric flow over the weir per weir length. The residual height, h_r , is only taken into account for sieve trays. Bennett's method (see Lockett, pp. 81) is:

$$h_r = \left(\frac{6}{1.27 \rho_L} \right) \left(\frac{\sigma}{g} \right)^{2/3} \left(\frac{\rho_L - \rho_V}{d_h} \right)^{1/3} \quad (\text{A.8})$$

Dry tray pressure, h_d , is calculated with:

$$h_d = K \frac{\rho_G}{\rho_L} u_h^2 \quad (\text{A.9})$$

$$K = \frac{\xi}{2g} \quad (\text{A.10})$$

where the orifice coefficient ξ for sieve trays is computed according to Stichlmair and Mersmann (1978). For valve trays we use the method of Klein (1982) as described in Kister (1992, pp. 309-312) where K is given for the cases with the valves closed or open. It is extended for double weight valve trays as discussed by Lockett (1986, pp. 82-86). The dry tray pressure drop is corrected for liquid fractional entrainment.

The froth density is computed with

$$h_f = \frac{h_{cl}}{\alpha} \quad (\text{A.11})$$

The liquid gradient, h_{lg} , is computed according to Fair (Lockett, 1986, pp. 72):

$$R_h = \frac{W h_f}{W + 2 h_f} \quad (\text{A.12})$$

$$U_f = \frac{Q_L}{W h_{cl}} \quad (\text{A.13})$$

$$Re_f = \frac{R_h U_f \rho_L}{\eta_L} \quad (\text{A.14})$$

$$f = 7 \cdot 10^4 h_w Re_f^{-1.06} \quad (\text{A.15})$$

$$h_{lg} = \frac{Z f U_f^2}{g R_h} \quad (\text{A.16})$$

where W is the average flow-path width for liquid flow, and Z the flow path length. The height of liquid at the tray inlet is:

$$h_i = \sqrt{\frac{2}{g} \left(\frac{Q_L}{W_l} \right)^2 \left(\frac{1}{h_{cl}} - \frac{1}{h_c} \right) + \frac{2 \alpha h_f^2}{3}} \quad (\text{A.17})$$

where h_c is the height of the clearance under the downcomer. The pressure loss under downcomer (expressed as a liquid height) is

$$h_{udc} = \left(\frac{1}{2g} \right) \left(\frac{Q_L}{C_d W_l h_c} \right)^2 \quad (\text{A.18})$$

where $C_d = 0.56$ according to Koch design rules. The height of liquid in the downcomer can now be calculated with the summation:

$$h_{db} = h_{wt} + h_i + h_{udc} \quad (\text{A.19})$$

Bubble-cap liquid heights are done according to Perry's (1984) and Smith (1963). Additionally the liquid fraction of the froth is computed according to Kastanek (1970).

Entrainment is computed from the fractional liquid entrainment which is computed from Hunt's correlation and from figure 5.11 of Lockett (1986) for sieve trays:

$$\phi^L = 7.75 \cdot 10^{-5} \left(\frac{0.073}{\sigma} \right) M_v \left(\frac{U_v}{T_s - 2.5h_{cl}} \right)^{3.2} \quad (\text{A.20})$$

Weeping flows are estimated from a correlation by Lockett and Banik (1984) where the weep-point occurs at $Fr_h = 0.67$:

$$\phi_w = 0.02 Fr_h^{-1} - 0.03 \quad (\text{A.21})$$

where ϕ_w is the weep rate (m^3/s) per total hole area (m^2). The Froude hole number is determined from

$$Fr_h = u_h \sqrt{\frac{\rho_v}{g \rho_l h_{cl}}} \quad (\text{A.22})$$

However, the weeping and entrainment flows were not accounted for in the dynamic model.

Mass Transfer Coefficients

Binary mass transfer coefficients (MTC's) can be computed from Number of Transfer Units (NTU's = N) by:

$$k^V = N^V / t_V a^V \quad (\text{A.23})$$

$$k^L = N^L / t_L a^L \quad (\text{A.24})$$

where the vapor and liquid areas are calculated with

$$a^V = a_d / \epsilon h_f \quad (\text{A.25})$$

$$a^L = a_d / \alpha h_f \quad (\text{A.26})$$

AIChE (1958)

$$N^V = (0.776 + 4.57h_w - 0.238F_s + 104.8Q_L/W_l) / \sqrt{Sc_V} \quad (\text{A.27})$$

$$F_s = u_s \sqrt{\rho_t^V} \quad (\text{A.28})$$

$$Sc_V = \mu^V / \rho_t^V D^V \quad (\text{A.29})$$

$$N^L = 19700 \sqrt{D^L} (0.4F_s + 0.17)t_L \quad (\text{A.30})$$

$$t_L = h_L ZW_l / Q_L \quad (\text{A.31})$$

The clear liquid height h_L is computed from Bennett *et al.* (1983):

$$h_L = \alpha_e (h_w + C(Q_L / \alpha_e W_l)^{0.67}) \quad (\text{A.32})$$

$$\alpha_e = \exp(-12.55(u_s(\rho^V / (\rho^L - \rho^V))^{0.5})^{0.91}) \quad (\text{A.33})$$

$$C = 0.50 + 0.438 \exp(-137.8h_w) \quad (\text{A.34})$$

Chan-Fair (1984)

$$N^V = (10300 - 8670F_f)F_f \sqrt{D^V} t_V / \sqrt{h_L} \quad (\text{A.35})$$

$$t_V = (1 - \alpha_e)h_L / (\alpha_e u_s) \quad (\text{A.36})$$

For the liquid number of transfer units the same correlations as given for the AIChE method is used (h_L and α_e are also computed with the correlation of Bennett *et al.*).

Zuiderweg (1982)

The vapour phase mass transfer coefficient is

$$k^V = 0.13 / \rho_t^V - 0.065 / (\rho_t^V)^2 \quad (\text{A.37})$$

in which k^V becomes independent of the diffusion coefficient. The liquid mass transfer coefficient is computed from either:

$$k^L = 2.6 \cdot 10^{-5} (\mu^L)^{-0.25} \quad (\text{A.38})$$

or

$$k^L = 0.024 (D^L)^{0.25} \quad (\text{A.39})$$

Chen-Chuang (1993)

The numbers of transfer units for the vapour is:

$$t_V = \frac{h_l}{u_s} \quad (\text{A.40})$$

$$F_s = U_s \sqrt{\rho^V} \quad (\text{A.41})$$

$$N^V = 11 \frac{1}{\eta_L^{0.1} \beta^{0.14}} \left(\frac{\rho_L F_s^2}{\sigma^2} \right)^{1/3} \sqrt{D^V t_V} \quad (\text{A.42})$$

and for the liquid

$$t_L = \frac{\rho_L}{\rho_V} t_V \quad (\text{A.43})$$

$$N^L = 14 \frac{1}{\eta_L^{0.1} \beta^{0.14}} \left(\frac{\rho_L F_s^2}{\sigma^2} \right)^{1/3} \left(\frac{V}{L} \right) \sqrt{D_L t_L} \quad (\text{A.44})$$

Interfacial Area

The interfacial area is computed according to Zuiderweg (1982) in the spray regime from:

$$a_d h_f = \frac{40}{\phi^{0.3}} \left(\frac{U_s^2 \rho_t^V h_L F P}{\sigma} \right)^{0.37} \quad (\text{A.45})$$

or in the froth-emulsion regime:

$$a_d h_f = \frac{43}{\phi^{0.3}} \left(\frac{U_s^2 \rho_t^V h_L F P}{\sigma} \right)^{0.37} \quad (\text{A.46})$$

The transition from the spray to mixed froth-emulsion flow depends on the flow parameter (FP):

$$FP > 3bh_L \quad (\text{A.47})$$

where b is the weir length per unit bubbling area:

$$b = W_l / A_b \quad (\text{A.48})$$

and the clear liquid height is given by:

$$h_L = 0.6 h_w^{0.5} (pFP/b)^{0.25} \quad (\text{A.49})$$

The total interfacial area on a tray can be calculated with

$$a^I = a_i a_{bub} \quad (\text{A.50})$$

Appendix B. Flow model derivation

The derivations for the various flow models was done with the help of the symbolic math program MAPLE. The plug flow model calculation of the average composition is:

```
# Plug-flow model
restart;
d:=diff(X(z),z)=B*X(z);
ds:=dsolve({d,X(1)=Xout},X(z));
X(z):=rhs(ds);
Xbar:=int(X(z),z=0..1);
Xbar:=factor(Xbar);
```

The calculation of the average composition for the dispersion flow model is similar, except that the result of Maple is not easy to use. Therefore, we simplified the answer by hand and check equivalence:

```
# dispersion-flow model
restart;
d:=A*diff(X(z),z,z)-diff(X(z),z)-B*X(z);
e1:=A=1/(2*a);
e2:=B=(b^2/a-a)/2;
d:=subs(e1,e2,d);
ds:=dsolve({d,D(X)(1)=0,X(1)=Xout},X(z));
ds:=subs(a+b=p,a-b=m,ds);
X(z):=rhs(ds);
Xbar:=int(X(z),z=0..1);
# Find a better formula and check
Xb:=Xout/(2*b) * (p*Omegam-m*Omegap);
assign(Omegam,(exp(m)-1)/(exp(m)*m));
assign(Omegap,(exp(p)-1)/(exp(p)*p));
simplify(Xbar-Xb);
```


Appendix C. Flow and Mass Transfer models

Murphree efficiencies as a function of the fraction of flooding for eight data sets were obtained from FRI reports by Yanagi and Sakata (1979, 1981, 1982). Two systems were used in the FRI tests: the cyclohexane (cC6) - *n*-heptane (nC7) system at pressures of 28, 34, and 165 *kPa*, and the *i*-butane (iC4) - *n*-butane (nC4) system at pressures of 1138, 2056, and 2756 *kPa*. The experiments were carried out on two types of sieve tray columns operated at total reflux; one with a free area ratio (total hole area divided by total active area) of 8% and one of 14%.

In each of the following figures the back-calculated efficiencies are plotted as function of the fraction of flooding, using the AIChE, Chan-Fair, Zuiderweg, and Chen-Chuang mass transfer coefficient correlation, respectively. For each mass transfer coefficient correlation four flow model combinations with increasing efficiency are plotted: Vapor mixed - Liquid mixed, Vapor plug flow - Liquid mixed, Vapor plug flow - Liquid dispersion flow, and Vapor plug flow - Liquid plug flow. The last two models usually result in similar efficiencies. The experimental FRI data are displayed with circles.

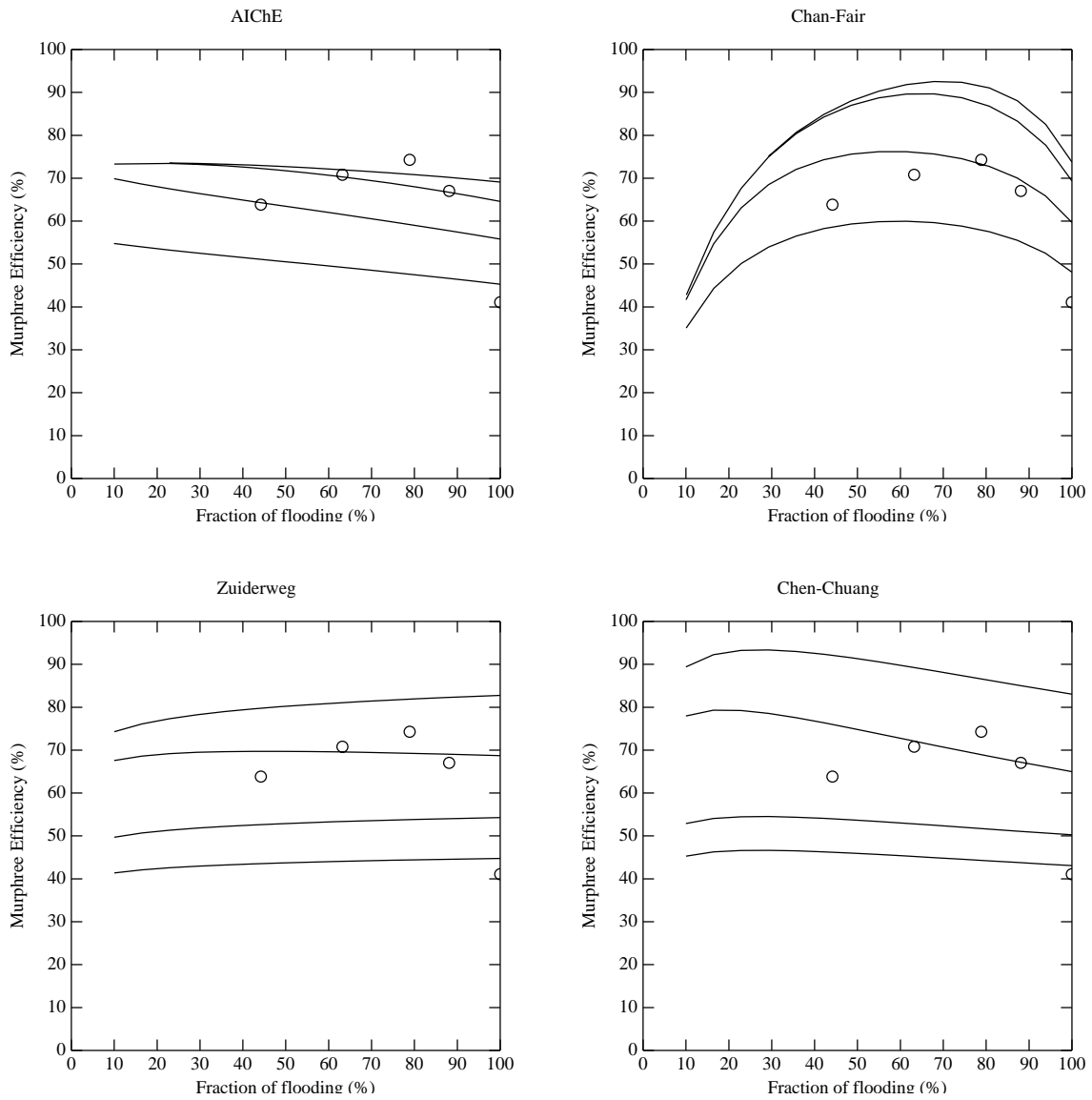


Figure C.1: Experimental FRI data cC6-nC7 at 34 kPa , 14% Sieve plate.

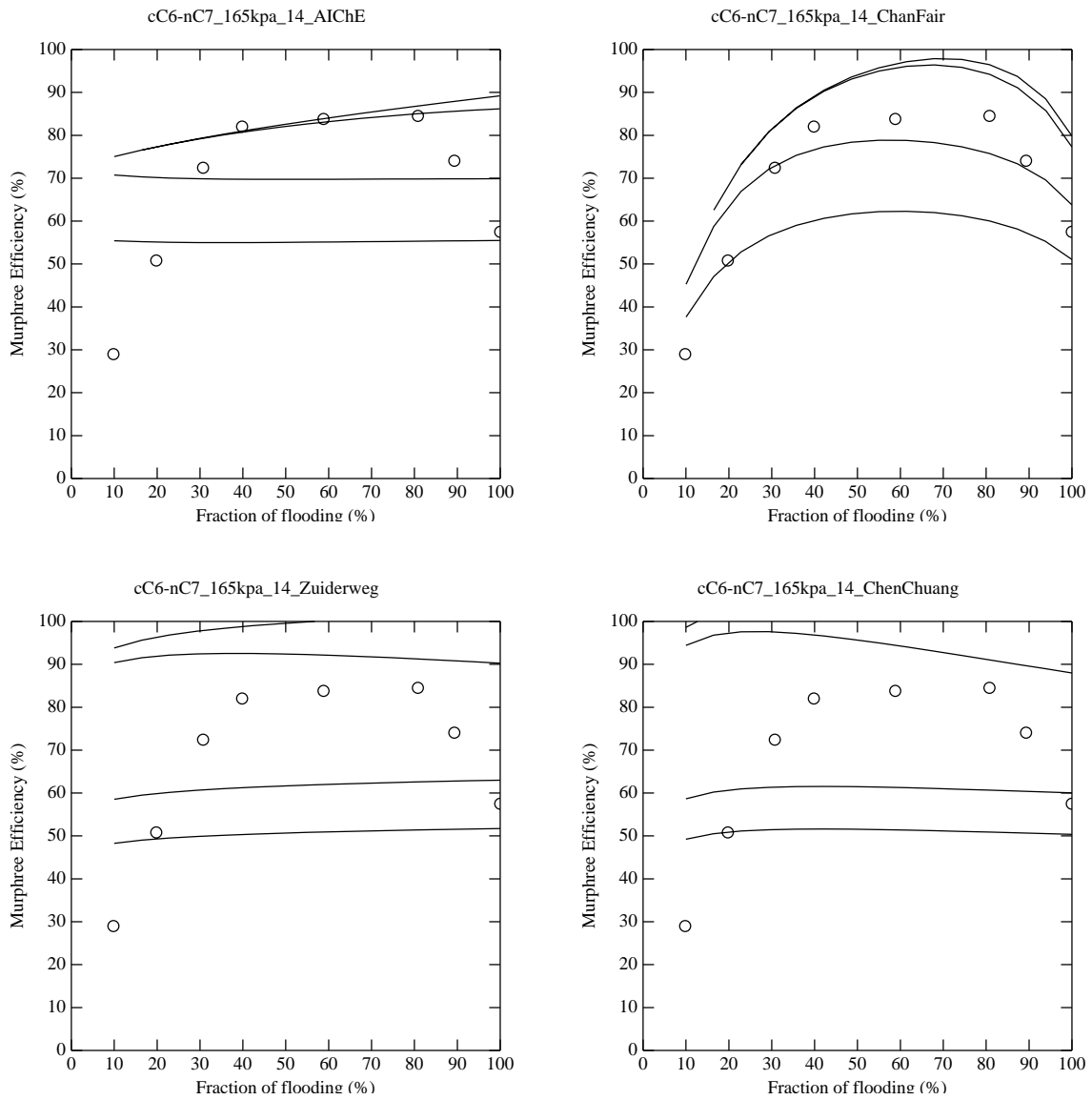


Figure C.2: Experimental FRI data cC6-nC7 at 165 *kPa*, 14% Sieve plate.

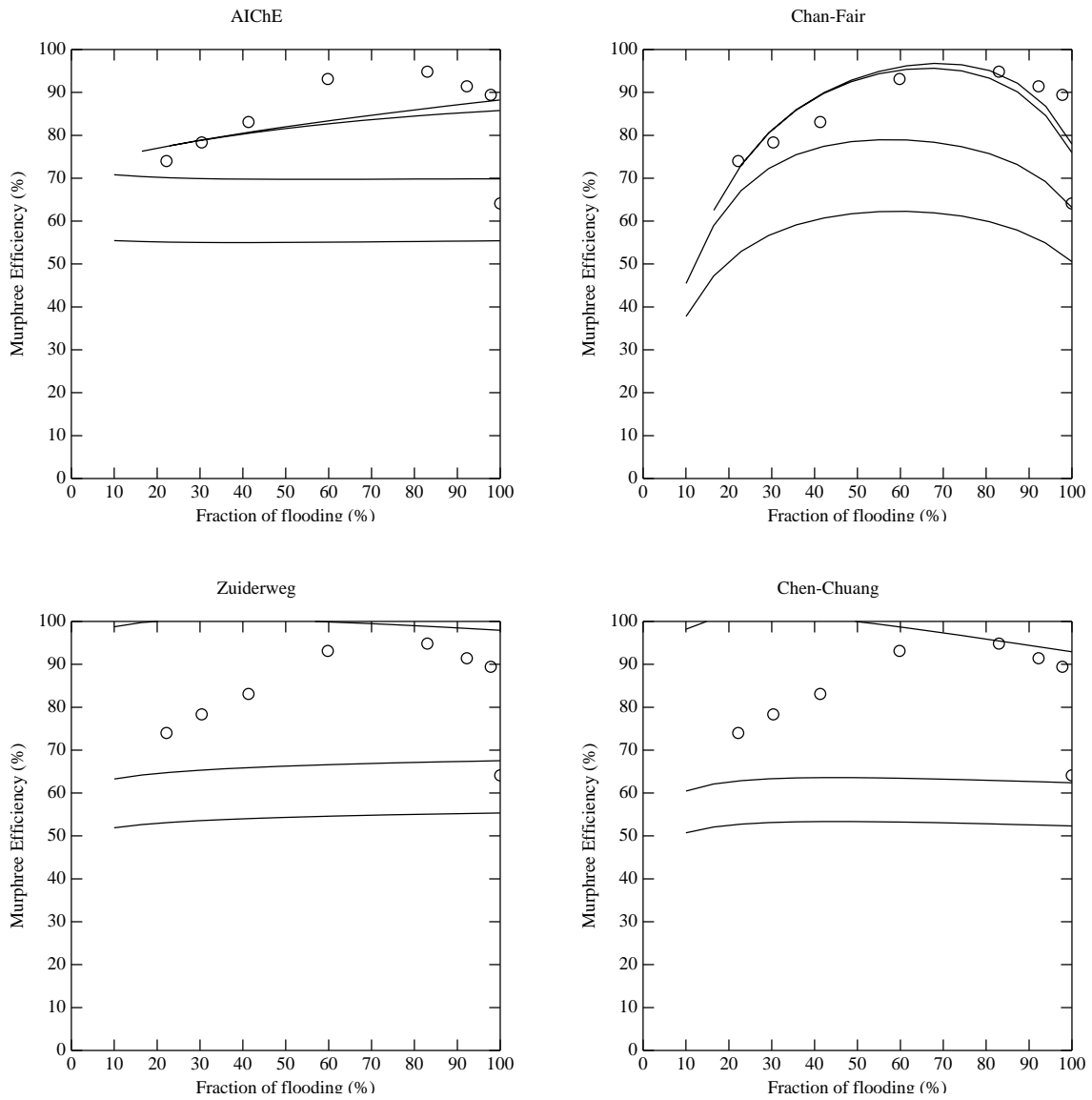


Figure C.3: Experimental FRI data cC6-nC7 at 165 kPa, 8% Sieve plate.

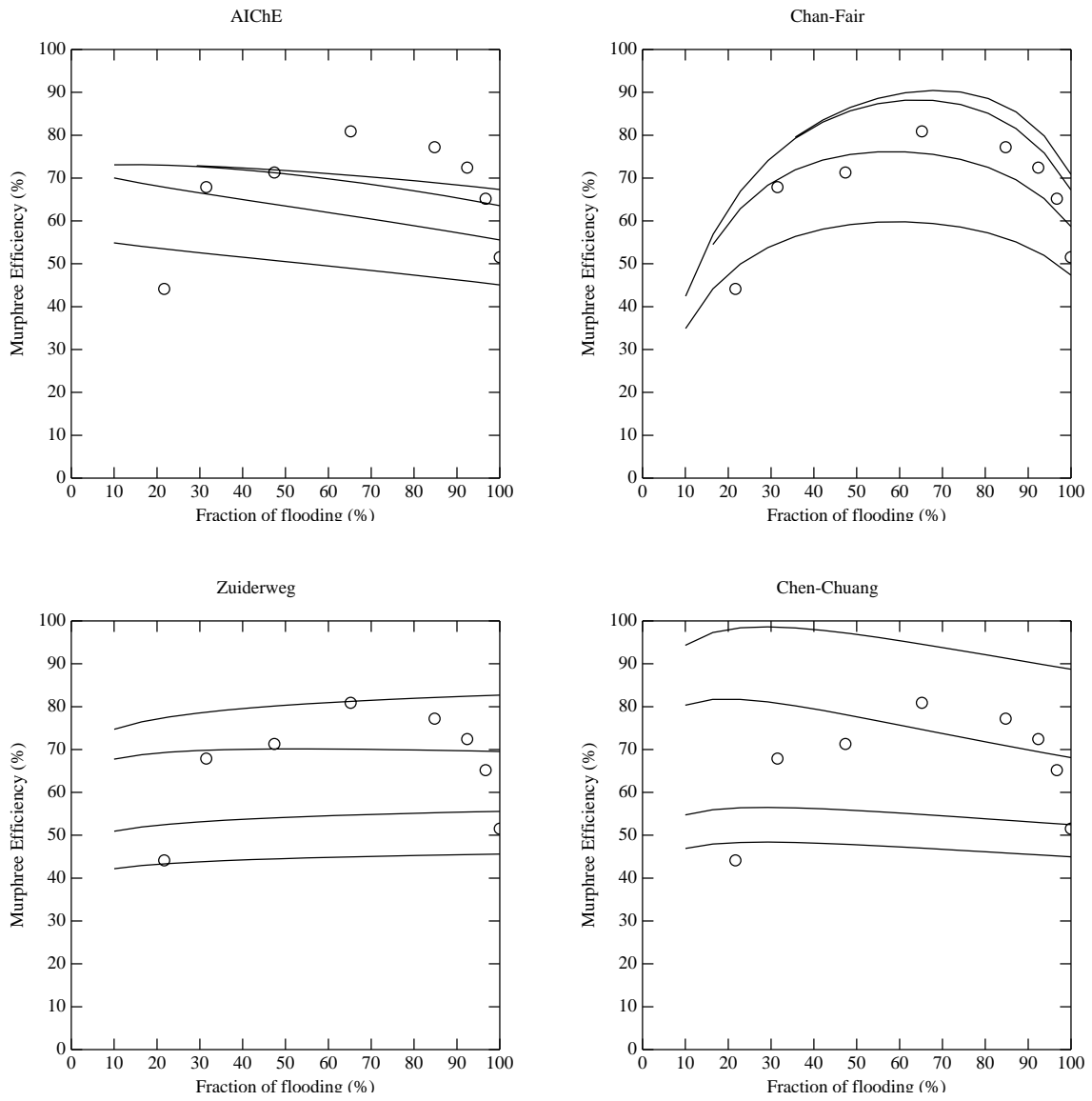


Figure C.4: Experimental FRI data cC6-nC7 at 28 kPa, 8% Sieve plate.

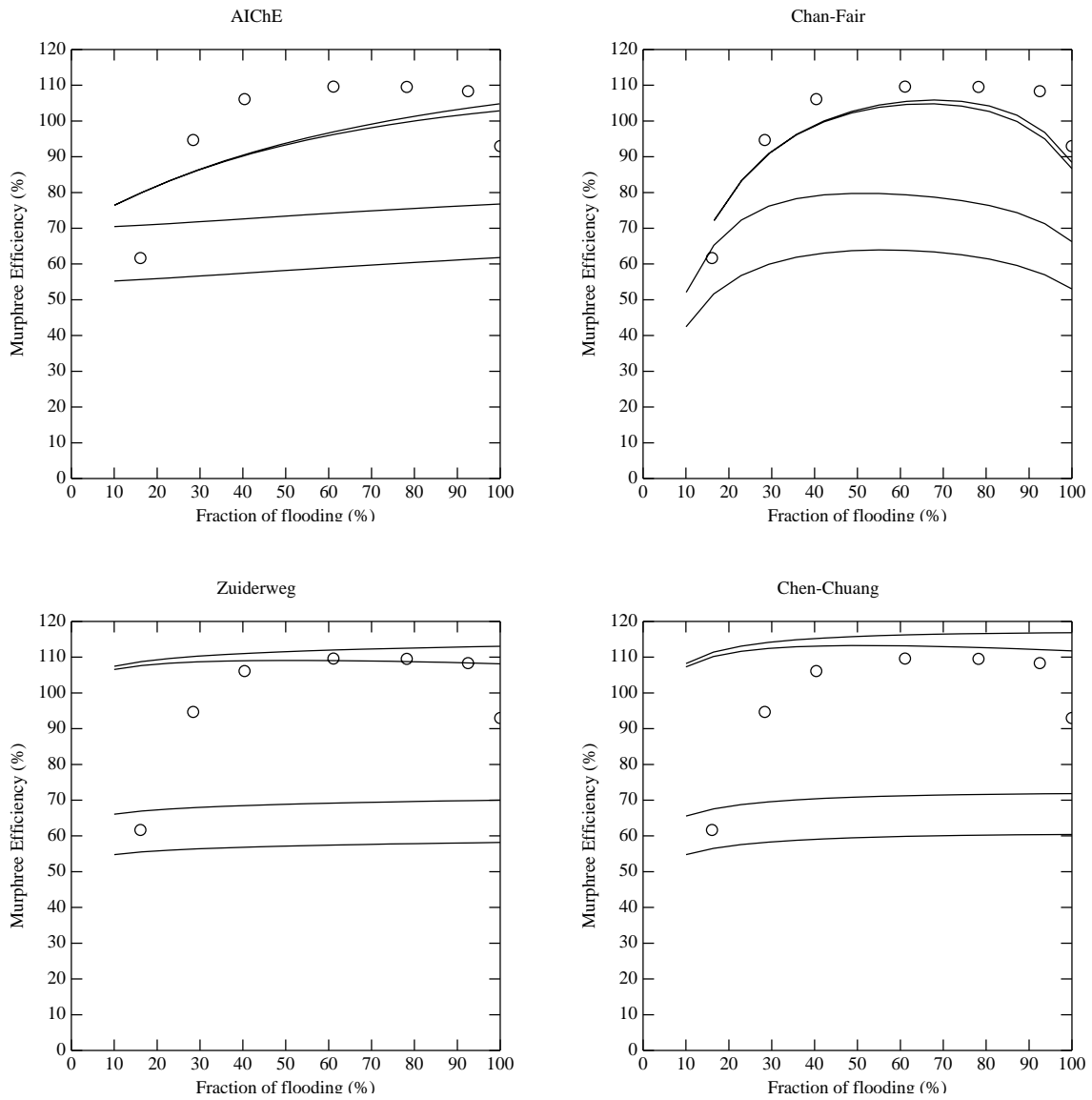


Figure C.5: Experimental FRI data iC4-nC4 at 1138 kPa , 14% Sieve plate.

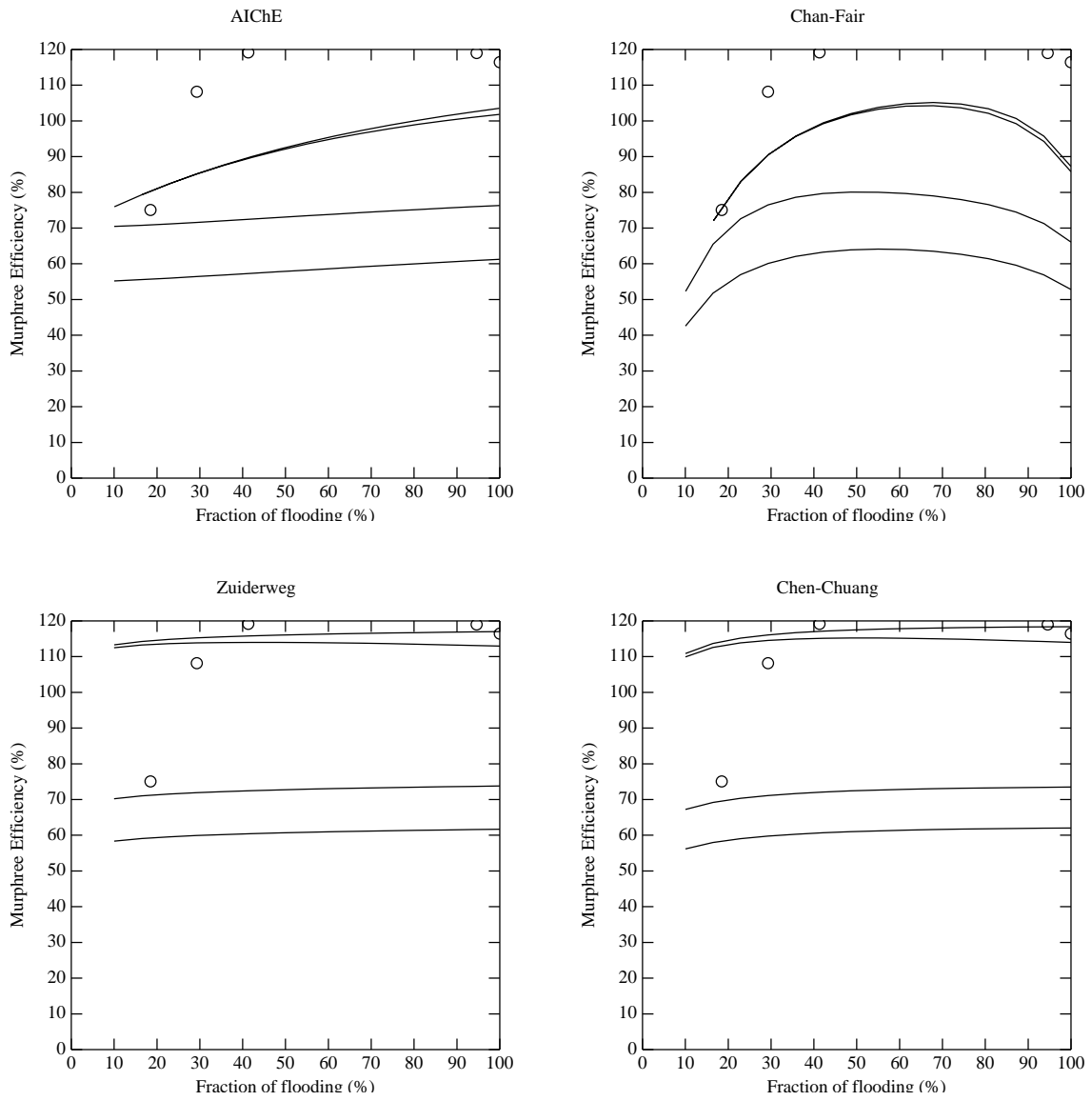


Figure C.6: Experimental FRI data iC4-nC4 at 1138 *kPa*, 8% Sieve plate.

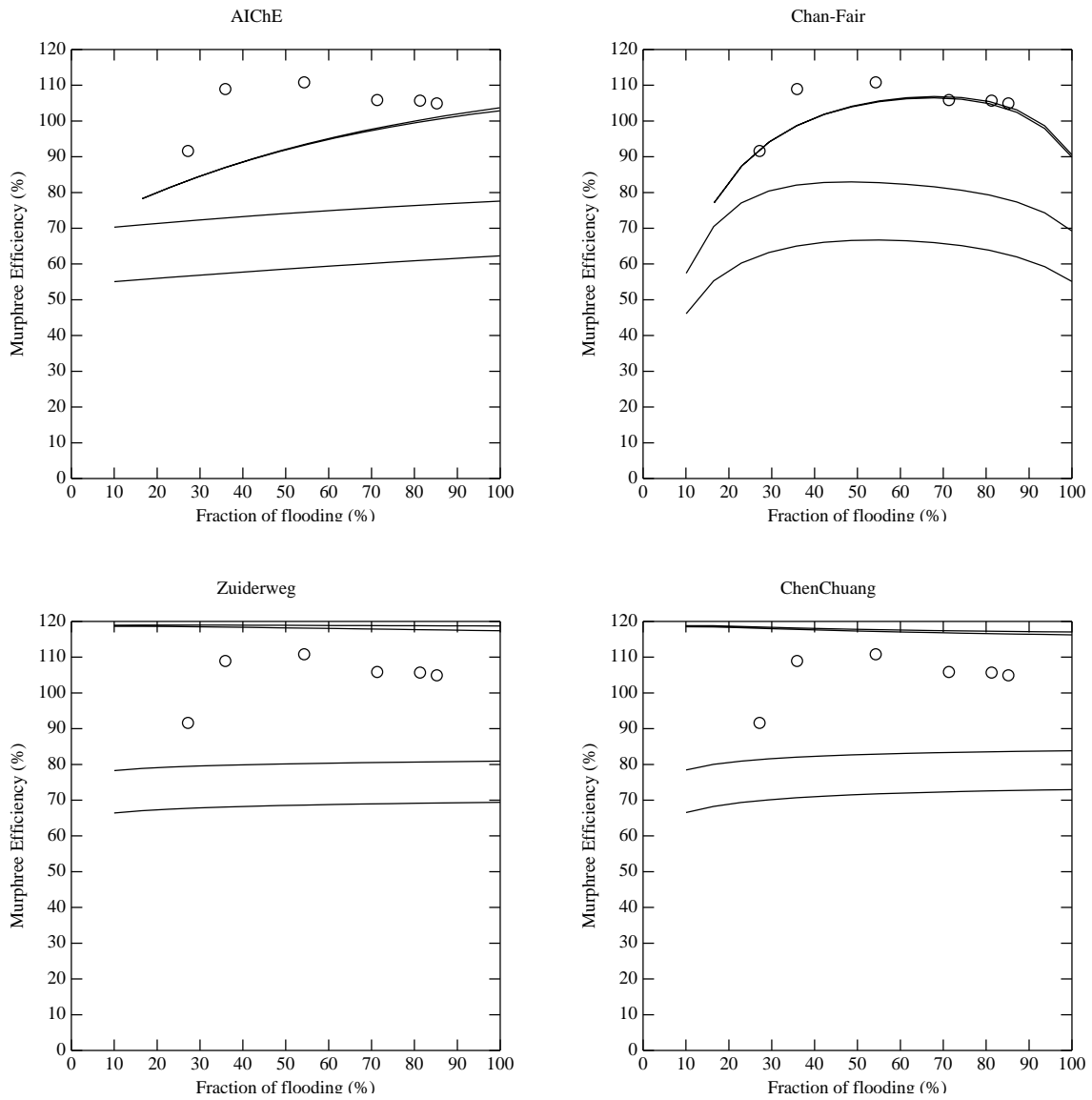


Figure C.7: Experimental FRI data iC4-nC4 at 2068 kPa , 8% Sieve plate.

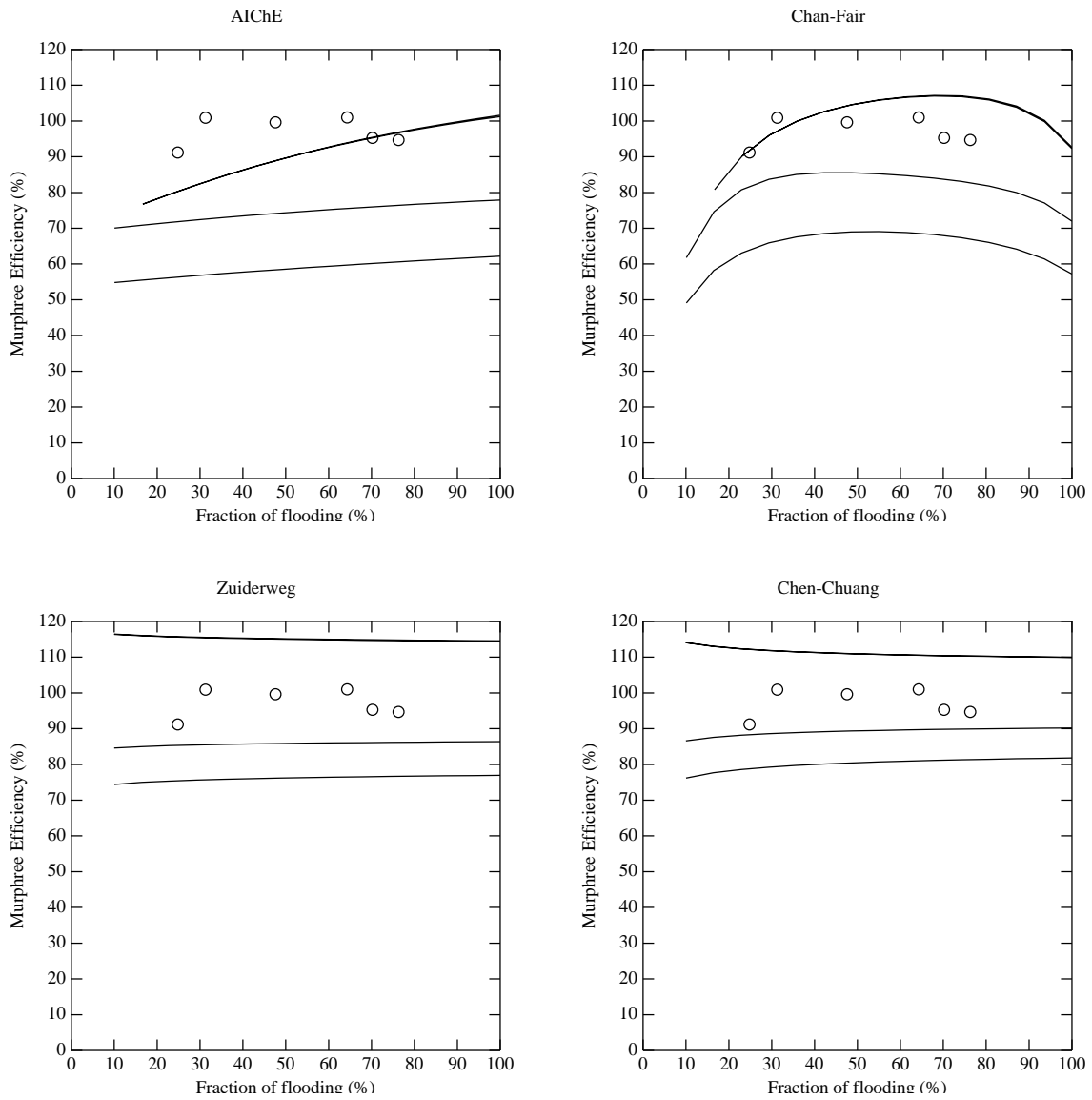


Figure C.8: Experimental FRI data iC4-nC4 at 2756 *kPa*, 8% Sieve plate.

Appendix D. BESIRK

Since solving systems of Differential-Algebraic Equations (DAE's) with multi-step codes (Brenan and Petzold, 1989) like DASSL requires initial derivative information and will have problems with discontinuities, our preference was to use a single-step method. Holland and Liapis (1983) solved the system of differential-algebraic equations resulting from his dynamic distillation column model by using a generalized Semi-Implicit Runge-Kutta method of Michelsen (1976) combined with Richardson extrapolation. The integration is computationally intensive.

To improve the method a Bulirsch-Stoer extrapolation approach was tested and shown to be more effective. The approach is similar to work by Bader and Deuffhard (1983) and Deuffhard *et al.* (1987) as described in Hairer (1991, 1994). A variety of stiff ODE problems taken from the literature have been solved and the results compared with DASSL and the Implicit Midpoint Rule method of Bader and Deuffhard. BESIRK is shown to have the better overall performance for the given set of test problems. The Fortran code solves differential-algebraic systems with constant differential coefficients.

The method requires more Jacobian evaluations than some other codes but it reduces execution times on a set of ODE test problems by about 30 percent. Performance on DAE problems equals that of multi-step codes. The algorithm is simple and compact, and may easily be tailored to the user's needs (to handle sparse systems, for example).

Algorithm

A system of DAE's can be written as:

$$\mathbf{A}\mathbf{y}' = \mathbf{f}(\mathbf{y}, \mathbf{z}, t) \quad (\text{D.51})$$

$$\mathbf{0} = \mathbf{g}(\mathbf{y}, \mathbf{z}, t) \quad (\text{D.52})$$

where (1) and (2) are the differential and algebraic set of equations respectively. Both sets are dependent on the differential variables, \mathbf{y} , the algebraic variables, \mathbf{z} , and the independent variable, t . \mathbf{A} is the coefficient matrix for all the differential terms. If the system (1,2) is written as

$$\mathbf{A}\mathbf{y}' = \mathbf{f}(\mathbf{y}, \mathbf{z}, t) \quad (\text{D.53})$$

$$\epsilon \mathbf{z}' = \mathbf{g}(\mathbf{y}, \mathbf{z}, t) \quad (\text{D.54})$$

with ϵ taken to approach zero, then the resulting ODEs can be solved by numerical integration methods that can handle stiff problems. Such methods are (Semi/Diagonal) Implicit Runge-Kutta (S/D IRK) methods or the Backward Differentiation Formulae (BDF) methods. There are many articles describing implementations (see, for example Gear (1971a); Hindmarsh (LSODE, 1980); Prokopakis and Seider (1981); Petzold (DASSL, 1983); Cameron (1983); Brenan *et al.* (1989); Cash and coworkers (1989,1990,1992); and many others). Bader and Deuffhard (1983) presented a method based on the Implicit Midpoint Rule (IMR) combined with a Bulirsch-Stoer (1966) extrapolation technique, Deuffhard (1983) discusses an implementation of this method. Deuffhard *et al.* (1987) developed the code LIMEX which employs an implicit Euler method with extrapolation. Here a Bulirsch-Stoer (BS) extrapolation technique is combined with a third order SIRK from Michelsen (1976).

To solve the system:

$$\mathbf{y}' = \mathbf{f}(t, \mathbf{y}) \quad (\text{D.55})$$

we can use Michelsen's (1976) third order SIRK method:

$$\mathbf{y}_{n+1} = \mathbf{y}_n + R_1 \mathbf{k}_1 + R_2 \mathbf{k}_2 + R_3 \mathbf{k}_3 \quad (\text{D.56})$$

where \mathbf{k}_1 , \mathbf{k}_2 , and \mathbf{k}_3 are obtained by solving:

$$[\mathbf{I} - ha_1 \mathbf{J}(\mathbf{y}_n)] \mathbf{k}_1 = h \mathbf{f}(t_n, \mathbf{y}_n) \quad (\text{D.57})$$

$$[\mathbf{I} - ha_1 \mathbf{J}(\mathbf{y}_n)] \mathbf{k}_2 = h \mathbf{f}(t_n + c_2 h, \mathbf{y}_n + b_2 \mathbf{k}_1) \quad (\text{D.58})$$

$$[\mathbf{I} - ha_1 \mathbf{J}(\mathbf{y}_n)] \mathbf{k}_3 = (b_{31} \mathbf{k}_1 + b_{32} \mathbf{k}_2) \quad (\text{D.59})$$

with h being the step in the independent variable t and \mathbf{I} the identity matrix. The Jacobian $\mathbf{J}(\mathbf{y}_n)$ is defined by:

$$\mathbf{J}(\mathbf{y}_n) = \frac{\partial \mathbf{f}(\mathbf{y}_n)}{\partial \mathbf{y}_n} \quad (\text{D.60})$$

The numerical constants are:

$$\begin{aligned} a_1 &= 0.4358665215084590 & c_2 &= 0.84375 \\ b_2 &= 3/4 & b_{32} &= -0.2423378912600453 \\ b_{31} &= -0.6302020887244526 & R_2 &= 0.8349304838526379 & R_3 &= 1 \\ R_1 &= 1.037609496131860 \end{aligned}$$

Precise values for these coefficients are important to maintain accuracy. The calculation of \mathbf{y}_{n+1} from (5)-(9) requires only one matrix decomposition and three back-substitutions. This method has been found to be one of the more efficient semi-implicit Runge-Kutta methods.

To solve the DAE system (1) and (2) with Michelsen's method the system is written as:

$$\mathbf{B} \mathbf{y}' = \mathbf{f}(t, \mathbf{y}) \quad (\text{D.61})$$

where \mathbf{B} is a matrix with constant coefficients and \mathbf{f} is the set of functions dependent on the variable vector \mathbf{y} and independent variable t . For algebraic equations the rows of \mathbf{B} will be zero. Thus, (11) can represent differential, algebraic, and differential algebraic equations. This makes it possible to easily switch between different systems of equations. By partitioning the matrix \mathbf{B} (using ϵ) we can write:

$$\mathbf{y}' = \mathbf{B}^{-1}\mathbf{f}(t, \mathbf{y}) \quad (\text{D.62})$$

\mathbf{k}_1 is obtained from:

$$[\mathbf{I} - ha_1\mathbf{B}^{-1}\mathbf{J}(\mathbf{y}_n)]\mathbf{k}_1 = h\mathbf{B}^{-1}\mathbf{f}(t_n, \mathbf{y}_n) \quad (\text{D.63})$$

This can be rewritten as:

$$[\mathbf{B} - ha_1\mathbf{J}(\mathbf{y}_n)]\mathbf{k}_1 = h\mathbf{f}(t_n, \mathbf{y}_n) \quad (\text{D.64})$$

Similarly, we can obtain \mathbf{k}_2 and \mathbf{k}_3 as:

$$[\mathbf{B} - ha_1\mathbf{J}(\mathbf{y}_n)]\mathbf{k}_2 = h\mathbf{f}(t + c_2h, \mathbf{y}_n + b_2\mathbf{k}_1) \quad (\text{D.65})$$

$$[\mathbf{B} - ha_1\mathbf{J}(\mathbf{y}_n)]\mathbf{k}_3 = \mathbf{B}(b_{31}\mathbf{k}_1 + b_{32}\mathbf{k}_2) \quad (\text{D.66})$$

The nice properties of Michelsen's algorithm have been retained; only one decomposition per iteration is needed.

We use the Bulirsch-Stoer (BS) extrapolation method to integrate from t to $t + H$, with H being a "big" step. The ideas behind BS methods are clearly articulated by Press *et al.* (1992), Bader and Deuffhard (1983) and Deuffhard (1983). Here we have adapted the original BS method to use the SIRK method for the integration.

The integration from t to $t + H$ is done several times while using n_j ($j = 1, 2, \dots$) smaller steps of size h_j , where $h_j = H/n_j$. Every j^{th} integration the number of steps increases, and thus, h_j decreases. After each integration (except for $j = 1$) we try to fit the values of $\mathbf{y}(t + H)$ as a function of stepsize h_j^p (with integer p depending on the order of the extrapolation method) and extrapolate to obtain $\mathbf{y}(t + H)$ at $h_j = 0$ (corresponding to taking an infinite number of steps). Current extrapolation methods include polynomial extrapolation and rational extrapolation, the former being favored (Press *et al.*, 1992). The extrapolation conveniently provides both the solution and an estimate of the error. If the error is not acceptable we integrate again using the next higher value of n_j . When, after integrating k times, the errors are within the integration tolerances we accept the step H_m . By estimating the number of integrations for the next step, k_{m+1} , we can obtain the next step as $H_{m+1} = H_m n_{k_{m+1}} / n_{k_m}$. The optimum value of k_{m+1} is denoted by q . Of course, the best q can be dependent on the required tolerances and the local problem conditions. Furthermore, increments of k need to be limited to a maximum increment, k^* , in order to maintain stability (see Deuffhard, 1983).

If the error estimates obtained from the extrapolation are too large the stepsize H is reduced. This prevents the extrapolation from becoming unbounded which can lead to (fatal) floating point errors. The error estimates obtained from the extrapolation should decrease as n_j increases. If the error estimates increase then the previous approximations are probably incorrect due to too large a step in h_j and H should be reduced. Unbounded extrapolations or increasing error estimates rarely occurred in our test computations but were adequately dealt with in this way.

Normally $k^* = 1$ is used throughout the integration. To improve the efficiency of the method $k^* = 2$ is used when k is constant during a step, and $k^* = 1$ when k changes during a step. This method of adjusting k works quite well as long as q is high. Furthermore, the new stepsize is limited to maximum 10 times the previous stepsize. The new stepsize is given by:

$$\begin{array}{ll}
 \text{for: } & k < q - 1, \quad k + k^* < q & H_{m+1} = H_m n_{k+k^*} / n_k \\
 & k < q - 1, \quad k + k^* \geq q & H_{m+1} = H_m n_{q-1} / n_k \\
 & k = q - 1 & H_{m+1} = 1.1 H_m \\
 & k = q & H_{m+1} = 0.9 H_m \\
 & k > q & H_{m+1} = H_m n_{q-1} / n_k \\
 \\
 \text{with:} & & H_{m+1} / H_m \leq 10
 \end{array}$$

Step sequences $\{n_j\}$ that have been employed in BS methods are:

$$\begin{array}{ll}
 \text{Bulirsch:} & \{ 2,4,6,8,12,16,24,32,48,64,96, \dots \} \\
 \text{Bader and Deuffhard:} & \{ 2,6,10,14,22,34,50, \dots \}
 \end{array}$$

With either of these step sequences there will be certain points in between t and $t + H$ where the right hand side of (11) is evaluated more than once. To avoid this we used a sequence that consisted of prime numbers:

$$\{ 1,2,3,5,7,11,17,23,31,47,61,89, \dots \}$$

causing the right hand side of (11) to be evaluated only once at any point other than at t and at $t + H$. We found that this improved the accuracy and stability of the method without effecting the efficiency. Both polynomial and rational extrapolation were tested, where polynomial extrapolation performs 50 to 100% better.

Using a semi-implicit integration method requires Jacobian information. While integrating with small steps of h_j we have the option of updating the Jacobian at each step or to evaluate it only at the beginning of each "big" step (H) and to reuse it in each small step (to approximate the Jacobian with Broyden's method does not work here). Reusing the Jacobian dramatically reduces the amount of work needed to evaluate Jacobians and to carry out matrix decompositions. However, reusing the Jacobian can have negative consequences for the convergence and stability of the extrapolation method. Usually the stepsize H has to be reduced to maintain stability which results in performing more function evaluations.

Both approaches of updating and reusing the Jacobian were tested on ODE problems taken from Enright and Pryce (1987), test set A-F, and from Cash and Considine (1992), test sets G-I. Test set J consists of

Table D.1: Results for the test problems with and without updating of the Jacobian. Absolute tolerances of 10^{-4} are used and the initial step is 10^{-3} .

Test Set	Reused Jacobian			Updated Jacobian		
	NF	NJ	time	NF	NJ	time
A	1500	113	10.0	560	226	5.6
B	4803	199	19.6	1303	538	8.3
C	9251	291	29.9	1552	660	7.7
D	2120	164	5.9	800	324	3.1
E	1310	148	4.3	605	242	2.7
Total A-E	18984	915	69.6	4820	1990	27.5
F	15622	230	36.0	3103	1376	12.1
G	19588	445	81.4	4856	2180	31.0
H	4330	369	10.2	1535	614	4.9
I	30571	367	68.3	7910	3488	26.0
Total F-I	70111	1411	195.9	17404	7658	74.0
J	6084	100	20.8	908	386	8.3
Total	95179	2426	286.3	23132	10034	109.8

three index one DAE problems. The index one pendulum problem taken from Brenan et al. (1989), an example from Gear (1971b) and the following simple (exponential) problem integrated from $t = 0 \dots 4$ starting from $y_i(0) = 1$:

$$y_1' = y_1 y_2^2 y_3^2 \quad (\text{D.67})$$

$$y_2' = (y_1^2 - 3y_3) y_2^2 \quad (\text{D.68})$$

$$0 = y_2 y_3 - 1 \quad (\text{D.69})$$

The solution to this simple problem is (e^t, e^{-2t}, e^{2t}) .

The integration is started with an initial stepsize of 10^{-3} for all problems (see Bader and Deuffhard, 1983). The equations and variables were unscaled and absolute tolerances were used. For all problems except E4 and I3 the Jacobian was evaluated from analytical derivatives. The number of function and Jacobian evaluations for each test set can be found in Table D.1. The reported execution time is the computer time used on a 66MHz Intel 486 based PC while compiling with WATFOR77 (WATCOM, 1988). WATFOR77 executables tend to be much slower than those generated by other compilers and they are not optimized.

When the Jacobian is reused the method fails on problem I4 (the time, NF, and NJ spent on I4 are not included in Table D.1). The results in Table D.1 shows that updating the Jacobian is to be preferred, especially for the more difficult test problems (sets F, G, and I).

The method described in this appendix has been implemented in a Fortran code we call BESIRK (for Bulirsch Extrapolated Semi-Implicit Runge-Kutta). The user supplies routines that will calculate the

function vector and Jacobian, checks the tolerances, updates the variable vector, and reports the variables. Standard versions of the tolerance check, update, and report routines are included. If required, BESIRK can produce informative messages on each internal step. The user can opt for numerical Jacobian evaluation (by simple forward differencing) which eliminates the burden of writing code for the analytical Jacobian evaluation (a common source of errors). The code has no preset limits on the size of the system. It requires the user to pass workspace arrays and a check whether these are properly sized is carried out. The Fortran code is extensively commented and, we believe, relatively easy to understand compared to multi-step codes like DASSL.

Comparison with other codes

To see how BESIRK performs relative to other codes we have also solved the test problems mentioned in the previous section with DASSL and an implementation of the IMR from the book by Press *et al.* (1992). The results are displayed in Table D.2. In order to obtain a proper comparison, we used absolute error criteria for each method. The IMR method had problems solving D6, I2, and I4. The number of evaluations and time spent on these problems by the IMR code are excluded from Table D.2. The totals for the IMR code also do not include problem set J (DAE's) since the IMR code was not designed for such problems. The corrected totals in Table D.2 represent the totals after excluding the results for problems D6, I2, I4, and set J in order to make a better comparison. Totals A-E represents the DE test set of Enright and Pryce (1987). For this test the IMR had the lowest total time, BESIRK was about 25 percent slower, and DASSL is 2.6 times slower than the IMR code. Problems F-I are the more difficult ones and BESIRK outperforms both DASSL and the IMR code by a factor of 1.2 and 1.75 respectively. DASSL performs only slightly slower than BESIRK on the DAE systems (set J) although the number of test problems is rather small.

The total calculation times will depend on whether one Jacobian evaluation is (much) more expensive to compute than n function evaluations, where n is the number of variables. None of the test problems had large n or computationally involved Jacobians. For sparse systems where the Jacobian evaluation can be much faster than n function evaluations updating the Jacobian can have a significant advantage.

References

G. Bader, P. Deuffhard, "A Semi-Implicit Mid-Point Rule for Stiff Systems of Ordinary Differential Equations", *Num. Math.*, **41**, (1983), pp. 373-398.

K.E. Brenan, S.L. Campbell, L.R. Petzold, *Numerical Solution of Initial-Value problems in Differential-Algebraic Equations*, North Holland (1989).

R. Bulirsch, J. Stoer, "Numerical treatment of Ordinary Differential Equations by Extrapolation Methods", *Num. Math.*, **8**, (1966), pp. 1-13.

Table D.2: Results for the test problems using DAES, IMR, and DASSL. Absolute tolerances of 10^{-4} are used and the initial step is 10^{-3} .

Test Set	BESIRK			IMR			DASSL		
	NF	NJ	time	NF	NJ	time	NF	NJ	time
A	560	226	5.6	1022	42	4.1	1060	122	13.0
B	1303	538	8.3	2834	84	7.0	2169	129	19.9
C	1552	660	7.7	3274	90	6.9	1611	143	13.1
D	800	324	3.1	933	45	1.6	922	140	6.1
E	605	242	2.7	873	41	1.7	641	117	4.2
Total A-E	4820	1990	27.4				6403	651	56.2
Corr. A-E	4760	1970	27.1	8936	302	21.3	6327	640	55.8
F	3103	1376	12.0	15502	492	25.9	2781	194	18.7
G	4856	2180	30.9	15578	336	42.8	2361	375	20.8
H	1535	614	5.0	1169	81	1.8	1132	174	6.7
I	7910	3488	26.0	27414	842	45.8	6774	390	41.8
Total F-I	17404	7658	73.9				13048	1133	88.0
Corr. F-I	14475	6396	66.3	59663	1751	116.3	10605	944	75.3
J	908	386	8.3	–	–	–	919	62	9.5
Total	23132	10034	109.8				20370	1850	153.7
Corr. total	19235	8366	93.4	68599	2053	137.6	16932	1584	131.0

I.T. Cameron, "Solution of Differential-algebraic Systems Using Diagonally Implicit Runge-Kutta Methods", *J. Num. Analys.*, **3**, (1983), pp. 273-289.

J.R. Cash, "A Block 6(4) Runge-Kutta Formula for Nonstiff Initial Value Problems", *ACM Trans. Math. Soft.*, **15**, 1, (1989), pp. 15-28.

J.R. Cash, A.H. Karp, "A variable Order Runge-Kutta Method for Initial Value Problems with Rapidly Varying Right-Hand Sides", *ACM Trans. Math. Soft.*, **16**, 3, (1990), pp. 201-222.

J.R. Cash, S. Considine, "An MEBDF Code for Stiff Initial Value Problems", *ACM Trans. Math. Soft.*, **18**, 2, (1992), pp. 142-155.

P. Deuffhard, "Order and Step-size Control in Extrapolation Methods", *Num. Math.*, **41**, (1983), pp. 399-422.

P. Deuffhard, E. Hairer, J. Zugck, "One step and extrapolation methods for differential-algebraic systems", *Num. Math.*, 51, (1987), pp. 501-516.

W.H. Enright, J.D. Pryce, "Two FORTRAN Packages for Assessing Initial Value Methods", *ACM Trans. Math. Soft.*, **13**, 1, (1987), pp. 1-27.

C.W. Gear, *Numerical Initial Value problems in Ordinary Differential Equations*. Prentice-Hall (1971a).

C.W. Gear, "Simultaneous numerical solution of differential-algebraic systems", *IEEE Trans. Circ.*

Theory, CT-18, 1 (1971b), pp. 85-95.

E. Hairer, S.P. Norsett, G. Warner, *Solving Ordinary Differential Equations I. Nonstiff Problems*, 2nd Ed., Springer-Verlag, Berlin (1994).

E. Hairer, G. Warner, *Solving Ordinary Differential Equations II. Stiff and Differential-Algebraic Problems*, Springer-Verlag, Berlin (1991).

A.C. Hindmarsh, "LSODE and LSODI, two new initial value ordinary differential equation solvers", *ACM-SIGNUM Newsletters*, **15**, (1980), pp. 10-11.

C.D. Holland, A.I. Liapis, *Computer Methods for Solving Dynamic Separation Problems*. McGraw-Hill (1983).

M.L. Michelsen, "An Efficient General Purpose Method of Integration of Stiff Ordinary Differential Equations", *AIChE J.*, **22**, 3, (1976) pp. 544.

L.R. Petzold, "A Description of DASSL: A Differential/Algebraic System Solver", in *Scientific Computing*, R.S. Stepleman *et al.* (Eds.), North Holland, Amsterdam (1983), pp. 65-68.

H.P. Press, S.A. Teukolsky, W.T. Vetterling, B.P. Flannery, *Numerical Recipes in Fortran*, 2nd Ed., Cambridge University Press, Cambridge, England (1992).

G.J. Prokopakis, W.D. Seider, "Adaptive Semi-Implicit Runge-Kutta Method for Solution of Stiff Ordinary Differential Equations", *Ind. Eng. Chem. Fundam.*, **20**, 3, (1981), pp. 255-266.